BIOMECHANICAL REGULATION OF HOOK BASAL BODY ASSEMBLY IN SALMONELLA ENTERICA

by

Eli Joseph Cohen

A dissertation submitted to the faculty of
The University of Utah
in partial fulfillment of the requirements for the degree of

Doctor of Philosophy

Department of Biology

The University of Utah

August 2017

The University of Utah Graduate School

STATEMENT OF DISSERTATION APPROVAL

The dissertation of **Eli Joseph Cohen**

has been approved by the following supervisory committee members:

Kelly T. Hughes	, Chair	**5/19/2017** Date Approved
Kent Golic	, Member	**5/19/2017** Date Approved
David Blair	, Member	**5/19/2017** Date Approved
Colin Dale	, Member	Date Approved
David Belnap	, Member	**5/19/2017** Date Approved

and by **M. Denise Dearing**, Chair/Dean of the Department/College/School of **Biology**

and by David B. Kieda, Dean of The Graduate School.

ABSTRACT

Bacteria swim through liquid environments by rotating extracellular propellers known as flagella. Extending up to 10 μm in length, the cell-external flagellar filament self-assembles from ~10,000 copies of a single protein and constitutes the bulk of the flagellum. However, the nanometer-scale hook basal body (HBB), which powers the flagellar filament and anchors it to the cell body, is constructed from ~25 unique protein subunit types that must self-assemble into an ion-powered motor of precise dimensions. Thus, the HBB represents the structurally and mechanically more complex component of the flagellum and has been the subject of intense study for several decades.

The HBB is composed of three substructures: i) the MS-C-ring rotor in the cytoplasm that encloses the flagellar-specific Type III Secretion apparatus, ii) the periplasmic driveshaft, and iii) the extracellular hook. The rigid driveshaft, known as the rod, is the first axial structure of the flagellum to assemble and resides entirely in the periplasmic space between the inner and outer membranes. The rod transmits the torque generated by the flagellar motor embedded in the cytoplasmic membrane to the cell-external components of the flagellum.

Until recently, the mechanisms that regulate rod assembly and the switch from rod-to-hook polymerization remained unknown. Specifically, it was unclear how the flagellum, which self-assembles from thousands of individual subunits to predetermined

dimensions, ensured the rod substructure did not grow past its mature wild type length of ~25 nm. Secondly, while it was known that the transition from rod polymerization to hook polymerization was somehow coordinated with penetration of the outer membrane by the nascent flagellar structure, the molecular mechanism that coupled these two events was unknown.

Using genetic, biochemical and microscopic techniques, we have elucidated both the means by which rod length is controlled as well as the mechanism that synchronizes outer membrane penetration with the switch from rod-to-hook assembly. We have also provided insight into the molecular basis for the difference in flexibility between the rod and the hook and the significance of the rod's relative inflexibility with respect to flagellar form and function.

Dedicated to mammy and pappy

TABLE OF CONTENTS

LIST OF FIGURES

LIST OF TABLES

CHAPTER 1

INTRODUCTION

Motility, the ability of an organism to propel itself through its environment, represents a major milestone in the evolution of life on earth. With the development of self-directed movement, the first motile organisms were transformed from passive inhabitants of their environment to active participants within it. Motility provided the means to locate food sources, avoid unfavorable environments and seek out sites for colonization.

Although prokaryotes have evolved several distinct types of motility and associated machinery, the bacterial flagellum represents the most extensively studied prokaryotic motility organelle. Resembling a corkscrew, the flagellar filament is a rigid multi-megadalton propeller that extends from the cell surface up to ten times the length of the cell body. The filament is anchored to the cell body, and is energized, by a structurally complex, ion-powered motor known as the hook basal body (HBB)(1-3). Once assembled, the flagellum of *Salmonella enterica* rotates at ~300 revolutions per second, propelling cells through aqueous environments at speeds of several body lengths per second (4-5). Whereas the filament is constructed from ~10,000-20,000 subunits of a single protein, flagellin (FliC and/or FljB), the HBB is composed of ~25 unique proteins and can be considered several distinct substructures in and of itself.

The Hook Basal Body (HBB) of *Salmonella enterica*

Construction of the flagellum (Fig. 1.1) begins with the assembly of a cytoplasmic membrane-embedded disk known as the MS-ring, which is composed of ~30 subunits of the FliF protein. The MS-ring acts as an assembly platform for the cytoplasmic C-ring, the flagellar Type 3 Secretion System (fT3SS) and the axial flagellar structures (i.e. the rod, hook and filament) (3, 6).

The cytoplasmic C-ring acts as the rotor of the flagellar motor. Stators (MotA and MotB) convert the energy released by ions (H^+ or Na^+) flowing down the electrochemical gradient established across the cytoplasmic membrane (the proton motive force) by the electron transport chain (ETC) during respiration. The energy made available by protons flowing across the cytoplasmic membrane is transduced into rotational movement of the flagellum through conformational changes at C-ring/stator interfaces (Fig. 1.2).

In order for proteins that form the axial flagellar structures to be translocated from the cytoplasm, where they are translated from mRNA, to the periplasm and external environment, where they assemble, they must be secreted through a pore in the cytoplasmic membrane. The secretion pore is formed within the MS-ring from three integral membrane proteins, FliP, FliQ and FliR, and one membrane-anchored protein, FliO (Fig. 1.2). FliP is believed to form the actual pore in the inner membrane through which flagellar substrates pass into the periplasm. The three other proteins (FliO, FliQ and FliR) play roles in pore formation, stability and function, although their exact functions, positions and stoichiometries relative to one another remain unknown. Unlike FliP, FliQ and FliR, which are all predominantly embedded in the inner membrane, FliO is a largely cytoplasmic protein that is tethered to the inner membrane by a short

transmembrane segment that is dispensable for its function. The *fliO* gene is absent in some bacterial species and is believed to stabilize FliP and promote FliP oligomerization within the MS-ring. Translocation of flagellar substrates through the membrane-embedded pore requires an energized secretion apparatus that is selective, ensuring that only the correct proteins are secreted across the cytoplasmic membrane. This requirement is fulfilled by two transmembrane proteins, FlhA and FlhB, that complex with one another within the MS-ring and associate with the FliOPQR pore. The FlhAB complex couples the energy released by ions (H^+ or Na^+, depending on the species of bacteria) (Fig. 1.2) flowing down an electrochemical gradient established across the cytoplasmic membrane to the secretion of flagellar protein subunits toward the external environment at rates of thousands of amino acid residues per second (9-10). In contrast, the Sec secretion system, which also secretes proteins across the cytoplasmic membrane, translocates proteins at a rate of ~10 residues/second (11).

The large cytoplasmic C-terminal portion of FlhA ($FlhA_C$) interacts with a soluble ATPase complex composed of the FliH, FliI and FliJ proteins that associate with the flagellar basal body via interactions between FliH and FliN of the C-ring. The ATPase complex is composed of FliH (~12 copies), FliI (6-12 copies) and FliJ (1-2 copies) that together form a doughnut-shaped structure within the C-ring (6). The FliHIJ ATPase complex and the F_1F_0 ATP synthase found in all living organisms are presumed to have descended from a common ancestral set of cellular machinery as the two share a significant degree of homology. Together, the FliOPQR/FlhAB/FliHIJ macromolecular complex is referred to as the **f**lagellar **T**ype **III S**ecretion **S**ystem (fT3SS).

For years it was presumed that flagellar substrate secretion was energized by

FliHIJ-dependent ATP hydrolysis. However, recent studies have demonstrated that secretion of flagellar proteins is energized by the proton motive force (PMF) or the sodium motive force (in marine species of bacteria). Nevertheless, FliHIJ is important for the assembly process and is thought to use the energy obtained from ATP hydrolysis to unfold secreted substrates and promote productive substrate/secretion apparatus interactions, thereby increasing the secretion efficiency (9-10). Because the secretion channel of the flagellum is ~2 nm in diameter, fT3SS substrates must travel through the central channel of the growing structure in an unfolded state and only assume their native 3D conformations once they reach the tip of the nascent flagellum (12).

Biomechanical Regulation of Axial Structure Assembly and Function

The first axial structure of the flagellum to be constructed resides entirely in the periplasm and is known as the rod. The rod acts as a driveshaft, coupling the torque generated by the flagellar rotary motor to the cell-external flagellar components. At only ~25 nm in length, the rod is nevertheless divided into two distinct substructures: the ~7 nm proximal rod and the ~18 nm distal rod (14-15).

The proximal rod, composed of four different protein subunit types (FliE, FlgB, FlgC and FlgF), bridges the distance between the inner membrane and peptidoglycan layer. Relatively little is known about the proximal rod, including how it assembles, how its length is regulated or why four protein types are required for its construction when the distal rod, hook and filament only require a single subunit type. It is thought that FliE is the first proximal rod protein to assemble and acts as an adaptor that couples the planar MS-ring to the axial flagellar components. Following FliE, the order of proximal rod

assembly was shown to be FlgB → FlgC → FlgF in *Borrelia* (16), and is presumed to follow the same order in *Salmonella*. Each subunit type forms a single stack in the proximal rod. Completion of the FlgF layer positions the tip of the proximal rod at the cell-proximal side of the peptidoglycan layer (17).

The peptidoglycan layer of gram-negative species of bacteria is comprised of several layers of extensively crosslinked glycan chains, forming a mesh that resides between the inner and outer membranes (18). The highly crosslinked mesh character of the peptidoglycan layer endows it with considerable strength while also allowing it to be both flexible and permeable to small molecules. Although the crosslinking of neighboring peptide strands is not uniform, the average gap size in the mesh of the peptidoglycan is ~4 nm and is therefore too small to allow the ~11 nm diameter rod to pass through (19).

In order for the nascent flagellar structure to reach, and ultimately pass through, the outer membrane, a hole with a diameter sufficiently large enough to accommodate the rod must be made in the peptidoglycan layer. In gram negative species of bacteria, the solution to this problem is to digest a hole in the peptidoglycan layer at the site of rod assembly via peptidoglycan hydrolyzing enzymes (PGases). In the β- and γ-proteobacteria, the requirement to digest a hole in the peptidoglycan layer has led to the evolution of a dual domain protein, FlgJ, that possesses a domain responsible for promoting rod assembly and a separate β-N-Acetylglucosaminidase (PGase) domain (19-20).

The N-termini of the *Salmonella* FlgJ protein serves a scaffolding function by capping the rod substructure and promoting incorporation of rod subunits as they reach

the tip of the growing structure (19). FlgJ also prevents premature incorporation of hook subunits prior to rod completion (17). The structure of the oligomeric FlgJ rod cap has yet to be determined, but is thought to resemble the FliD filament cap, which forms a homopentamer on the tip of the growing filament and promotes incorporation of flagellin subunits (21). In *Salmonella* mutants possessing truncated versions of FlgJ possessing only the N-terminus, flagellar structures referred to as candlesticks are formed. Candlestick structures possess distal rod subunits with P-rings, but lack L-rings (discussed below) and hooks/filaments, demonstrating that the rod scaffolding function of FlgJ is attributable entirely to its N-terminus (19).

The C-terminus of *Salmonella* FlgJ is responsible for the PGase activity of the protein, and is separated from the N-terminus rod capping domain by a ~55 residue unstructured linker region that is largely dispensable for FlgJ function. Phylogenetic analysis suggests that the dual domain character of FlgJ proteins in the β- and γ-proteobacterial clades is the result of a gene fusion. This fusion occurred in the last shared ancestor of these two lineages and fused the FlgJ scaffolding domain to a PGase located elsewhere in the chromosome. This is supported by the observation that flagellated species of bacteria in all other genera of proteobacteria possess single domain homologs of FlgJ with no C-terminal PGase. Additionally, a member of the δ-proteobacteria, *Desulfovibrio desulfuricans*, possesses a dual domain FlgJ where the C-terminal PGase is a M23/37-family peptidase (Pep), as opposed to the β-N-Acetylglucosaminidase found in the β- and γ-proteobacteria (20). This demonstrates that the evolution of dual domain FlgJ's has occurred by at least two independent events.

For gram-negative species possessing single domain (i.e. *sans* PGase activity)

FlgJ homologs, soluble periplasmic PGases are thought to be recruited by the rod in order to locally digest the peptidoglycan. Indeed, the FlgB and FlgF rod proteins of *Rhodobacter sphaeroides* have recently been shown to both bind to and activate a cell wall hydrolyzing protein, SltF (22). It is worth noting that efforts to identify proteins responsible for peptidoglycan hydrolysis in the flagellated gram-positive species *Bacillus subtilis* have been unsuccessful, raising questions as to how the rod passes through the thick gram-positive cell wall.

Once the peptidoglycan layer has been breached, distal rod assembly can continue to the outer membrane. Unlike the proximal rod, which requires four different protein types to span the distance between the cytoplasmic membrane and peptidoglycan, the distal rod bridges the space between the peptidoglycan and outer membrane using ~50 copies of a single protein, FlgG (15). FlgG subunits stack helically upon one another, adding length to the growing structure with each subunit added, until the inner leaflet of the outer membrane is reached. At this point, distal rod growth ceases. Due to its intrinsic rigidity, the rod projects from the cytoplasmic membrane perpendicular to the outer membrane, with the tip of the distal rod flush with the outer membrane (17, 23-24). Positioning the rod in this manner is thought to be important for the next step of flagellar synthesis, which is the penetration of the outer membrane.

Penetration of the outer membrane requires a large ring complex, the PL-ring, to form around the distal rod. The PL-ring is built from approximately 25-30 subunits each of the FlgI (P-ring) and FlgH (L-ring) proteins. FlgI and FlgH (and a FlgI folding chaperone, FlgA) are distinct in that they are not secreted to the periplasm via the fT3SS. Instead, these three proteins are secreted into the periplasm through the Sec type II

secretion system (25-26).

Assembly of the PL-ring is sequential, the P-ring must be present on the rod before the L-ring can polymerize. While the specific FlgG residues or motifs that promote P-ring assembly are unknown, it is clear that the FlgI subunits recognize the distal rod and, with assistance from FlgA, polymerize around it to form the P-ring. This is evident from the observation that mutations that cause the distal rod to grow past its wild type length of ~18 nm accumulate multiple P-rings along the length of the distal rod as opposed to just one (23). Additionally, a handful of mutations in the *flgG* gene that allow distal rod assembly but preclude P-ring assembly have been isolated.

The FlgH protein possesses a canonical lipobox motif (discussed below) at its N-terminus and is consequently localized to, and inserted in, the outer membrane. FlgH is targeted to the Sec machinery via an N-terminal secretion signal that is cleaved from the protein during its translocation to the periplasm, resulting in a cysteine residue occupying the N-terminal position of the mature FlgH protein. This cysteine is lipoylated, which facilitates insertion into the inner leaflet of the outer membrane, thereby anchoring FlgH in the outer membrane. As a consequence of being anchored in the outer membrane, the tip of the distal rod must be positioned flush with the outer membrane in order for the L-ring to polymerize around it (17, 23). Similar to the P-ring, the specifics of L-ring assembly, including conformational changes that take place during assembly and which residues of FlgI and/or FlgG are recognized by FlgH, remain unknown.

Following outer membrane penetration, approximately 130 FlgE subunits self-assemble to form the hook, a universal joint that allows the rigid filament to articulate relative to the cell body (1, 3, 27-28). Similar to both the distal rod and filament, hook

polymerization by FlgE subunits requires the presence of a capping scaffold (FlgD) to promote proper subunit folding and incorporation into the growing structure. FlgE and FlgG share 40% amino acid identity and are presumed to have descended from a single, ancestral, proto rod-hook flagellar protein. Despite the high degree of conservation between the two subunit types, the rod and the hook behave differently: the former is rigid while the latter is flexible. This difference is thought to arise from the insertion of a large globular domain in FlgE not found in FlgG, and a ~40 residue domain in FlgG, truncated significantly in FlgE, known as the L-stretch.

FlgE polymerization continues until the hook has reached its mature WT length of ~55 nm. Termination of hook polymerization, and the switch to flagellin secretion, depends on the action of a secreted molecular ruler, FliK. FliK takes intermittent measurements of the hook as it assembles, with approximately 5-6 FliK molecules secreted per hook, or about one FliK per 30 secreted hook subunits. FliK possesses globular domains at its N- and C-termini, connected by a long, unstructured linker. The C-terminus of FliK ($FliK_C$) interacts with the FlhB component of the fT3SS, which energizes substrate secretion using the proton motive force (PMF) and specifies which class of flagellar substrates are secreted. Interaction of $FliK_C$ with FlhB induces a secretion specificity switch in FlhB, causing it to cease targeting rod-hook type subunits and begin to target filament-type substrates for secretion (27-28).

Prevention of interaction of the $FliK_C$ with FlhB prior to HBB completion, and therefore premature substrate specificity switching, depends on the speed of FliK secretion. When the hook is short, i.e. < ~40 nm, the N-terminus of FliK exits the tip of the growing hook and assumes its secondary, globular structure. The thermodynamic

forces driving re-folding of the FliK N-terminus as it exits the tip of the hook are thought to pull the rest of the FliK molecule through the secretion channel at high velocity (28). The speed at which the re-folding of the FliK N-terminus pulls the C-terminal globular domain past FlhB is fast enough to prevent a productive interaction of FlhB with $FliK_C$, thereby preventing specificity switching. However, once the hook has reached a length of at least ~40 nm, the N-terminus remains in the central channel of the growing hook as $FliK_C$ approaches FlhB at a slow rate of secretion, which allows $FliK_C$ to interact with FlhB and catalyze the secretion specificity switch. In the absence of FliK, the hook will continue polymerizing indefinitely. Specificity switching allows for secretion of late substrates to occur and is coupled to a switch in flagellar gene transcription from genes coding for early structures to those coding for later structures (e.g. the filament) (1, 29-30).

Genetic Regulation of Flagellar Assembly

A single flagellum represents ~1% of the total cellular protein. Flagellated species of bacteria, such as *E. coli* and *Salmonella*, construct ~4-6 flagella per cell. Thus, flagellar morphogenesis amounts to a significant energy and resource expenditure for the cell. Consequently, bacteria have evolved genetic regulatory mechanisms to ensure that flagella are assembled only when motility is required and that the expression of flagellar genes occurs in a hierarchical fashion. The genes required to assemble late structures, e.g. the filament and stators, are only expressed once assembly of the HBB is complete (1, 29-30).

The flagellar regulon is composed of ~60 genes transcribed in a hierarchy of three promoter classes. The co-transcribed *flhD* and *flhC* genes are the sole class I flagellar genes and sit at the top of the flagellar genetic hierarchy (30). The *flhDC* operon encodes the proteins that together act as the flagellar master regulator, the $FlhD_4C_2$ heteromer (Fig. 1.3). $FlhD_4C_2$ recruits the σ^{70} transcription factor to class II genes whose expression is required for construction of the HBB. Integration of environmental stimuli (e.g. the cells nutritional state, outer membrane stress, etc.) occurs at the level of *flhDC* expression. Seven repressors and three enhancers of flagellar gene expression have been identified that bind to the large (~500 bp) *flhDC* promoter region and 5' UTR (31). In addition to structural HBB genes, the $FlhD_4C_2/\sigma^{70}$/RNA polymerase (RNAP) complex drives expression of class III protein secretion chaperones as well as another, flagellar class III-specific σ factor, *fliA* (σ^{28}) (32).

Prior to hook completion and subsequent FliK-dependent secretion specificity switching at FlhB, class III genes are not expressed, despite the presence in the cytoplasm of FliA. This is due to the fact that FliA is prevented from directing RNAP to class III promoters by FlgM, a small (97 amino acid residues) protein that forms a complex with FliA and prevents FliA from binding DNA (Fig. 1.3) (33).

FlgM is one of a small number of proteins expressed from class II promoters that possess class III secretion signals, and thus is not secreted prior to hook completion. Only after the secretion specificity switch occurs is FlgM recognized and targeted for secretion by the fT3SS. FlgM secretion allows free FliA to bind, and therefore recruit RNAP, to class III promoters (33). In this way, biomechanical regulation of the switch from early to late structure construction by FliK is coupled to the genetic switch from class II to class

III gene expression. Prevention of premature class III gene expression precludes the accumulation of tens of thousands of flagellin molecules in the cytoplasm and accompanying cytotoxic effects.

Two other proteins possessing class III secretion signals that are expressed from class II promoters are FlgK and FlgL, which form a filament adaptor complex at the tip of the completed hook. The FlgKL adaptor defines the junction between the hook and filament and are required for filament assembly (34-35). By expressing *flgKL* along with the class II HBB structural genes, i.e. prior to *fliC*/*fljB*, the handful of FlgKL subunits needed to polymerize on the tip of the hook need not compete with the much more numerous flagellin subunits.

In contrast to class II secretion substrates, secreted class III proteins are known to require secretion chaperones for efficient secretion through the fT3SS (36). In addition to its function as a transcription factor, FliA serves as the secretion chaperone for FlgM, delivering it to the fT3SS to be secreted (37). The dual functionality of FliA is a conserved phenomenon among chaperone proteins. The FlgK and FlgL chaperone FlgN and the filament cap (FliD) chaperone FliT both have secondary regulatory functions that modulate flagellar gene expression.

FlgN promotes flagellar assembly by binding to FlgK and FlgL, protecting them from degradation by proteases, preventing premature FlgKL aggregation in the cell and directing them to the fT3SS once hook assembly is complete (38-39). Once FlgK and FlgL have been secreted, FlgN is free to fulfill its second role, increasing translation of FlgM mRNA. The FlgN-dependent increase of FlgM translation is thought to be a mechanism for the cell to fine-tune late flagellar gene expression by altering the levels of

free FliA in the cytoplasm.

FliT also regulates flagellar gene expression. Once FliD has been secreted following the secretion specificity switch, FliT is free to perform its second function, targeting $FlhD_4C_2$ for proteolysis. Free FliT binds specifically to the FlhC subunits of the $FlhD_4C_2$ complex and targets them to the ClpXP proteasome. It is interesting to note that FliT is only capable of binding free $FlhD_4C_2$; when $FlhD_4C_2$ is bound to DNA as part of the $FlhD_4C_2/\sigma^{70}$/RNAP holoenzyme, it ($FlhD_4C_2$) is protected from FliT-directed ClpXP degradation (38). This is in contrast to another regulator of flagellar gene expression, RflP (YdiV), that also promotes ClpXP-mediated proteolysis of $FlhD_4C_2$. RflP is expressed in response to nutrient limitation and, unlike FliT, will remove $FlhD_4C_2$ from class II promoters (41). Thus, FliT allows the cell to gradually taper off flagellar gene expression as flagellar morphogenesis progresses, while RflP promotes the rapid downregulation of flagellar gene expression that is thought to be important for, e.g., evading the host immune system during establishment of infection.

Mutations in *flgG* that Result in Filamentous Rods

The wild type distal rod contains ~50 FlgG subunits and polymerizes to ~18 nm, a length slightly longer than twice the length of the ~7 nm proximal rod (15). Termination of distal rod assembly places the tip of the rod at the inner leaflet of the outer membrane (17, 23-24). In the absence of the proteins that make up the L- and P-rings (FlgI and FlgH, respectively), outer membrane penetration and hook assembly do not occur. Since the mature rod is ~25 nm long and FliK will only catalyze the secretion specificity switch once a flagellar axial structure of a minimal length of ~70 nm has polymerized (25 nm

rod + 45 nm hook), FlgM secretion and class III gene expression do not occur in a Δ*flgHI* background.

The inability to secrete FlgM, and therefore express class III genes in a Δ*flgHI* background, has allowed for the development of genetic selections and screens designed to isolate mutants capable of bypassing the WT requirement for outer membrane penetration and hook assembly prior to secretion specificity switching (42). By constructing gene fusions, we have been able to to isolate said bypass mutants that allow FlgM secretion and class III gene expression in a Δ*flgHI* background.

To isolate mutants that secrete FlgM in a Δ*flgHI* background, the gene required to degrade β-lactam antibiotics (i.e. ampicillin), *bla*, is fused to the N-terminal region of FlgM containing its class III fT3SS secretion signal. Ampicillin exerts its cytotoxic effects by blocking peptidoglycan synthesis in the periplasm. Consequently, β-lactamase (Bla) must localize to the periplasm in order to confer ampicillin resistance (Ap^R) to the cell. Normally, secretion of β-lactamase to the periplasm is accomplished by the Sec secretion machinery and depends on Bla's N-terminal Sec secretion signal. By fusion of the *bla* gene lacking its N-terminus to the C-terminus of the FlgM coding region, resistance to ampicillin necessarily demands secretion of FlgM-Bla through the fT3SS.

In the case of class III gene expression in a Δ*flgHI* background, the genes required to utilize lactose (*lacZYA*) as a carbon source have been placed under control of flagellar class III promoters (e.g. *fliC* or *motAB*). This allows one to select for class III gene expression in a Δ*flgHI* background simply by selecting for growth on media where the only available carbon source is lactose.

Using these tools, mutants have been isolated that undergo secretion specificity

switching in the absence of the PL-ring complex. These include mutations in both *flgM* and *fliA* (e.g. *flgM* nulls and mutants of FliA that are defective in interaction with FlgM), as well as mutations in *flhAB*, *flhE* and *flk*. These alleles are detailed elsewhere and will not be discussed further as they are beyond the scope of this dissertation.

In addition to the mutations discussed above, a class of mutants were isolated in the gene encoding the distal rod subunit, *flgG*, that allowed secretion specificity switching to occur in the absence of the FlgHI PL-ring (23, 42). Approximately 25 *flgG* alleles were isolated that conferred an Ap^R phenotype in the Δ*flgHI flgM-bla* background and were termed *flgG** alleles. Upon examination by transmission electron microscopy (TEM), it was found that all of the *flgG** alleles allowed the distal rod to continue polymerizing well past its wild type length of ~18 nm. Rather than terminating growth at ~18 nm, rod length in *flgG** backgrounds was determined by the FliK molecular ruler normally responsible for measuring hook length. In a $fliK^+$ background, the average *flgG** rod length was found to peak at ~70 nm. When *fliK* was deleted, rods grew to uncontrolled lengths of up to ~500 nm.

Further investigation revealed three other features of *flgG** flagellar structures: i) *flgG** filamentous rods accumulated multiple P-rings, ii) filament assembly could occur in the absence of the hook (FlgE) and/or the hook cap (FlgD) on the tip of a *flgG** filamentous rod once FliK triggered the secretion specificity switch and iii) in the absence of FliK, ~25% of the polyrod structures transitioned to polyhook structures (17, 23), indicating spontaneous loss of the FlgJ rod cap, possibly dislodged by continuous secretion of FlgD and/or FlgE subunits. Thus, the rod-to-hook transition could occur independently of PL-ring complex assembly. Each of these observations are discussed

separately below.

The accumulation of multiple P-rings along the length of *flgG** filamentous rods suggests that the nucleation signal for individual FlgI subunits to polymerize and form the P-ring is the distal rod itself, as opposed to, e.g., FlgF, the FlgF/FlgG junction or the peptidoglycan layer. Additionally, several *flgG** mutants that produce filamentous rods failed to accumulate P-rings in a $flgI^{+}$ background, supporting the hypothesis that the signal for P-ring assembly depends on specific residues or motifs within FlgG. However, despite the accumulation of P-ring on filamentous rods, the maximum number of L-rings found on any given *flgG** rod was always one (17). L-ring polymerization to form the mature PL-ring complex invariably terminates distal rod assembly and promotes the transition to hook polymerization. This is the focus of Chapter 2 of this dissertation.

As mentioned previously, FlgE and FlgG share ~40% amino acid identity. Nevertheless, it was not expected that filaments would attach directly to the rod in a *flgG** Δ*flgDE* background. This suggested that the FlgKL hook-filament junction was capable of recognizing and assembling directly on top of the distal rod and reinforced the notion that FlgE and FlgG must possess common structural features in the mature flagellum. Consequently, the inability of the *flgG** distal rod to terminate growth at ~18 nm resulted in periplasmic filament assembly, regardless of whether *flgHI* and/or *flgDE* is present. Filament growth in the periplasm causes *flgG** strains to be poorly motile in swim agar and display severe morphological defects.

When *flgG** basal bodies from Δ*flgHI* Δ*fliK* backgrounds were isolated, a heterogeneous mixture of structures was observed. The majority of structures, ~75%, possessed only the MS-ring, proximal rod and extended *flgG** distal rods that were

termed polyrods (23). The remaining ~25% of structures possessed MS-rings, proximal rods and polyrods followed by polyhooks. Under normal circumstances, the assembly of the PL-ring complex will dislodge the FlgJ distal rod cap (see Chapter 2). Thus, while it appears that the presence of the FlgJ rod cap blocks FlgD from polymerizing on the rod tip and promoting premature hook assembly, the association of the FlgJ rod cap on the rod tip must be somewhat labile. Furthermore, the length of the polyrods with hooks attached isolated from Δ*flgHI* Δ*fliK* were found to cluster around 80-90 nm (23). One explanation for this observation is that, at any given distal rod length, there is a small chance that FlgJ will be dislodged from the rod tip during FlgG polymerization. This probability is presumed to be low, and thus does not occur with appreciable frequency in wild type backgrounds. However, as distal rod assembly proceeds unchecked in a Δ*flgHI* Δ*fliK flgG** background, the probability that FlgJ will be dislodged and replaced by a FlgD cap as the distal rod grows longer approaches 100% by or before the time the polyrod reaches ~80-90 nm.

The identification of numerous missense mutations in *flgG* that allow extended distal rod polymerization, coupled to the likelihood that FlgG and FlgE likely diverged from a common, ancestral protein, presented a paradox: If FlgE is capable of polymerizing indefinitely and requires the action of a molecular ruler to determine hook length, how does the wild type distal rod regulate its length in the absence of any such ruler molecule?

Based on experimental observations, and previous work that had estimated the total number of FlgG subunits in the mature distal rod was ~26 (13), a model for distal rod length control was proposed that depended solely on FlgG-FlgG interactions. The

flagellar axial components consist of 11 protofilaments that together form a hollow, tubular structure (43). Twenty-six FlgG subunits would be enough to complete two full helical turns of FlgG subunits, meaning that only two stacks of FlgG would be present in the completed distal rod. However, a recent structure of the HBB generated using electron cryo-tomography demonstrated that the number of FlgG subunits in the wild type distal rod is closer to fifty, which was not compatible with the FlgG-intrinsic model of distal rod length control. Our recent work supports a model for distal rod length control that depends on the outer membrane, which is the topic of Chapter 3 of this dissertation.

Lipoprotein secretion, processing and membrane anchoring

The extracytoplasmic compartment residing between the inner and outer membrane of gram-negative species of bacteria is referred to as the periplasmic space. In addition to housing the flagellar rod subtructure, hundreds of different proteins localize to this compartment (44). Periplasmic proteins take part in a variety of important cellular processes including nutrient transport, secretion and outer membrane homeostasis. Proteins that are translocated to the periplasm can be broadly divided into two classes: lipid-modified proteins known as lipoproteins that are membrane-anchored (e.g. FlgH), and those that are soluble in the periplasmic matrix (e.g. FlgI).

In general, periplasmic proteins are secreted across the cytoplasmic membrane by one of two systems, the generalized **sec**retory system (Sec) or the **t**win **a**rginine **t**ransport (Tat) system, both of which are found in all three domains of life (11). The Sec and Tat systems fulfill complementary roles in the translocation of proteins across the inner

membrane: The Sec system secretes proteins in an unfolded state and is also responsible for insertion of integral membrane proteins in the cytoplasmic membrane, while the Tat system translocates folded proteins across the inner membrane. All of the secreted proteins discussed in this dissertation are translocated by either the fT3SS or the Sec system.

The Sec secretion system (Fig. 4) is energized by both ATP hydrolysis and the PMF. It consists of a protein conducting channel (PCC, made up of SecYEG) that spans the cytoplasmic membrane, a PCC-associated ATPase in the cytoplasm (SecA) that pushes unfolded secretory proteins through the PCC and a soluble protein chaperone (SecB) that binds Sec-targeted proteins post-translationally and delivers them to the SecA/SecYEG machinery in an unfolded state. In some cases, such as proteins that possess transmembrane domains (TMD) and require insertion in the cytoplasmic membrane, targeting and secretion through SecYEG occurs co-translationally. During co-translational secretion, signal recognition particle (SRP) recognizes and binds to the Sec-specific N-terminal secretion signal amino acid sequence as it exits the ribosome's E-site and directs the ribosome/SRP/protein complex to the Sec machinery in the cytoplasmic membrane (11, 46-47).

All Sec-secreted proteins identified to date have a canonical N-terminal secretion signal encompassing their first ~20 residues. Although the amino acid sequence of the secretion signal is not conserved, the electrochemical properties of the secretion signal are invariant and contain: i) a stretch of positively charged residues at the N-terminus, ii) a polar C-terminal region and iii) a run of hydrophobic residues sandwiched between the two. The secretion signal is cleaved from Sec-secreted proteins as they are being

translocated by either type I signal peptidase (soluble periplasmic proteins) or type II signal peptidase (lipoproteins) (11).

The fate of a Sec-secreted protein depends on the identities of the residues directly preceding and following the signal peptidase cleavage site. If the +1 position (the first amino acid residue following the cleavage site) is a cysteine residue and the -3 to -1 positions are a Leu-(Ala/Ser)-(Gly/Ala) motif, the protein is destined to become a lipoprotein. The Leu-(Ala/Ser)-(Gly/Ala)-Cys amino acid sequence is referred to as the lipobox motif and is widely conserved across all domains of life (11). Bioinformatics approaches analyzing the *E. coli* genome predict that this species possesses ~100 unique lipoproteins. Similar approaches in other species for whom genome sequences are available suggest that this is the approximate number of lipoproteins possessed by a number of bacterial species (45).

Maturation of a prolipoprotein to a fully processed, membrane-anchored lipoprotein involves several steps. Prior to signal sequence cleavage, a diacylglycerol moiety is covalently attached via thioether linkage to the sulfhydryl group of the +1 cysteine by phosphatidylglycerol/prolipoprotein diacylglycerol transferase (Lgt). Attachment of diacylglycerol is followed by signal sequence cleavage and N-acylation of the Cys residue by apolipoprotein *N*-acyltransferase (Lnt) to produce the mature, membrane-anchored lipoprotein (48-49). Whether a processed lipoprotein is retained in the cytoplasmic membrane or localized to the outer membrane depends on the identities of the +2 and, to a lesser degree, +3 residues. A serine residue at +2 directs the mature lipoprotein to the outer membrane, while an aspartate residue leads to retention in the cytoplasmic membrane (11).

To reach the outer membrane, hydrophobic lipoproteins like FlgH, the L-ring protein and LppA, the major outer membrane lipoprotein, must transit the hydrophilic space between the inner and outer membranes. This transit is performed by the localization of lipoproteins (Lol) system, an inner membrane-to-outer membrane lipoprotein shuttle essential for cell viability (Fig. 1.4). The Lol system consists of a cytoplasmic membrane-associated complex (LolCDE), a soluble periplasmic lipoprotein shuttle (LolA) and an outer membrane bound receptor (LolB) that accepts lipoproteins from LolA and inserts them in the inner leaflet of the outer membrane (48-49).

Once inserted in the inner leaflet of the outer membrane, Lol-shuttled lipoproteins may be subject to further modification. In the case of LppA, the C-terminus of the protein is covalently crosslinked to the peptidoglycan layer to promote outer membrane stability (50-51) (see Chapter 3). It is becoming increasingly clear that a number of lipoproteins are solvent exposed, i.e. they ultimately localize to the outer leaflet of the outer membrane (52-54). This is thought to require the action of poorly understood "flippases" that flip specific lipoproteins from the periplasmic side of the outer membrane to the extracellular face of the outer membrane.

References

1. Chevance FF, Hughes KT, Coordinating assembly of a bacterial macromolecular machine. *Nat. Rev. Microbiol.* 6:455–465 (2008).

2. Kearns DB. 2010. A field guide to bacterial swarming motility. *Nat. Rev. Microbiol.* 8:634–644 (2010).

3. Macnab RM, How bacteria assemble flagella. *Annu. Rev Microbiol.* 57: 77-100 (2003).

4. Berg HC, The rotary motor of bacterial flagella. *Annu. Rev. Biochem.* 72:19–54

(2003).

5. Berg HC, Anderson RA, Bacteria swim by rotating their flagellar filaments. *Nature* 245: 380-382 (1971).

6. Minamino T, Macnab RM, Components of the Salmonella flagellar export apparatus and classification of export substrates. *J. Bacteriol.* 181:1388–1394 (1999).

7. DeRosier DJ, The turn of the screw: the bacterial flagellar motor. *Cell* 93:17–20. (1998).

8. Barker CS, Meshcheryakova IV, Kostyukova AS, Samatey FA, FliO Regulation of FliP in the Formation of the Salmonella enterica Flagellum. PLoS Genet. 6:e1001143 (2010).

9. Paul K, Erhardt M, Hirano T, Blair DF, Hughes KT, Energy source of flagellar typeIII secretion. *Nature* 451:489-492 (2008).

10. Kojima S, Yamamoto K, Kawagishi I, Homma M, The polar flagellar motor of vibrio cholera is driven by an Na^+ motive force. *J. Bacteriol* 181:1927-1930 (1999).

11. Natale P, Bruser T, Driessen AJM, Sec- and tat-mediated protein secretion across the bacterial cytoplasmic membrane- distinct translocases and mechanisms. *Biochim. Biophys. Acta* 1778:1735-1756 (2008).

12. Yonekura K, Maki-Yonekura S, Namba K, Growth mechanism of the bacterial flagellar filament. *Res. Microbiol.* 153:191–197 (2002)

13. Jones CJ, Macnab RM, Okino H, Aizawa S. 1990. Stoichiometric analysis of the flagellar hook-(basal-body) complex of Salmonella typhimurium. *J. Mol. Biol.* 212:377–387 (1990).

14. Homma M, Kutsukake K, Hasebe M, Iino T, Macnab RM. 1990. FlgB, FlgC, FlgF and FlgG. A family of structurally related proteins in the flagellar basal body of Salmonella typhimurium. *J. Mol. Biol.* 211:465–477 (1990).

15. Fujii T *et al.*, Identical folds used for distinct mechanical functions of the bacterial flagellar rod and hook. *Nat. Commun.* 8:14276 (2016).

16. Liu J *et al.*, Intact flagellar motor of borrelia burgdorferi revealed by cryo-electron tomography: evidence for stator ring curvature and rotor/C-ring assembly flexion. *J. Bacteriol.* 191:5026-5036 (2009).

17. Cohen EJ, Hughes KT, Rod-to-hook transition for extracellular flagellum assembly is catalyzed by the l-ring-dependent rod scaffold removal. *J. Bacteriol.* 196:2387-2395. (2014).

18. Vollmer W, Holtje JV, The architecture of the murein (peptidoglycan) in gram-negative bacteria: vertical scaffold or horizontal layer(s)? *J. Bacteriol.* 186:5978-5987 (2004).

19. Nambu T, Minamino T, Macnab RM, Kutsukake K, Peptidoglycan-hydrolyzing activity of the FlgJ protein, essential for flagellar rod formation in Salmonella typhimurium. *J. Bacteriol.* 181:1555-1561 (1999).

20. Nambu T, Inagaki Y, Kutsukake K, Plasticity of the domain structure in FlgJ, a bacterial protein involved in flagellar rod formation. *Genes Genet. Syst.* 81:381-389 (2006).

21. Yonekura K *et al.*, The bacterial flagellar cap as the rotary promoter of flagellin self-assembly. *Science* 290:2148-2152 (2000).

22. De la Mora J *et al.*, The C terminus of the flagellar muramidase SltF modulates the interaction with FlgJ in Rhodobacter sphaeroides. *J. Bacteriol* 194:4513-4520 (2012).

23. Chevance FF *et al.*, The mechanism of outer membrane penetration by the eubacterial flagellum and implications for spirochete evolution. *Genes Dev*. 21:2326–2335 (2007).

24. Cohen EJ, Ferreira JL, Ladinsky MS, Beeby M, Hughes KT, Nanoscale-length control of the flagellar driveshaft requires hitting the tethered outer membrane. *Science* 356:197-200 (2017)

25. Jones CJ, Homma M, Macnab RM, L-, P-, and M-ring proteins of the flagellar basal body of Salmonella typhimurium: gene sequences and deduced protein sequences. *J. Bacteriol.* 171:3890–3900 (1989).

26. Nambu T, Kutsukake K, The Salmonella FlgA protein, a putative periplasmic chaperone essential for flagellar P ring formation. *Microbiology* 146:1171–1178 (2000).

27. Minamino T, Moriya N, Hirano T, Hughes KT, Namba K, Interaction of FliK with the bacterial flagellar hook is required for efficient export specificity switching. *Mol. Microbiol.* 74:239–251 (2009).

28. Erhardt M, Singer HM, Wee DH, Keener JP, Hughes KT, An infrequent molecular ruler controls flagellar hook length in Salmonella enterica. *EMBO J.* 30:2948–2961 (2011).

29. Aldridge P, Hughes KT, Regulation of flagellar assembly. *Curr. Opin. Microbiol.* 5:160–165 (2002).

30. Chilcott GS, Hughes KT, Coupling of flagellar gene expression to flagellar assembly in Salmonella enterica serovar Typhimurium and Escherichia coli. *Microbiol. Mol. Biol. Rev.* 64:694–708 (2000).

31. Mouslim C, Hughes KT, The effect of cell growth phase on the regulatory cross-talk between flagellar and Spi1 virulence gene expression. *PLoS Pathog.* 10:e1003987 (2014).

32. Ohnishi K, Kutsukake K, Suzuki H, Iino T, Gene fliA encodes an alternative sigma factor specific for flagellar operons in Salmonella typhimurium. *Molec. Gen. Genetic.* 221:139 (1990).

33. Hughes KT, Gillen KL, Semon MJ, Karlinsey JE, Sensing structural intermediates in bacterial flagellar assembly by export of a negative regulator. *Science* 262:1277-1280 (1993).

34. Homma M, Kutsukake K, Iino T, Yamaguchi S, Hook-associated proteins essential for flagellar filament formation in Salmonella typhimurium. *J. Bacteriol.* 157:100-108 (1984).

35. Homma M, Iino T, Locations of hook-associated proteins in flagellar structures of Salmonella typhimurium. *J. Bacteriol.* 162:183-189 (1985).

36. Lee SH, Galan JE, Salmonella Type III Secretion-associated chaperones confer secretion-pathway specificity. *Mol. Microbiol* 51:483-495 (2003).

37. Aldridge PD *et al.*, The flagellar-specific transcription factor, σ28, is the Type III Secretion chaperone for the flagellar-specific anti-σ28 factor FlgM. *Genes and Dev.* 20:2315-2326 (2006).

38. Sato Y, Takaya A, Mouslim C, Hughes KT, Yamamoto T, FliT selectively enhances proteolysis of FlhC subunit in $FlhD_4C_2$ complex by an ATP-dependent protease, ClpXP. *JBC* 289:33001-33011 (2014).

39. Aldridge P, Karlinsey J, Hughes KT, The Type III Secretion chaperone FlgN regulates flagellar assembly via a negative feedback loop containing its chaperone substrates FlgK and FlgL. *Mol. Microbiol.* 49:1333-1345 (2003).

40. Karlinsey JE, Lonner J, Brown KL, Hughes KT, Translation/secretion coupling by Type III Secretion systems. *Cell* 102:487-497 (2000).

41. Wada T *et al.*, EAL domain protein YdiV acts as an anti-FlhD4C2 factor responsible for nutritional control of the flagellar regulon in Salmonella enterica serovar Typhimurium. *J. Bacteriol.* 193:1600–1611 (2011).

42. Hirano T, Mizuno S, Aizawa SI, Hughes KT, Mutations in Flk, FlgG, FlhA, and FlhE That affect the flagellar Type III Secretion specificity switch in Salmonella enterica. *J. Bacteriol.* 191:3938-3949 (2009).

43. Samatey FA *et al*., Structure of the bacterial flagellar hook and implication for the molecular universal joint mechanism. *Nature* 431:1062-1068 (2004).

44. Stock JB, Rauch B, Roseman S, Periplasmic space in Salmonella typhimurium and Escherichia coli. *J. Biol. Chem*. 252:7850-7861 (1977).

45. Brokx SJ *et al.*, Genome-wide analysis of lipoprotein expression in Escherichia coli MG1655. *J. Bacteriol.* 186:3254-3258 (2004).

46. Beckwith J, Silhavy TJ, Genetic analysis of protein export in Escherichia coli. *Methods Enzymol.* 97:3-11 (1983).

47. Danese PN, Silhavy TJ, Targeting and assembly of periplasmic and outer-membrane proteins in Escherichia coli. *Annu. Rev. Genet.* 32:59-94 (1998).

48. Tokuda H, Matsuyama SI, Sorting of lipoproteins to the outer membrane in E. coli. *Biochim. Biophys. Acta* 1693:5-13 (2004).

49. Zuckert WR, Secretion of bacterial lipoproteins: through the cytoplasmic membrane, the periplasm and beyond. *Biochim. Biophys. Acta* 1843:1509-1516 (2014).

50. Braun V, Covalent lipoprotein from the outer membrane of Escherichia coli. *Biochim. Biophys. Acta* 415:335–377 (1975).

51. Magnet S *et al.*, Identification of the L,D-Transpeptidases responsible for attachment of the braun lipoprotein to Escherichia coli peptidoglycan. *J. Bacteriol.* 189:3927-3931 (2007).

52. Cowles CE, Li Y, Semmelhack MF, Cristea IM, Silhavy TJ, The free and bound forms of Lpp occupy distinct subcellular locations in Escherichia coli. *Mol. Microbiol* 79:1168-1181 (2011).

53. Konovalova A, Perlman DH, Cowles CE, Silhavy TJ, Transmembrane domain of surface-exposed outer membrane lipoprotein RcsF is threaded through the lumen of β-barrel proteins. *PNAS* 111:4350-4358 (2014).

54. Bernstein HD, The double life of a bacterial lipoprotein. *Mol. Microbiol* 79:1128-1131 (2011).

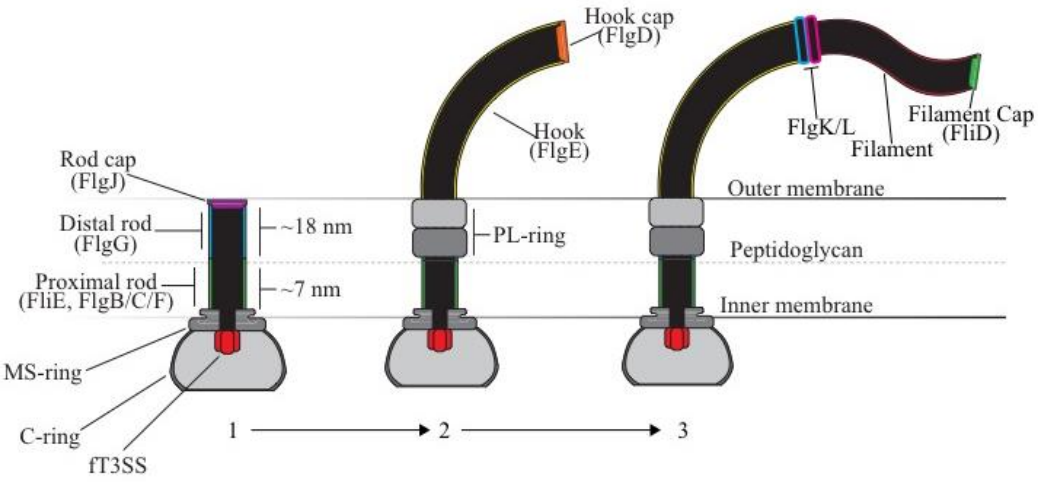

Fig. 1.1: The flagellum of *Salmonella enterica*
Assembly of the flagellum is sequential. The MS-ring is the first component of the flagellum to assemble and acts as a platform for assembly of the fT3SS, the C-ring and the rod. PL-ring formation around the distal rod dislodges the rod cap and forms a hole in the outer membrane for the growing structure to pass through. The hook is the first cell-external structure of the flagellum and grows to a mature length of ~55 nm. Following hook completion and the assembly of the hook-filament junction from FlgK and FlgL subunits, filament assembly commences. The filament grows to length up to ~10 μm and is composed of ~10,000 subunits of FliC and/or FljB.

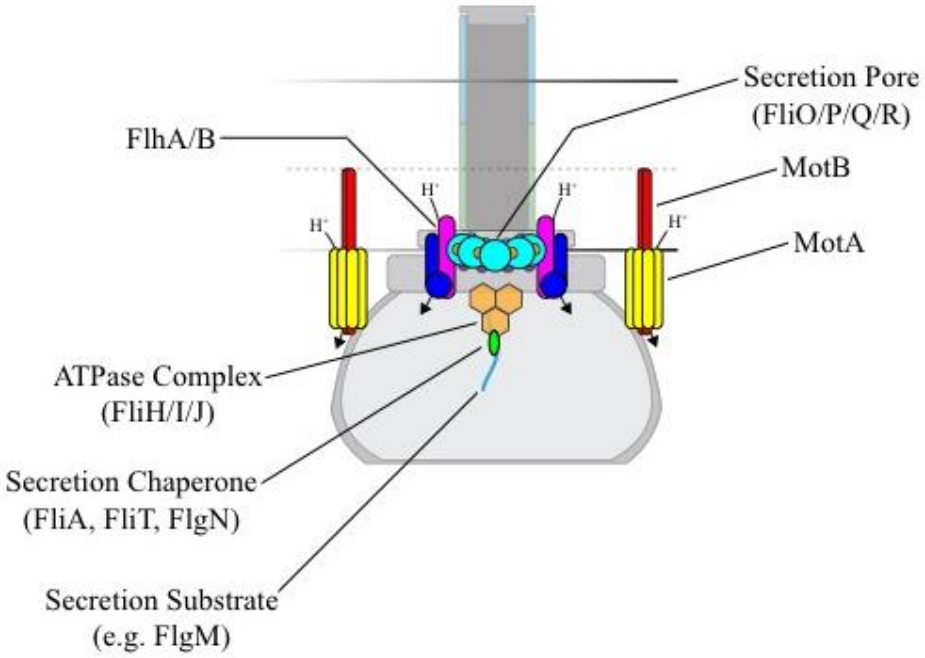

Fig. 1.2: The hook basal body (HBB) of *Salmonella enterica*
The HBB is an ion-powered rotary motor and secretion apparatus as well as the assembly scaffold for the flagellar axial components (i.e. the rod, hook and filament). The secretion pore, composed of FliO, FliP, FliQ and FliR, assembles within the MS-ring in the cytoplasmic membrane. Secreted flagellar substrates are secreted through the pore by FlhA and FlhB, which couple the energy of proton (H^+) diffusion across the cytoplasmic membrane to substrate secretion. The stators (MotA and MotB) generate torque at rotor-stator interfaces using H^+ diffusion across the inner membrane.

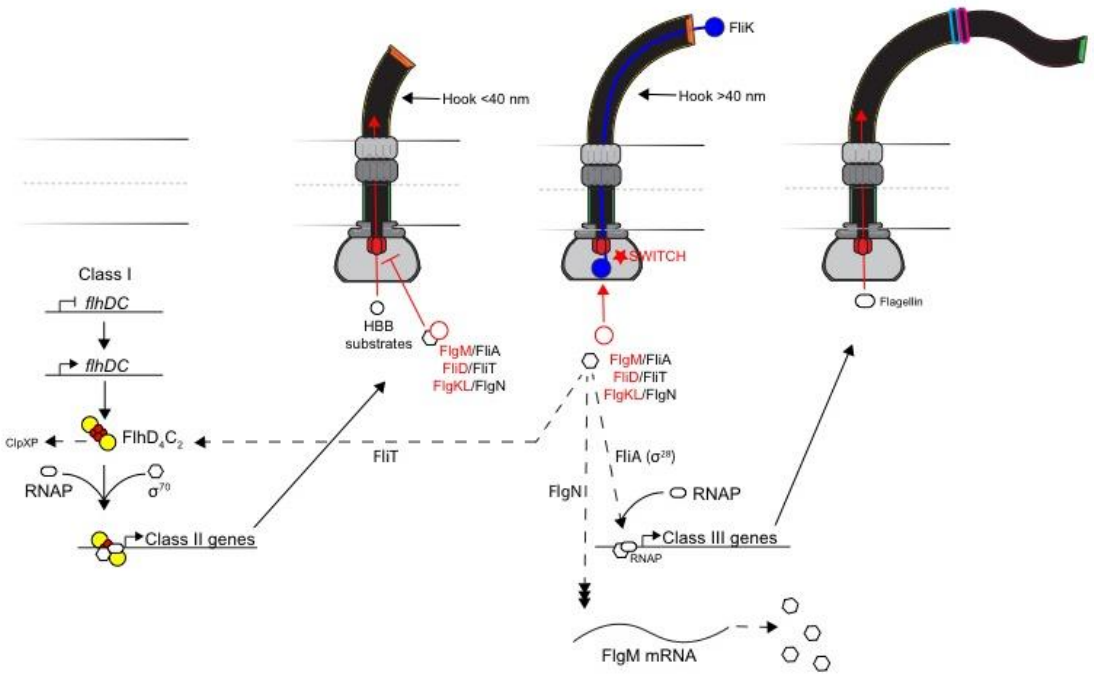

Fig. 1.3: Genetic regulation of flagellar morphogenesis
Expression of flagellar genes is hierarchical, the genes required to build early structures are expressed prior to those needed to construct later ones. *flhDC* is at the top of the hierarchy and is the master regulator of flagellar gene expression. Expression of *flhDC* in response to environmental signals produces the $FlhD_4C_2$ complex that directs σ^{70} and RNAP to class II promoters. Class II genes code for the HBB structural proteins as well as several class III secretion substrates (FlgM, FlgKL) and their secretion chaperones (FliA, FliT, FlgN). Prior to hook completion, class III substrates are not secreted. Once the secretion specificity switch is catalyzed by the interaction of $FliK_C$ with FlhB, class III substrates are secreted. Secretion of FlgM frees FliA σ^{28} to recruit RNAP to late gene (e.g. *fliC*) promoters.

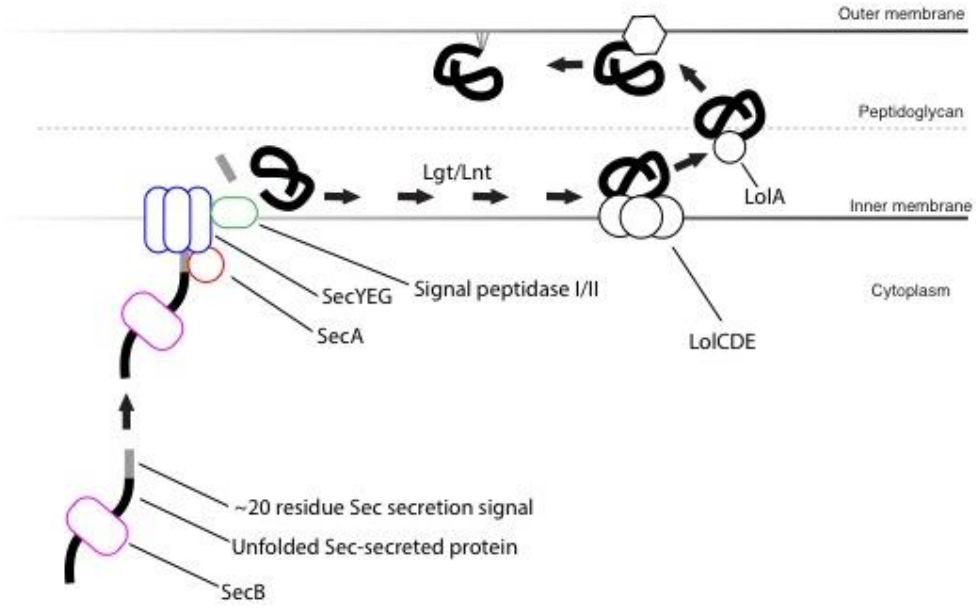

Fig. 1.4: Secretion of lipoproteins through the Sec type II secretion system
Sec secreted proteins are targeted to the cytoplasmic membrane-associated SecA/YEG apparatus via an N-terminal signal sequence. The signal sequence encompasses the first ~20 residues of the protein and is cleaved during translocation by one of two signal peptidases. Secreted proteins are bound in an unfolded state and delivered to the secretion apparatus by SecB if they are secreted post-translationally or by signal reconition particle (SRP, not shown) if they are secreted co-translationally. As lipoproteins are translocated to the periplasm they are lipoylated at an invariant N-terminal cysteine residue by Lnt and Lgt. For lipoproteins that localize to the outer membrane, the Lol shuttle system mediates the transfer from the inner to outer membrane.

CHAPTER 2

ROD-TO-HOOK TRANSITION FOR EXTRACELLULAR FLAGELLUM ASSEMBLY IS CATALYZED BY THE L-RING-DEPENDENT ROD SCAFFOLD REMOVAL

Eli J. Cohen and Kelly T. Hughes

Journal of Bacteriology
2014, Vol. 196(13): 2387-2395
doi:10.1128/JB.01580-14

JB Journals.ASM.org

Rod-to-Hook Transition for Extracellular Flagellum Assembly Is Catalyzed by the L-Ring-Dependent Rod Scaffold Removal

Eli J. Cohen, Kelly T. Hughes

Department of Biology, University of Utah, Salt Lake City, Utah, USA

In *Salmonella*, the rod substructure of the flagellum is a periplasmic driveshaft that couples the torque generated by the basal body motor to the extracellular hook and filament. The rod subunits self-assemble, spanning the periplasmic space and stopping at the outer membrane when a mature length of ~22 nm is reached. Assembly of the extracellular hook and filament follow rod completion. Hook initiation requires that a pore forms in the outer membrane and that the rod-capping protein, FlgJ, dislodges from the tip of the distal rod and is replaced with the hook-capping protein, FlgD. Approximately 26 FlgH subunits form the L-ring around the distal rod that creates the pore through which the growing flagellum will elongate from the cell body. The function of the L-ring in the mature flagellum is also thought to act as a bushing for the rotating rod. Work presented here demonstrates that, in addition to outer membrane pore formation, L-ring formation catalyzes the removal of the FlgJ rod cap. Rod cap removal allows the hook cap to assemble at the rod tip and results in the transition from rod completion in the periplasm to extracellular hook polymerization. By coupling the rod-to-hook switch to outer membrane penetration, FlgH ensures that hook and filament polymerization is initiated at the appropriate spatial and temporal point in flagellar biosynthesis.

The bacterial flagellum exemplifies nanoscale engineering that microbes have been perfecting over billions of years (1). This supramolecular structure is composed of approximately 25 distinct protein subunits and self-assembles to final lengths of up to 20 μm, several times the length of the cell itself (2). The flagellum enables a bacterium to colonize surfaces, search for food, and avoid noxious substances in its environment (3). To orchestrate the ordered assembly of a flagellum, flagellated species of bacteria have evolved numerous regulatory mechanisms. Flagellar biosynthesis is regulated at the genetic level by mechanisms that couple gene expression to assembly (4, 5) and at the biomechanical level with many flagellar proteins possessing inherent self-assembly characteristics (6–8).

Synthesis of the flagellum begins with the assembly of a basal body composed of several substructures (9). First to assemble is the MS-ring within the cytoplasmic membrane, followed by the cytoplasm-facing C-ring, which serves as both the rotor for the flagellar motor and as an affinity site for the secretion and assembly of other flagellar structures (10). The flagellum-specific type three secretion (T3S) system assembles in the inner membrane within the MS- and C-rings. The flagellar T3S system secretes flagellar subunits from the cytoplasm to be assembled at the tip of the growing flagellum (11, 12). The rod assembles through the periplasmic space to the outer membrane and transmits the torque generated by the basal body to the extracellular hook and filament (13).

The rod initially assembles into a proximal rod structure that lies between the MS-ring and the cell wall and is composed of FliE and approximately 6 subunits each of FlgB, FlgC, and FlgF (14). It is thought that FliE acts as an adaptor that joins the axial rod to the planar MS-ring, with FlgB, FlgC, and FlgF assembling atop one another until the cell wall is reached (15, 16). The distal rod structure is about the same length as the proximal rod (~11 nm) and is composed of approximately 26 FlgG subunits (14).

In order for rod assembly to proceed to the outer membrane, a hole must be made in the cell wall, a role fulfilled by FlgJ. FlgJ is a dual-domain protein composed of an N-terminal scaffolding domain required for polymerization of the distal rod and a C-terminal acetylmuramidase domain required for forming a hole in the cell wall (1). Once FlgJ has made a hole in the cell wall, about 26 subunits of the distal rod protein, FlgG, are secreted and assemble in two stacks underneath FlgJ, thereby spanning the remaining distance between the cell wall and the outer membrane (16, 17). What is not known is whether FlgJ assembles prior to proximal rod assembly or distal rod assembly. If FlgJ assembles prior to proximal rod assembly, then FlgJ would serve as a scaffold for 4 different proteins (FlgB, FlgC, FlgF, and FlgG). If the FlgJ cap assembles after proximal rod completion, then, similar to FlgD and FliD, which are scaffolds for FlgE (hook) and FliC (filament), respectively, FlgJ would serve as a scaffold for a single protein, FlgG.

After the distal rod has polymerized, a hole forms in the outer membrane for construction of the extracellular hook and filament to proceed from the cell surface. For this to happen, FlgA, FlgH, and FlgI are secreted via the Sec type II secretion system into the periplasm. FlgI forms the P-ring, whose assembly is facilitated by FlgA, and FlgH forms the L-ring (18–20). FlgI polymerizes around the distal rod in close proximity to the cell wall and directs assembly of the L-ring (17). Assembly of the L-ring forms a pore in the outer membrane required for hook polymerization to commence. In addition to forming a hole in the outer membrane, it has been suggested that the P- and L-rings function as bushings for the rod (21).

PL-ring completion and outer membrane pore formation is followed by hook polymerization. This requires that the FlgD rod scaffold replace the FlgJ scaffold in order for the hook (FlgE) to

Received 16 February 2014 **Accepted** 11 April 2014
Published ahead of print 18 April 2014
Address correspondence to Kelly T. Hughes, hughes@biology.utah.edu.

doi:10.1128/JB.01580-14

polymerize from the rod tip at the cell surface. Hook polymerization terminates by the action of a molecular ruler, FliK (22). FliK is secreted during hook polymerization, and when the hook reaches a minimal length of about 40 nm, the C terminus of FliK interacts with the FlhB component of the flagellar T3S system, resulting in a conformational change in FlhB (23, 24). FlhB specifies which substrates are secreted through the flagellar T3S system. Prior to FliK interaction, FlhB allows secretion of the rod-hook class of protein subunits. After hook completion and interaction with FliK, FlhB becomes specific for late, or filament class, substrate secretion. The hook-associated proteins (HAPs), FlgK, FlgL, and FliD, and the FlgM regulatory protein are secreted next. The assembly of the HAPs dislodges the hook scaffold FlgD. The filament then polymerizes beneath the FliD filament cap to lengths up to about 15 μm.

The enteric flagellum is composed of 11 protofilaments (9). Subunits that make up the axial structures, the rod hook filament, are added 5.5 subunits per turn of the helix. As a result, it takes two helical additions to add a full layer of subunits to the structure. Thus, the estimated 26 subunits of FlgG would include more than 4 helical additions. Based on mutations in the *flgG* gene that allow continuous polymerization of FlgG subunits, it was proposed that FlgG has an intrinsic stacking mechanism where subunits polymerize on each other and stop, which would result in addition of only 22 FlgG subunits (17). The mutations in *flgG* that allow continuous polymerization of FlgG subunits, called *flgG**, produce filamentous rod structures whose lengths are controlled by the FliK molecular ruler (25).

MATERIALS AND METHODS

Bacterial strains, plasmids, and media. Detailed information about bacterial strains and plasmids used in this study are listed in Table 1. Cells were cultured in lysogeny broth (LB). The following antibiotic supplements were added as needed: chloramphenicol (12.5 μg ml^{-1}), kanamycin (50 μg ml^{-1}), tetracycline (15 μg ml^{-1}), and anhydrotetracycline (ATc; 1 μg ml^{-1}). Gene expression from the arabinose promoter was induced by addition of 0.2% L-arabinose. The generalized transducing phage of *Salmonella enterica* serovar Typhimurium P22 *HT105/1 int-201* was used in all transductional crosses (26).

Isolation and measurement of HBBs. Hook basal body (HBB) isolation was carried out by the methods described previously (27), with minor modifications. Flagellar samples were not collected by CsCl gradient centrifugation but were pelleted at 60,000 × *g* for 1 h using a Beckman 50.2Ti rotor at 4°C. Hook lengths were measured using NIH ImageJ 1.42q software.

Electron microscopy. Purified HBB samples were negatively stained with 2% uranyl acetate on copper-coated grids. Images were captured using a Hitachi H-7100 electron microscope at an acceleration voltage of 125 kV.

SDS-PAGE sample preparation and immunoblotting. Overnight cultures were diluted 1:100 into defined media (E-salts plus 0.2% glucose) with LB added to a final concentration of 20%. LB was added in order to provide a small amount of carrier protein to aid in the precipitation of secreted proteins during sample preparation. Cultures were grown at 37°C with aeration. ATc, when used, was added to cultures to a final concentration of 0.7 μg ml^{-1}. Cells were harvested via centrifugation at 3,550 × *g* for 10 min in an Eppendorf 5430 benchtop centrifuge. Supernatants were then filtered through 0.45-μm cellulose acetate filters to remove any cells remaining after centrifugation. Supernatant protein was precipitated by the addition of 100% (wt/vol) trichloroacetic acid (Sigma) to a final concentration of 20 to 25% and precipitated on ice overnight. Following overnight precipitation, samples were spun at 14,000 rpm for 30 min in a Sorvall RC5-B centrifuge followed by two washes with −20°C acetone. Precipitated protein was resuspended in 30 to 40 μl 2× SDS sample buffer with 5% β-mercaptoethanol (βME) (recipe per Bio-Rad). Cell pellets were simply boiled in 2× SDS sample buffer with 5% βME. For SDS-PAGE, 10-well, 1-mm, 11% acrylamide gels were used. For supernatant samples, ~2,000 to 3,000 optical density (OD) equivalents were loaded in each lane of the gel. For cell pellets, ~100 to 200 OD equivalents were loaded. Protein was transferred to a 0.2-μm nitrocellulose membrane (Optitran BA-S 83 reinforced NC; GE Healthcare) by semidry transfer (Trans-Blot SD semidry transfer cell; Bio-Rad). After blocking in Tris-buffered saline (TBS) with 5% nonfat powdered milk for 30 min, blots were incubated with anti-HA monoclonal antibody from mouse ascites fluid (Covance), anti-DnaK mouse monoclonal antibody (Abcam), and/or anti-FlgE/anti-FlgM rabbit-derived antibody in TBST (TBS with 0.02% Tween 20) with 5% nonfat milk at 4°C with gentle agitation overnight.

Blots were then washed 3× with TBST and exposed to goat anti-mouse and/or anti-rabbit 2° antibodies (Dylight 800 and Li-Cor IRDye 680RD, respectively) in TBST with 10% milk for 1 h with agitation. After being washed of 2° antibodies, blots were imaged using a LI-COR Biosciences Odyssey infrared imaging system.

TABLE 1 List of strains used in this study

Strain	Genotype
TH9614	*flgG5664*(G53C)
TH10082	*flgG5677*(G53R)
TH10354	*flgG6705*(G65R)
TH12005	*flgG6755*(S64P)
TH12334	*flgG7327*(G53S)
TH20653	*flgG8192*(G53D)
TH13929	Δ*flgG7661*
TH13636	Δ*araBAD972*::*flgH*$^+$*I*$^+$*A*$^+$
TH20800	*flgG5664*(G53C) Δ*araBAD972*::*flgH*$^+$*I*$^+$*A*$^+$
TH20801	*flgG5677*(G53R) Δ*araBAD972*::*flgH*$^+$*I*$^+$*A*$^+$
TH20802	*flgG6705*(G65R) Δ*araBAD972*::*flgH*$^+$*I*$^+$*A*$^+$
TH20803	*flgG6755*(S64P) Δ*araBAD972*::*flgH*$^+$*I*$^+$*A*$^+$
TH20807	*flgG7327*(G53S) Δ*araBAD972*::*flgH*$^+$*I*$^+$*A*$^+$
TH20809	*flgG8192*(G53D) Δ*araBAD972*::*flgH*$^+$*I*$^+$*A*$^+$
TH20838	*flgG5677*(G53R) Δ*araBAD1008*::*flgE*$^+$
TH20839	*flgG5677*(G53R) Δ*araBAD925*::*tetRA*
TH12850	*flgG6705*(G65R) Δ*araBAD972*::*flgH*$^+$*I*$^+$*A*$^+$ Δ*fliK6137*::*tetRA*
TH20840	Δ*flgH7662* Δ*flgM5794*::FCF
TH20842	Δ*flgH7662* Δ*flgM5794*::FCF Δ*araBAD1008*::*flgE*$^+$
TH20843	Δ*flgH7662* Δ*araBAD925*::*tetRA*
TH20844	Δ*flgH7662* Δ*araBAD1008*::*flgE*$^+$
TH17693	*flgJ8013*::3×HA
TH17820	*flgJ8021*::3×HA Δ*flgHI1958* Δ*araBAD941*::*flgH*$^+$*I*$^+$ *fljB*^{enx} *vh2*
TH20753	*flgJ8021*::3×HA Δ*flgHI1958* Δ*araBAD941*::*flgH*$^+$*I*$^+$ $P_{flhDC8089}$::*tetR* P_{tetA} *fljB*^{enx} *vh2*
TH20757	*flgJ8021*::3×HA Δ*flgHI1958* Δ*flgD6543* Δ*araBAD941*::*flgH*$^+$*I*$^+$ $P_{flhDC8089}$::*tetR* P_{tetA} *fljB*^{enx} *vh2*
TH20765	*flgJ8013*::3×HA Δ*flgH7662* Δ*araBAD1001*::*flgH*$^+$ $P_{flhDC8089}$::*tetR* P_{tetA}
TH20769	*flgJ8013*::3×HA Δ*flgH7662* Δ*flgD6543* Δ*araBAD1001*::*flgH*$^+$ $P_{flhDC8089}$::*tetR* P_{tetA}

RESULTS

PL-ring gene overexpression suppresses motility defect in G53 filamentous rod mutants of distal rod gene *flgG*. The rod component of the HBB grows to 22 nm and stops (25). This places the rod tip perpendicular to the outer membrane. The P-ring polymerizes around the 2 helical stacks of FlgG distal rod subunits. This is followed by L-ring formation, outer membrane penetration, and hook polymerization from the cell surface (Fig. 1). Hook

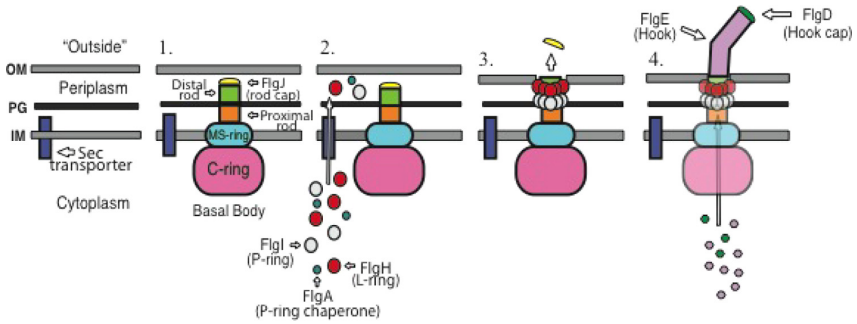

FIG 1 Model for the PL-ring-mediated switch from rod to hook polymerization during flagellar morphogenesis. The assembly of the flagellum is a hierarchical process. (Step 1) The first structures to assemble are the MS-ring in the inner membrane (IM) and the cytoplasmic C-ring. The inner membrane components of the flagellar T3S system are believed to assemble within the MS-ring, while the cytoplasmic components of the flagellar T3S system associate with the C-ring. The first secreted subunits to assemble are FliE, FlgB, FlgC, and FlgF, which form the proximal rod. FlgJ, the rod scaffold, associates with the rod at some point during this process in order to form a hole in the cell wall. FlgG polymerizes to form the distal rod on top of the proximal rod and underneath FlgJ. Distal rod assembly ceases once the rod has reached the outer membrane (OM), positioning the tip of the rod perpendicular to the outer membrane. PG, peptidoglycan. (Step 2) The subunits required for PL-ring formation, FlgA, FlgH, and FlgI, are secreted into the periplasm through the Sec secretion system. Once in the periplasm, FlgA assists FlgI in the assembly of the P-ring around the distal rod. FlgH forms the L-ring around the distal rod in close proximity to the P-ring. (Step 3) Formation of the L-ring around the distal rod by FlgH forms a pore in the outer membrane and also causes the rod scaffold, FlgJ, to dissociate from the tip of the distal rod into the extracellular environment. (Step 4) Once the rod cap has been dislodged from the rod, FlgD is able to form the hook scaffold and direct assembly of the hook by FlgE.

polymerization continues until the molecular tape measure, FliK, is secreted through a hook with a minimal length of 40 nm. FliK then catalyzes a conformational change in the FlhB component of the flagellar T3S system that results in the secretion specificity switch from rod-hook secretion substrates to late, or filament-type, secretion substrates. Filamentous rod mutants in FlgG (*flgG**) do not stop polymerizing at the outer membrane but do stop polymerizing when FliK catalyzes the secretion specificity switch after the rod has reached 40 nm or longer.

Rod completion and PL-ring formation are uncoupled processes. The proteins required for PL-ring formation, FlgA, FlgH, and FlgI, are secreted into the periplasm through the Sec type II secretion system. FlgA facilitates polymerization of the FlgI P-ring structural subunits around the distal rod. Formation of the P-ring is followed by assembly of the L-ring by FlgH directly adjacent to the P-ring.

We wondered if overexpression of the PL-ring components suppresses the *flgG** motility defect. It was thought that by increasing the pool of PL-ring components available in the periplasm, the PL-ring might be able to form while the rod was still perpendicular to the outer membrane and allow the flagellar structure to penetrate the outer membrane and grow beyond the cell surface. All 25 *flgG** mutants isolated to date were tested for the ability of PL-ring gene overexpression to suppress the *flgG** motility defect. Only one allele, the G53R substitution, showed a high degree of suppression when the *flgA*, *flgH*, and *flgI* genes were overexpressed (Fig. 2). Three other single-amino-acid substitution mutants, G53D, G53S, and S64P, also showed suppression at a low but reproducible level (Fig. 2). We presumed that these FlgG alleles polymerized slowly enough to allow PL-rings to form at short rod lengths, thereby allowing motility.

We then tested if PL-ring genes could form on an *flgG** polyrod mutant if we did not demand suppression of the motility defect using an *fliK* null mutant background. In the absence of FliK, FlgG polymerization continues, resulting in polyrod structures that measured up to a micron in length (17). When the *flgG** G65R mutant was grown under the PL-ring overexpression conditions, the strain remained defective in motility. The polyrod structures of the *flgG** (G65R) *fliK* double mutant grown under PL-ring gene overexpression were isolated and examined by electron microscopy to see if PL-rings could form on polyrods (Fig. 3). In this background, the filamentous rod was accompanied by many P-rings along the length of the distal rod, and some single L-rings had assembled around the rod in very close proximity to the most distal P-ring. When this occurred, rod formation ceased and hook polymerization commenced at the PL-ring junction. This suggested that FlgI will form P-rings around FlgG indefinitely so long as there is a sufficient length of rod to form a P-ring around. However, formation of the L-ring only occurs at the tip of the rod in very close proximity to the P-ring. Therefore, when the rod of an *flgG** mutant continues to polymerize after the addition of a P-ring, a gap between the P-ring and the rod tip is formed before

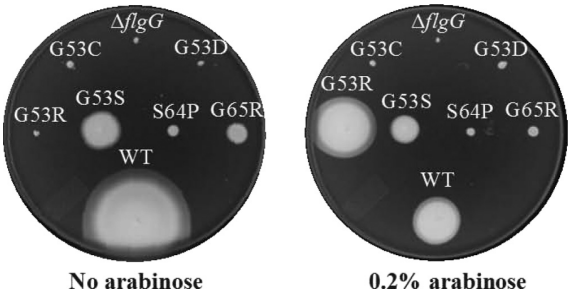

FIG 2 Overexpression of *flgA*, *flgH*, and *flgI* suppresses the motility defect of the *flgG** G53R filamentous rod mutant. The genes required for PL-ring formation (*flgA*, *flgH*, and *flgI*) were cloned into the arabinose-inducible Δ*araBAD* locus in every filamentous rod mutant isolated to date. The chromosomal copies of *flgA*, *flgH*, and *flgI* were left intact in the *flg* operon. The motility defect of the G53R mutant was suppressed to nearly WT levels when inoculated in soft agar with 0.2% arabinose added. WT, DaraBAD::flgAHI.

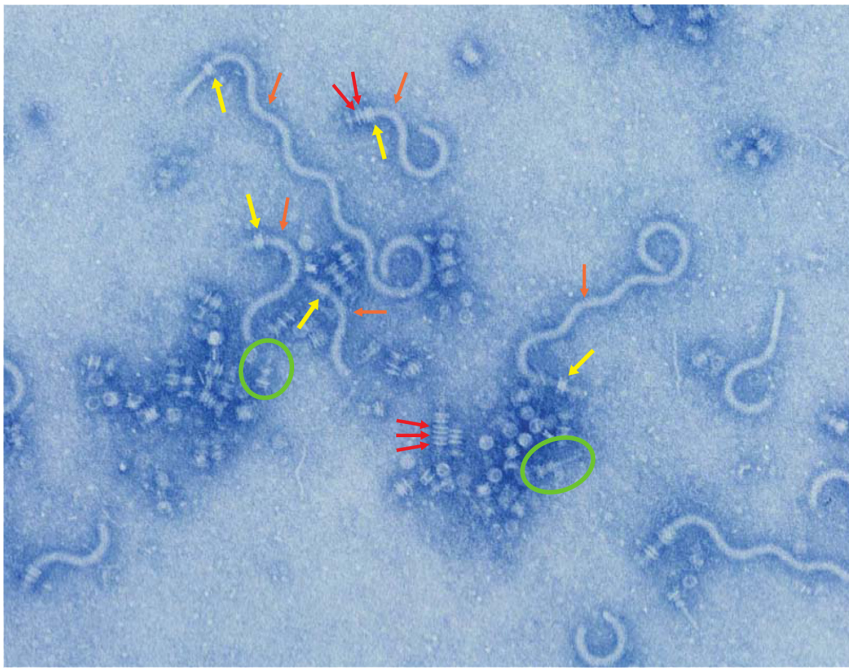

FIG 3 PL-ring assembly triggers a switch from rod polymerization to hook polymerization in the *flgG**(G65R) Δ*fliK* Δ*araBAD*::*flgH*$^+$*I*$^+$*A*$^+$ background. The *flgG** G65R mutant produces distal rods that fail to stop polymerizing at the WT length of ~12 nm, forming aberrantly long rod structures termed filamentous rods. When the intact genes required for PL-ring assembly (*flgH*$^+$, *flgI*$^+$, and *flgA*$^+$) are overexpressed in this background, rods of a variety of lengths are produced. Many P-rings (red arrows) are able to form along the length of the distal rod in this background. When a PL-ring (yellow arrows) forms, the switch from rod to hook polymerization occurs. Deletion of the hook length gene *fliK* results in hooks (orange arrows) that are hundreds of nanometers long, known as polyhooks. Two injectisome structures are circled in green. The injectisome shares many common structural features with the flagellum and possesses its own T3S system needed for the construction of the injectisome as well as to translocate effector proteins into host cells in order to establish infection.

FlgH can associate with both the rod tip and the P-ring, thereby preventing formation of the L-ring by FlgH.

We tested the hypothesis that the abrupt switch from rod assembly to hook assembly in the G65R *fliK* null background upon formation of the PL-ring was a result of PL-ring-dependent removal of FlgJ. As discussed above, FlgJ performs two roles in the construction of the flagellum: penetration of the cell wall and acting as a scaffold for FlgG (distal rod) subunit polymerization. The FlgD hook cap remains associated with a completed hook until it is dislodged by FlgK polymerization. In a similar manner, we wondered if FlgJ remains associated with the tip of the rod following rod completion, awaiting the addition of L-ring subunits to dislodge it. In doing so, FlgJ could act as a cap to prevent assembly of the hook scaffold, FlgD, prior to outer membrane penetration.

Loss of FlgM or FlgE overexpression partially restores the motility defect of an *flgH* deletion allele. In the original characterization of *flgG** alleles, about 25% of the polyrod structures that form in the absence of both FliK and the PL-rings had attached polyhooks (17). This suggested that PL-rings were not absolutely required for the removal of FlgJ and the transition from rod to hook polymerization. This is consistent with an earlier study showing that overexpression of FlgE (hook) from a high-copy-number plasmid vector partially suppresses the nonmotile phenotype of a mutant lacking L-rings (28). This suggests that the interaction of FlgJ at the rod tip is weak enough that continuous passage of FlgE subunits eventually dislodges FlgJ, but L-ring formation is required for efficient removal of FlgJ. In the case of an L-ring-defective strain (Δ*flgH*), we expect there will be 6 to 8 basal body structures per cell. If *flgE* overexpression dislodged FlgJ from only a single structure, the suppression of the motility might be hindered by the accumulation of FlgM, since it would be secreted by a single basal structure and may still accumulate to an extent that σ^{28}-dependent transcription of late flagellar genes, including the flagellin gene *fliC* (or *fljB*) and chemosensory genes, is limited by excess cellular FlgM. We tested whether loss of the rod cap in the absence of the L-ring occurred at a high enough frequency with normal rod structures (*flgG*$^+$) such that removal of FlgM alone could suppress the motility defect in a Δ*flgH* strain.

When a Δ*flgH* mutant is inoculated in soft agar and allowed to incubate for a day or two, some motility is observed for a fraction of the cells, giving the colony a speckled phenotype with small satellite colonies forming around the original, nonmotile cells (Fig. 4A). This indicates that in the absence of L-rings, some cells occasionally are able to form at least one functional flagellum. When this same protocol was followed for a strain deleted for both *flgH* and *flgM*, the colony still has a speckled phenotype, but the motility diameter of the colony was about twice that of the Δ*flgH* mutant (Fig. 4A). This indicated that the full σ^{28}-dependent transcription in a Δ*flgH* background increased the likelihood of L-ring-independent flagellar formation. When *flgE* was overexpressed from the arabinose locus in the Δ*flgH* Δ*flgM* double mutant, the diameter of the colony on soft agar was slightly larger

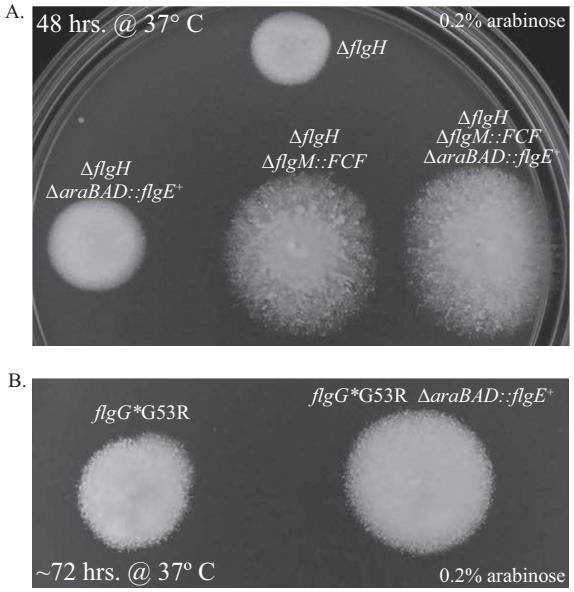

FIG 4 Nonmotile phenotype of mutants defective in PL-ring assembly can be partially suppressed by knocking out the anti-sigma factor *flgM* and/or overexpressing the hook protein, FlgE. Mutants that are unable to form PL-rings are largely nonmotile. The speckled phenotype of these mutants on soft agar indicates that the switch from rod to hook polymerization can occur without the PL-ring but at only a fraction of WT levels. (A) The motility defect of a mutant lacking L-rings (Δ*flgH*) is partially suppressed by overexpressing FlgE and/or knocking out *flgM*. (B) The phenotype of the *flgG** G53R mutant in soft agar is similar to that of the Δ*flgH* mutant. By overexpressing the subunits required for PL-ring assembly, motility was restored to a large degree (Fig. 3), suggesting that this mutant is defective in PL-ring assembly. Similar to a Δ*flgH* mutant, the motility defect of the G53R mutant can be partially suppressed by overexpressing the hook protein, FlgE.

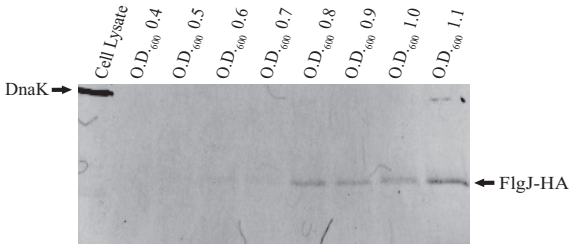

FIG 5 FlgJ is secreted extracellularly. Fifteen ml of culture from TH17693 (*flgJ8013*::HA) was collected at each OD_{600} unit from 0.4 to 1.1. Cells were removed, and the supernatant protein was concentrated and analyzed by SDS-PAGE using anti-HA antibody. Anti-DnaK antibody was added as a cell lysis control.

still (Fig. 4A). This demonstrates that some transition from rod to hook polymerization and outer membrane penetration by the flagellar structure will occur in the absence of the L-ring; however, the L-ring is required for this process to occur with close to 100% efficiency.

As discussed in the previous section, we managed to isolate a single, nonmotile *flgG** mutant (G53R) whose motility defect was suppressed by overexpression of PL-ring genes. We reasoned that the nonmotile phenotype of this mutant was due to a poor affinity of FlgH or FlgI for $FlgG^{G53R}$ that resulted in a ring-less rod. If this were the case, it was expected that the motility defect would be partially suppressed by overexpressing *flgE*, as is the case in a Δ*flgH* background. When *flgE* was overexpressed in the $flgG^{G53R}$ background, the diameter of the colonies inoculated in motility plates was about twice that observed for the $flgG^{G53R}$ strain with normal *flgE* expression (Fig. 4B).

FlgJ accumulates in the culture supernatant. The results described above demonstrate that PL-ring formation on the tip of the distal rod results in a transition from rod to hook polymerization. One mechanism that would account for this observation is that L-ring formation dislodges the rod scaffold, which is made up of FlgJ protein subunits. Removal of the FlgJ rod scaffold might be required to allow the hook scaffold, which is composed of FlgD subunits, to form on the rod tip and the transition to hook polymerization. We tested the hypothesis that PL-ring formation was coupled to release of FlgJ from the rod. Previous work suggested that FlgJ dissociates or dislodges from the rod and, under overexpression conditions, is accumulated in the periplasmic space (29). The filament cap protein, FliD, forms a pentamer that associates with the filament tip and acts as a scaffold for filament polymerization (7). Wild-type (WT) cells possess about six flagella; therefore, they only require that ~30 FliD subunits be translocated from the cytoplasm to the filament tips. FlgJ has also been postulated to form a cap composed of only a few subunits (30). If this were the case, one would expect that the amount of FlgJ dislodged into the supernatant would be small. As such, a sensitive method to assay for the presence of extracellular FlgJ was needed. To that end, the influenza virus-derived hemagglutinin (HA) tag was inserted into the chromosomal *flgJ* gene in the linker region between the N- and C-terminal domains believed to be unstructured (31). The resulting FlgJ-3×HA chimera (TH17693) exhibited wild-type motility and allowed for sensitive and unambiguous identification of FlgJ, expressed from its native, chromosomal locus, by standard Western blot analysis.

An overnight culture of TH17693 was diluted 1:100 into 100 ml of liquid media and grown to an OD at 600 nm (OD_{600}) of 0.1, at which point 15 ml of culture was placed on ice. This was repeated at each 0.1 OD_{600} unit up to an OD_{600} of 1.1. Cells were removed by centrifugation and filtration, and the secreted protein was concentrated and subjected to Western blot analysis probing for HA. Contrary to previous findings where FlgJ produced by a plasmid overexpression system accumulated in the periplasm, we observed that chromosomally expressed FlgJ was present in the secreted extracellular fraction. The presence of extracellular FlgJ was detected at an OD of ~0.6 (Fig. 5). Previous investigations may have failed to detect FlgJ in the supernatant due to insufficient culture volumes. Even with ≥15-ml cultures, detection of FlgJ-3×HA was difficult.

FlgH is responsible for the accumulation of FlgJ in the supernatant. FlgH forms a pore in the outer membrane; therefore, it was assumed to be required for FlgJ (or any other secreted flagellar protein) to accumulate in the supernatant. We hypothesized that FlgH was responsible for the accumulation of extracellular FlgJ by destabilizing or dislodging FlgJ from the rod. To test this model, a series of strains was constructed with either the L-ring structural gene *flgH* or both *flgH* and the P-ring structural gene *flgI* deleted from their chromosomal location in the *flg* operon and placed under the control of the arabinose-inducible *araBAD* promoter

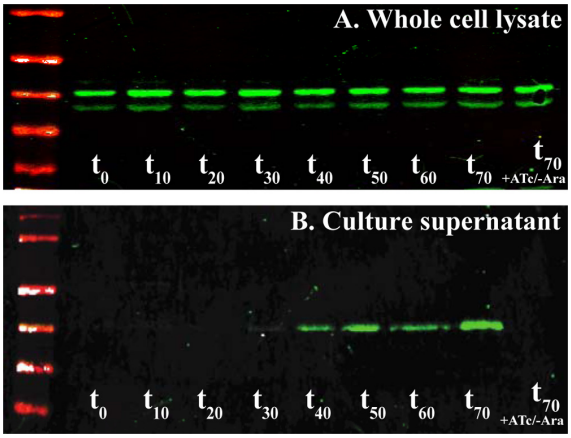

FIG 6 Secretion of FlgJ into the supernatant is dependent on PL-ring formation. Liquid culture of TH20753 (*flgJ8021*::3×HA Δ*flgHI1958* Δ*araBAD941*::*flgH*$^{+}$*I*$^{+}$ P$_{flhDC8089}$::*tetR* P$_{tetA}$ *fljB*^{enx} *vh2*) was grown to an OD$_{600}$ of ~0.3, at which point anhydrotetracycline (ATc) was added to induce *flhDC* expression and basal body assembly. After 10 min of incubation with ATc, arabinose (Ara) was added to the culture to induce expression of *flgH*$^{+}$. Samples were collected at 10-min intervals. Translation was arrested by the addition of spectinomycin, and the cells were placed on ice. Pellet and supernatant samples from each time point were subjected to Western blot analysis with probing for FlgJ-HA with anti-HA antibody. Time point zero (t$_0$) represents samples taken after 10 min of incubation with ATc immediately prior to addition of Ara to the culture. (A) Levels of FlgJ-HA in the whole-cell lysates remained constant for the duration of the experiment. The upper band is full-length FlgJ-HA, and the lower band is presumed to be partially degraded FlgJ-HA. (B) In the supernatant samples, FlgJ-3×HA began to accumulate at ~30 min after the addition of arabinose and continued to accumulate throughout the remainder of the experiment. In the supernatant, FlgJ-HA is present in the full-length form only. The supernatant of the sample that received ATc and saline (t_{70} + ATc/−Ara) had no detectable FlgJ-HA.

(P$_{araBAD}$). The flagellar master regulon, *flhDC*, was also placed under the control of the *tetA* promoter (P$_{tetA}$), which is induced by addition of either tetracycline (Tc) or its nonantibiotic analog, anhydrotetracycline (ATc), to the growth medium. This inducible promoter allows for the controlled time of induction of the flagellar regulon and subsequent flagellum assembly. This was accomplished by replacing the *flhDC* promoter region with P$_{tetA}$ and an adjacent *tetR* repressor gene, resulting in the ΔP$_{flhDC8089}$::*tetR* P$_{tetA}$ allele. Thus, flagellar gene expression and flagellum assembly could be synchronized with the addition of ATc.

Overnight cultures were diluted into liquid media and grown to early- to mid-log phase (OD$_{600}$ of ~0.3). At this point, ATc was added to induce *flhDC* expression and subsequent flagellar basal body-rod construction. At 10 min post-*flhDC* induction, either arabinose or saline was added to the cultures. Ten-ml aliquots of each culture were taken every 10 min for 1 h following arabinose induction. mRNA translation was arrested with the addition of spectinomycin, and the cells were placed on ice. As before, cells were removed by centrifugation followed by filtration, and the supernatant samples were prepared for Western blot analysis. It was found that FlgJ-HA was detected in the supernatant ~30 to 40 min after *flhDC* induction with the subsequent addition of arabinose and continued to accumulate throughout the remainder of the experiment (Fig. 6B). Cultures that received ATc without the subsequent addition of arabinose expressed FlgJ, but this was only found in the cellular fraction. Without arabinose induction, we were unable to detect any FlgJ in the supernatant, even at 70 min post-ATc induction. The intensity of the FlgJ-HA band in the cellular fraction remained stable over the course of the experiment, in contrast to the supernatant bands, which increase from one time point to the next. Furthermore, the HA signal detected in the cellular fractions appeared not as a single band, as in the supernatant samples, but as two bands ~5 kDa apart and of about the same intensity (Fig. 6A). This indicates that either cytoplasmic or periplasmic FlgJ was subject to degradation.

If FlgH pore formation dislodged the rod cap, FlgJ should appear in the supernatant before or at the same time as other secreted flagellar proteins. To determine if this was the case, the same protocol as that used before was followed but with assaying for FlgE (hook) and FlgM in addition to FlgJ-HA by Western blotting. FlgE polymerizes on top of FlgG and is the first extracellular component of flagellum assembly. FlgM is an anti-sigma factor that binds σ^{28} in the cytoplasm, thereby preventing expression of flagellum class 3 promoters of genes required after HBB completion, such as filament and chemosensory-associated genes. Once hook synthesis has completed, the export apparatus of the basal body undergoes a secretion specificity switch from rod-hook substrate specificity to late-type substrate specificity including FlgM. If it is true that FlgH displaces FlgJ during L-ring formation and outer membrane penetration, FlgJ, FlgE, and FlgM would also be expected to accumulate in the supernatant around the same time following induction with ATc and arabinose. Moreover, neither FlgE nor FlgM should be found in the secreted fraction prior to FlgJ. After performing another time course experiment assaying for all three proteins, it was found that they are all detected in the supernatant at the same point in time, about 30 to 40 min after ATc and arabinose induction. In the absence of arabinose in the culture, no amount of FlgJ-HA, FlgE, or FlgM was detected (Fig. 7A).

The preceding lines of evidence demonstrate that FlgJ accumulates in the supernatant, and that the presence of FlgJ in the spent growth medium is dependent on L-ring formation. However, the possibility that FlgH forms a pore in the outer membrane but that FlgJ is dislodged from the rod by a different mechanism could not be ruled out (i.e., pore formation and the switch from rod to hook are simultaneous but mechanically independent events). If this were the case, the likely agent responsible for dislodging FlgJ was expected to be FlgD, the hook-capping protein, which assembles immediately after L-ring formation. FlgD forms a cap on top of the distal rod and acts as a scaffold for hook polymerization by FlgE. In the absence of FlgD, FlgE is secreted but unable to polymerize. Therefore, FlgD must be the subunit that polymerizes once FlgJ is dislodged in order for construction of the hook and filament to proceed. To determine if FlgD, and not FlgH, was responsible for dislodging FlgJ, the strain used in the preceding experiments (TH20753) was deleted for *flgD*. If FlgD was responsible for dislodging FlgJ, one would expect that FlgJ (and FlgE and FlgM) would be absent from culture supernatant after performing the protocol described above. When this experiment was performed, the resulting Western blot was almost indistinguishable from the previous blots. The absence of FlgD did not affect detection of FlgJ and FlgE in the supernatant, and the absence of FlgD did not affect the point in time following ATc and arabinose induction at which FlgJ and FlgE were detected (Fig. 7B).

FlgJ remains stably associated with the rod in the absence of FlgH. It was still possible that the FlgJ detected in culture super-

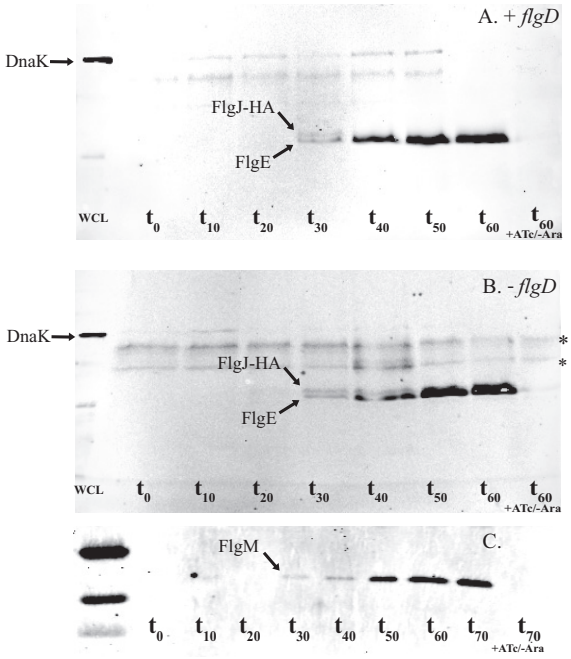

FIG 7 Outer membrane penetration and the secretion of flagellar subunits is dependent on FlgH and independent of the hook-capping protein, FlgD. The protocol described in the legend to Fig. 6 was followed, this time probing for FlgJ-HA, FlgE, and DnaK (as a cell lysis control). (A) FlgE and FlgJ-HA appear in the supernatant at the same time point (~30 min after addition of arabinose). (B) Western blot of TH20757 (*flgJ8021*::3×HA Δ*flgHI958* Δ*flgD6543* Δ*araBAD941*::*flgH*$^{+}$*I*$^{+}$ $P_{flhDC8089}$::*tetR* P_{tetA} *fljB*^{enx} *vh2*) probing for FlgE, FlgJ-HA, and DnaK. Knocking out *flgD* does not affect the secretion of FlgJ-HA or FlgE into the culture supernatant. (C) FlgM appeared in the supernatant at the same time as FlgE and FlgJ-HA following addition of arabinose to TH20753 (*flgJ8021*::3×HA Δ*flgHI958* Δ*araBAD941*::*flgH*$^{+}$*I*$^{+}$ $P_{flhDC8089}$::*tetR* P_{tetA} *fljB*^{enx} *vh2*). WCL, whole-cell lysate. t_0, sample taken ~10 min post-ATc induction, immediately before addition of arabinose. t_{60} + Atc/−Ara, control samples induced with anhydrotetracycline but not arabinose. *, nonspecific band.

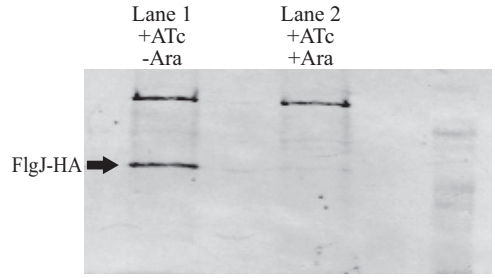

FIG 8 Rod scaffold protein FlgJ remains stably associated with the basal body until it is dislodged by FlgH. Two 500-ml aliquots of TH20769 (*flgJ8013*::3×HA Δ*flgH7662* Δ*flgD6543* Δ*araBAD1001*::*flgH*$^{+}$ $P_{flhDC8089}$::*tetR* P_{tetA}) were grown to mid-log phase and induced to construct basal bodies by adding anhydrotetracycline (ATc). After 10 min, one culture received arabinose (Ara) to induce expression of the L-ring protein, FlgH. The other culture received saline. Following an additional 25 min of incubation, mRNA translation was blocked in both cultures by the addition of spectinomycin. Basal bodies from both cultures were purified and subjected to SDS-PAGE. Western blot analysis probing for FlgJ-HA revealed that without L-ring formation, FlgJ-HA remained associated with the basal body (lane 1). The culture, which was induced to express FlgH, had only a trace amount of FlgJ-HA associated with purified basal bodies (lane 2).

natants in the preceding experiments was just cytoplasmic FlgJ secreted into the supernatant following outer membrane penetration by FlgH. In other words, the results did not prove that FlgJ forms a structure that caps the distal rod and awaits displacement by the L-ring. The possibility that the distal rod had no cap and premature FlgD/FlgE assembly was prevented via a different mechanism seemed implausible, but it was a possibility that could be ruled out.

To determine if FlgJ formed a stably associated rod cap, basal bodies before and after formation of the L-ring were purified. Two 500-ml cultures of strain TH20769 (Δ*flgH* Δ*araBAD*::*flgH*^{WT} $P_{flhDC8089}$::*tetR* P_{tetA} *flgJ-HA* Δ*flgD*) were grown to an OD_{600} of ~0.5 and induced with ATc. After ~10 min, one culture was induced with arabinose and the other with saline. The cultures were incubated an additional 25 min, arrested with spectinomycin, and allowed to incubate for five more minutes before being placed on ice. Cells from both cultures were pelleted and gently lysed. Basal bodies from both cultures were concentrated via ultracentrifugation, denatured with SDS sample loading buffer, and analyzed by Western blotting.

Samples induced with only ATc (+*flhDC*) had a prominent FlgJ band, whereas those induced with both ATc and arabinose (+*flhDC*, +*flgH*) had only a very faint FlgJ band (Fig. 8). The presence of FlgJ following the lengthy basal body purification indicates that in the absence of the L-ring, FlgJ forms a stable rod-associated structure.

DISCUSSION

The flagellar basal body of *S.* Typhimurium is composed of 22 different structural proteins followed by the hook, filament, and 3 hook-associated proteins (HAPs). The rod cap, hook cap, and hook length control protein FliK are transiently associated during HBB assembly. The periplasmic chaperone FlgA is required for assembly of the P-ring, and secretion chaperones FlgN (for FlgK and FlgL), FliT (for FliD), and FliS (for FliC/FljB) are required for efficient secretion of late secretion substrates. The FliK, FlgM, and σ^{28} proteins are required for the transition to the assembly of HAPs and filament and expression of chemosensory genes. Finally, motor force generators MotA and MotB are required as stators to drive flagellum rotation using the energy of the proton motive force. Thus, 38 different proteins are known to be required for the assembly of a functional flagellum. A remarkable feature of this structure is the requirement that subunits self-assemble onto the growing structure (32).

The process of self-assembly requires that some proteins are transiently associated with the structure at specific stages of the assembly process. The first structural subunit that is transiently associated is the rod scaffold protein FlgJ. FlgJ is thought to assemble prior to proximal rod formation, because severely truncated *flgJ* mutants produced MS-rings without rods (10). After rod completion, the FlgJ cap on the distal rod must be removed before the hook scaffold, FlgD, can assemble to allow hook subunits to polymerize onto the completed distal rod. The rod grows to a length of ~22 nm, which places the terminal end of the rod at the outer membrane. Mutants in the distal rod gene *flgG*, called *flgG** alleles, were described that resulted in rod lengths of ~50 nm.

Filaments that grow on these extended rod structures grow in the periplasm rather than outside the cell (17). The PL-ring structure was required for the transition from rod assembly to filament assembly for the formation of periplasmic flagella, but the hook was not required (25). Deletion of the hook gene did not prevent the growth of periplasmic flagella in the *flgG** mutant strains. This led to a model in which the wild-type distal rod subunit FlgG polymerizes on top of another assembled FlgG subunit only once (17). An interaction between stacked FlgG subunits prevents further polymerization of FlgG subunits and would terminate rod growth at ~22 nm. The *flgG** alleles are defective in this FlgG stacking interaction that prevents further FlgG polymerization. Termination of rod growth at ~22 nm would place the rod tip at the outer membrane. The PL-ring assembles around the distal rod and forms a pore in the outer membrane so that polymerization of the hook is external from the cell surface.

This checkpoint in flagellum assembly that couples (i) rod growth termination with (ii) PL-ring outer membrane pore assembly and (iii) the initiation of hook assembly predicts that a component of this checkpoint is associated with removal of the FlgJ rod scaffold to be replaced by the FlgD hook scaffold. The N-terminal 152 amino acids of FlgJ are required for rod polymerization, while the remaining C-terminal 164 amino acids include the muramidase domain required for rod penetration of the cell wall (30). FlgJ also has a heptad repeat (HR) domain of hydrophobic residues near its C terminus. Deletion of the FlgJ HR domain produced basal structures with P-rings but lacking the L-ring. This suggested that FlgJ does not dissociate from completed rods, but its presence at the rod tip is required for L-ring formation. Furthermore, FlgD, which is present in the secreted fraction in wild-type strains, is absent from the secreted fraction for *flgJ* mutants defective in L-ring assembly. This further supports the model in which the L-ring forms a pore for flagellar growth outside the cell.

The two remaining mechanisms for FlgJ scaffold removal we considered were that L-ring assembly displaced FlgJ or that the FlgD hook scaffold could dislodge FlgJ and assemble in its place. Because FlgD is continuously secreted into the periplasm prior to rod and PL-ring completion, the most plausible mechanism was that L-ring formation resulted in FlgJ removal from the rod tip.

The *flgG** mutant strains missing hook-length control protein FliK have a polyrod phenotype, where rod polymerization is uncontrolled and rods as long as 1 μm have been observed (17). When the PL-ring formation genes *flgA*, *flgH*, and *flgI* were overexpressed in an *flgG** *fliK* mutant background, we observed that PL-rings formed on polyrod structures and that their formation resulted in the transition from polyrod to polyhook formation. This supported the hypothesis that L-ring formation was responsible for FlgJ removal from the rod tip. Thus, we set up experiments to explore the possibility of FlgJ removal by L-ring formation.

It was previously reported that FlgJ was not secreted from the cell and was found only in the periplasmic fraction (29). We were concerned, because this result was obtained in strains that highly overexpressed FlgJ from a plasmid expression system. We suspected that, like the filament cap FliD, there were only 5 subunits of FlgJ per basal body, making it difficult to detect such a small amount of protein that might be released into the spent growth medium upon L-ring formation. We constructed an HA-tagged version of the chromosomal *flgJ* gene, placing the HA between the N-terminal scaffold domain and C-terminal muramidase domain of FlgJ. The resulting FlgJ-HA construct had wild-type motility, indicating that FlgJ-HA could form a perfectly functional rod cap and the HA tag would facilitate detection using anti-HA antibodies. Using this chromosomal FlgJ-HA construct, we could detect FlgJ in the secreted cell fraction. This suggested that L-ring pore formation in the outer membrane released FlgJ into the culture supernatant and not into the periplasm. By placing the L-ring structural gene (*flgH*) expression under the control of an arabinose-inducible promoter, we further showed that extracellular FlgJ required *flgH* expression. Furthermore, the presence of hook (FlgE) and FlgM in the secreted fraction does not occur before the appearance of secreted FlgJ. Finally, FlgJ was stably associated with basal structures lacking the L-ring, further supporting a model in which L-ring formation is coupled to the removal of FlgJ from the rod tip.

ACKNOWLEDGMENTS

We thank Shin-Ichi Aizawa for performing the electron microscopy presented in this work.

This work was supported by grant GM056141 from the National Institutes of Health to K.T.H.

We have no conflicts of interest to declare.

REFERENCES

1. **Erhardt M, Namba K, Hughes KT.** 2010. Bacterial nanomachines: the flagellum and type III injectisome. Cold Spring Harb. Perspect. Biol. **2:**a000299. http://dx.doi.org/10.1101/cshperspect.a000299.
2. **Chevance FF, Hughes KT.** 2008. Coordinating assembly of a bacterial macromolecular machine. Nat. Rev. Microbiol. **6:**455–465. http://dx.doi.org/10.1038/nrmicro1887.
3. **Kearns DB.** 2010. A field guide to bacterial swarming motility. Nat. Rev. Microbiol. **8:**634–644. http://dx.doi.org/10.1038/nrmicro2405.
4. **Aldridge P, Hughes KT.** 2002. Regulation of flagellar assembly. Curr. Opin. Microbiol. **5:**160–165. http://dx.doi.org/10.1016/S1369-5274(02)00302-8.
5. **Chilcott GS, Hughes KT.** 2000. Coupling of flagellar gene expression to flagellar assembly in *Salmonella enterica* serovar Typhimurium and *Escherichia coli*. Microbiol. Mol. Biol. Rev. **64:**694–708. http://dx.doi.org/10.1128/MMBR.64.4.694-708.2000.
6. **Minamino T, Macnab RM.** 1999. Components of the *Salmonella* flagellar export apparatus and classification of export substrates. J. Bacteriol. **181:**1388–1394.
7. **Yonekura K, Maki S, Morgan DG, DeRosier DJ, Vonderviszt F, Imada K, Namba K.** 2000. The bacterial flagellar cap as the rotary promoter of flagellin self-assembly. Science **290:**2148–2152. http://dx.doi.org/10.1126/science.290.5499.2148.
8. **Yonekura K, Maki-Yonekura S, Namba K.** 2002. Growth mechanism of the bacterial flagellar filament. Res. Microbiol. **153:**191–197. http://dx.doi.org/10.1016/S0923-2508(02)01308-6.
9. **Macnab RM.** 2003. How bacteria assemble flagella. Annu. Rev. Microbiol. **57:**77–100. http://dx.doi.org/10.1146/annurev.micro.57.030502.090832.
10. **Kubori T, Shimamoto N, Yamaguchi S, Namba K, Aizawa S.** 1992. Morphological pathway of flagellar assembly in *Salmonella typhimurium*. J. Mol. Biol. **226:**433–446. http://dx.doi.org/10.1016/0022-2836(92)90958-M.
11. **Emerson SU, Tokuyasu K, Simon MI.** 1970. Bacterial flagella: polarity of elongation. Science **169:**190–192. http://dx.doi.org/10.1126/science.169.3941.190.
12. **Iino T.** 1969. Polarity of flagellar growth in *Salmonella*. J. Gen. Microbiol. **56:**227–239. http://dx.doi.org/10.1099/00221287-56-2-227.
13. **Berg HC.** 2003. The rotary motor of bacterial flagella. Annu. Rev. Biochem. **72:**19–54. http://dx.doi.org/10.1146/annurev.biochem.72.121801.161737.
14. **Jones CJ, Macnab RM, Okino H, Aizawa S.** 1990. Stoichiometric analysis of the flagellar hook-(basal-body) complex of *Salmonella typhimurium*. J. Mol. Biol. **212:**377–387. http://dx.doi.org/10.1016/0022-2836(90)90132-6.
15. **Homma M, Kutsukake K, Hasebe M, Iino T, Macnab RM.** 1990. FlgB, FlgC, FlgF and FlgG. A family of structurally related proteins in the flagellar basal body of *Salmonella typhimurium*. J. Mol. Biol. **211:**465–477.
16. **Jones CJ, Macnab RM.** 1990. Flagellar assembly in *Salmonella typhimurium*: analysis with temperature-sensitive mutants. J. Bacteriol. **172:**1327–1339.

17. **Chevance FF, Takahashi N, Karlinsey JE, Gnerer J, Hirano T, Samudrala R, Aizawa S, Hughes KT.** 2007. The mechanism of outer membrane penetration by the eubacterial flagellum and implications for spirochete evolution. Genes Dev. **21:**2326–2335. http://dx.doi.org/10.1101/gad.1571607.
18. **Homma M, Komeda Y, Iino T, Macnab RM.** 1987. The flaFIX gene product of *Salmonella typhimurium* is a flagellar basal body component with a signal peptide for export. J. Bacteriol. **169:**1493–1498.
19. **Jones CJ, Homma M, Macnab RM.** 1989. L-, P-, and M-ring proteins of the flagellar basal body of *Salmonella typhimurium*: gene sequences and deduced protein sequences. J. Bacteriol. **171:**3890–3900.
20. **Nambu T, Kutsukake K.** 2000. The *Salmonella* FlgA protein, a putativeve periplasmic chaperone essential for flagellar P ring formation. Microbiology **146**(Part 5):1171–1178.
21. **DeRosier DJ.** 1998. The turn of the screw: the bacterial flagellar motor. Cell **93:**17–20. http://dx.doi.org/10.1016/S0092-8674(00)81141-1.
22. **Erhardt M, Singer HM, Wee DH, Keener JP, Hughes KT.** 2011. An infrequent molecular ruler controls flagellar hook length in *Salmonella enterica*. EMBO J. **30:**2948–2961. http://dx.doi.org/10.1038/emboj.2011.185.
23. **Minamino T, Ferris HU, Moriya N, Kihara M, Namba K.** 2006. Two parts of the T3S4 domain of the hook-length control protein FliK are essential for the substrate specificity switching of the flagellar type III export apparatus. J. Mol. Biol. **362:**1148–1158. http://dx.doi.org/10.1016/j.jmb.2006.08.004.
24. **Minamino T, Moriya N, Hirano T, Hughes KT, Namba K.** 2009. Interaction of FliK with the bacterial flagellar hook is required for efficient export specificity switching. Mol. Microbiol. **74:**239–251. http://dx.doi.org/10.1111/j.1365-2958.2009.06871.x.
25. **Takahashi N, Mizuno S, Hirano T, Chevance FF, Hughes KT, Aizawa S.** 2009. Autonomous and FliK-dependent length control of the flagellar rod in *Salmonella enterica*. J. Bacteriol. **191:**6469–6472. http://dx.doi.org/10.1128/JB.00509-09.
26. **Davis RW, Botstein D, Roth JR.** 1980. Advanced bacterial genetics. Cold Spring Harbor Laboratory, Cold Spring Harbor, NY.
27. **Aizawa SI, Dean GE, Jones CJ, Macnab RM, Yamaguchi S.** 1985. Purification and characterization of the flagellar hook-basal body complex of *Salmonella typhimurium*. J. Bacteriol. **161:**836–849.
28. **Ohnishi K, Homma M, Kutsukake K, Iino T.** 1987. Formation of flagella lacking outer rings by *flaM*, *flaU*, and *flaY* mutants of *Escherichia coli*. J. Bacteriol. **169:**1485–1488.
29. **Nambu T, Minamino T, Macnab RM, Kutsukake K.** 1999. Peptidoglycan-hydrolyzing activity of the FlgJ protein, essential for flagellar rod formation in *Salmonella typhimurium*. J. Bacteriol. **181:**1555–1561.
30. **Hirano T, Minamino T, Macnab RM.** 2001. The role in flagellar rod assembly of the N-terminal domain of *Salmonella* FlgJ, a flagellum-specific muramidase. J. Mol. Biol. **312:**359–369. http://dx.doi.org/10.1006/jmbi.2001.4963.
31. **Nambu T, Inagaki Y, Kutsukake K.** 2006. Plasticity of the domain structure in FlgJ, a bacterial protein involved in flagellar rod formation. Genes Genet. Syst. **81:**381–389. http://dx.doi.org/10.1266/ggs.81.381.
32. **Minamino T, Namba K.** 2004. Self-assembly and type III protein export of the bacterial flagellum. J. Mol. Microbiol. Biotechnol. **7:**5–17. http://dx.doi.org/10.1159/000077865.

CHAPTER 3

NANOSCALE-LENGTH CONTROL OF THE FLAGELLAR DRIVESHAFT REQUIRES HITTING THE TETHERED OUTER MEMBRANE

Reprinted with permission:

Cohen EJ, Ferreira JL, Ladinsky MS, Beeby M, Hughes KT

Science 14 Apr 2017:
Vol. 356, Issue 6334, pp. 197-200
DOI: 10.1126/science.aam6512

REPORT

SIZE CONTROL

Nanoscale-length control of the flagellar driveshaft requires hitting the tethered outer membrane

Eli J. Cohen,[1] Josie L. Ferreira,[2] Mark S. Ladinsky,[3] Morgan Beeby,[2] Kelly T. Hughes[1]*

The bacterial flagellum exemplifies a system where even small deviations from the highly regulated flagellar assembly process can abolish motility and cause negative physiological outcomes. Consequently, bacteria have evolved elegant and robust regulatory mechanisms to ensure that flagellar morphogenesis follows a defined path, with each component self-assembling to predetermined dimensions. The flagellar rod acts as a driveshaft to transmit torque from the cytoplasmic rotor to the external filament. The rod self-assembles to a defined length of ~25 nanometers. Here, we provide evidence that rod length is limited by the width of the periplasmic space between the inner and outer membranes. The length of Braun's lipoprotein determines periplasmic width by tethering the outer membrane to the peptidoglycan layer.

Length determination of linear filaments poses a particular problem, some of whose known examples are solved by using molecular rulers. The bacterial flagellum is one such linear filament composed of a series of axial structures that must be assembled to precise specifications to enable motility. The bacterial flagellum consists of a cytoplasmic, ion-powered rotary motor connected to a driveshaft (rod) that transmits torque to the external filament (propeller). The rod extends ~25 nm from the inner membrane through the peptidoglycan layer and periplasmic space to the outer membrane and terminates (Fig. 1). Termination of rod assembly positions the rod tip perpendicular to the outer membrane permitting an outer membrane–bound bushing complex, the periplasmic lipopolysaccharide ring (PL-ring), to assemble around the rod. The PL-ring forms an outer-membrane pore and results in the initiation of hook polymerization, which extends ~55 nm, followed by the filament. The hook acts as a universal joint connecting the rigid rod to the rigid filament, whose rotation propels the bacterium forward and allows the cell to alter its swimming trajectory (Fig. 1) (*1*–*5*). The length-control mechanism of the hook is well characterized and depends on the action of a secreted, molecular ruler, FliK. When the hook reaches a minimal length, the C terminus of FliK that is in the process of being secreted through the growing flagellar structure interacts with the FlhB gatekeeper protein of the flagellar type III secretion apparatus to switch secretion-substrate specificity from early, rod-hook secretion mode to late, filament secretion mode (*6*–*10*).

Although the flagellar hook serves as an excellent model for understanding length determination via the FliK molecular ruler, the length-control mechanism of another flagellar component, the rod, has remained enigmatic (*11*). The rod consists of two distinct substructures: the ~7-nm proximal and ~18-nm distal rod (*12*–*14*). The proximal rod is composed of four different proteins, and its mechanism of assembly remains unknown. In contrast, the distal rod is composed of ~50 copies of a single protein, FlgG. FlgG subunits must stack upon one another to reach the outer membrane (*14*). The self-stacking capability of FlgG poses a dilemma for the cell: Once initiated, what prevents continuously secreted FlgG subunits from polymerizing indefinitely?

A model for flagellar rod-length control was proposed on the basis of a set of mutations mapping to the *flgG* gene (*flgG** mutations) that resulted in increased rod lengths. The *flgG** rods grow beyond the wild-type (WT) length of ~25 nm to ~60 nm, which is determined by the FliK ruler (*15*). Because the *flgG** mutations resulted in extended distal rod growth, a rod length–control mechanism was proposed that depended on intrinsic FlgG subunit stacking interactions during distal rod assembly. This model was based on earlier reports that the distal rod consisted of ~26 FlgG subunits, which would constitute two stacks of FlgG in the distal rod (*16*). Recent work has determined that the number of FlgG subunits in the distal rod is actually ~50 (*14*), which does not support an intrinsic distal rod length–control model based on subunit stacking interactions.

The FlgG-intrinsic model for rod-length control predicted that rod length would be unaffected by the cytoplasmic FlgG concentration. However, overexpression of the *flgG* gene yielded an increase in the average rod length (Fig. 2). This result and the finding that the distal rod is composed of ~50 FlgG subunits forced us to explore other possible mechanisms of flagellar rod-length control.

A clue to the actual rod-length control mechanism came from the isolation of suppressor mutations of the *flgG** length-control mutants.

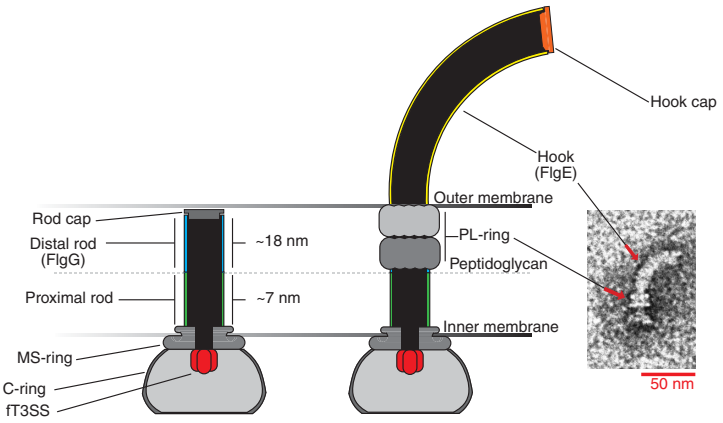

Fig. 1. The hook basal body of *Salmonella enterica*. Construction of the flagellum begins with the assembly of the transmembrane membrane supramembrane ring (MS-ring), the flagellar type 3 secretion system (fT3SS), and the cytoplasmic ring (C-ring) rotor complex. The proximal rod polymerizes on top of the MS-ring followed by the FlgG distal rod to span the distance between the peptidoglycan layer and the outer membrane. FlgJ, the rod cap, allows the growing structure to pass through the peptidoglycan layer through localized hydrolysis of the peptidoglycan (*28*). Once the distal rod has reached the outer membrane, formation of the periplasmic ring–lipopolysaccharide ring (P-ring–L-ring) complex simultaneously forms a hole in the outer membrane and dislodges the rod cap. Rod cap removal allows the hook cap (FlgD) to form on the tip of the nascent structure and to promote assembly of the hook by FlgE subunits.

[1]Department of Biology, University of Utah, Salt Lake City, UT 84112, USA. [2]Department of Life Sciences, Imperial College of London, London SW7 2AZ, UK. [3]Division of Biology and Biological Engineering 114-96, California Institute of Technology, Pasadena, CA 91125, USA.
***Corresponding author. Email: hughes@biology.utah.edu**

Because rod growth in these mutants continues to ~60 nm, we speculated that the placement of the rod tip was no longer perpendicular to the outer membrane, compromising PL-ring assembly and resulting in filament growth in the periplasm and a nonmotile phenotype (*11*, *17*). The nonmotile phenotype of *flgG** mutants allowed us to perform a selection for suppressor mutations that relieved these mutants of the motility defect. One class of mutants arose in a gene not previously implicated in flagellar morphogenesis, *lppA*.

The *lppA* gene encodes Braun's lipoprotein, which is the major outer-membrane lipoprotein of the cell in Gram-negative bacteria. Lpp is the most abundant protein in *Escherichia coli*, with 10^6 copies per cell. The LppA protein is secreted to the periplasm and processed to a final length of 58 amino acids that form homotrimers. N-terminal cysteine residues are acylated and anchor the LppA trimer in the outer membrane, whereas C-terminal lysine residues are covalently attached to the peptidoglycan layer (fig. S1) (*18*–*20*). Unlike the case in WT *Salmonella*, which displays a slight reduction in motility upon deletion of *lppA* (fig. S2), the *flgG** mutants exhibited a 2- to 3-fold increase in swim diameter on motility agar when *lppA* was deleted (fig. S3).

We hypothesized that without LppA, the space between the peptidoglycan and outer membrane would be less constricted and would allow *flgG** distal rods to be positioned perpendicular to the outer membrane as they grew longer than 25 nm, which would permit PL-ring pore formation. This predicted that the number of extracellular filaments assembled by *flgG** mutants would increase

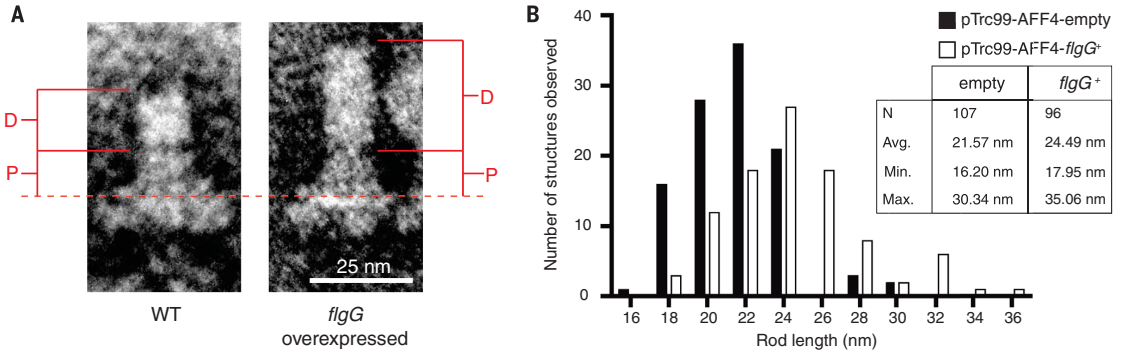

Fig. 2. Overexpression of *flgG* resulted in longer distal rods. To test the FlgG intrinsic model for length control of the distal rod, *flgG* was overexpressed from a plasmid vector to supplement *flgG* expression from its native chromosomal locus in a strain lacking the genes required for termination of distal rod assembly (*flgH*) and subsequent hook assembly (*flgD* and *flgE*). (**A**) Flagellar basal bodies were purified from the *flgG*-overexpression background and compared with those from an empty-vector control strain by transmission electron microscopy (TEM). (**B**) Measurements were taken from the top of the MS-ring [dashed line in (A)] to the tip of the rod (P, proximal rod; D, distal rod). Overexpression of *flgG* was found to significantly increase the length of the rod ($P < 0.0001$, Student's two-tailed *t* test, $N = 2$).

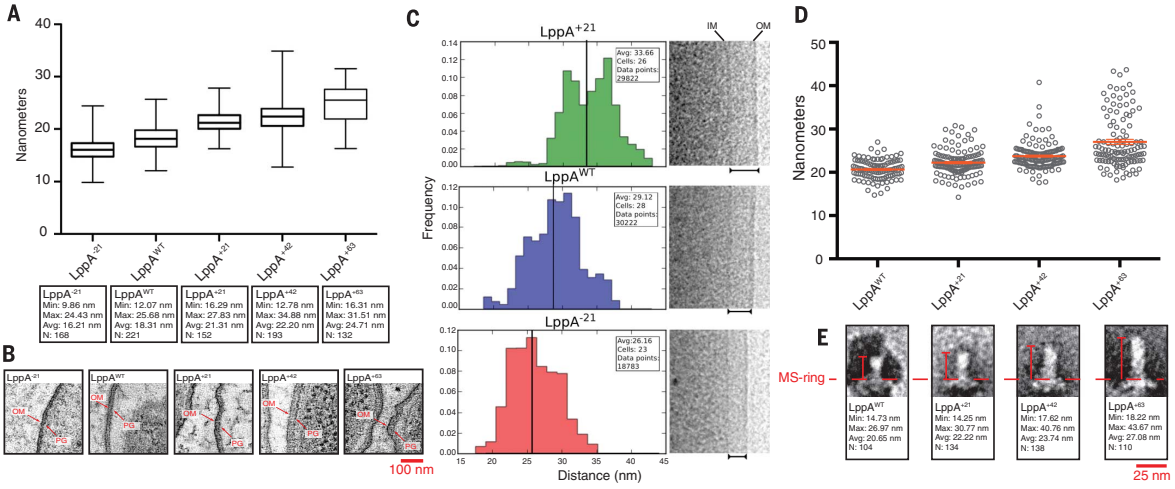

Fig. 3. The inner- to outer-membrane distance and flagellar rod length varied with LppA lengths. Resin-embedded LppA-length mutants, as well as WT control (TH22579 and TH22634 to TH22637) were thin-sectioned and observed by electron tomography. (**A** and **B**) The peptidoglycan-layer (PG)–to–outer-membrane (OM) distances for each strain were measured. As the length of LppA increased, we observed a corresponding increase in PG-to-OM distance [$P < 0.0001$, one-way analysis of variance (ANOVA)]. (**C**) To verify these results, cells from −21, +21, and WT LppA strains (TH22579, TH22634, and TH22635) were imaged via cryo-EM, and the distances between the inner membrane (IM) and OM were measured for each. The distances varied with LppA lengths ($P < 0.0001$, Student's two-tailed *t* test). (**D** and **E**) Flagellar rods from lengthened LppA variants (TH22574 to TH22577) were purified, imaged via TEM and measured. The average length of the rod increased ~1.5 to 2 nm for every three heptad repeats (21 residues) added [$P < 0.0001$, one-way ANOVA, $N = \geq 3$, data in (D) are means ± SEM].

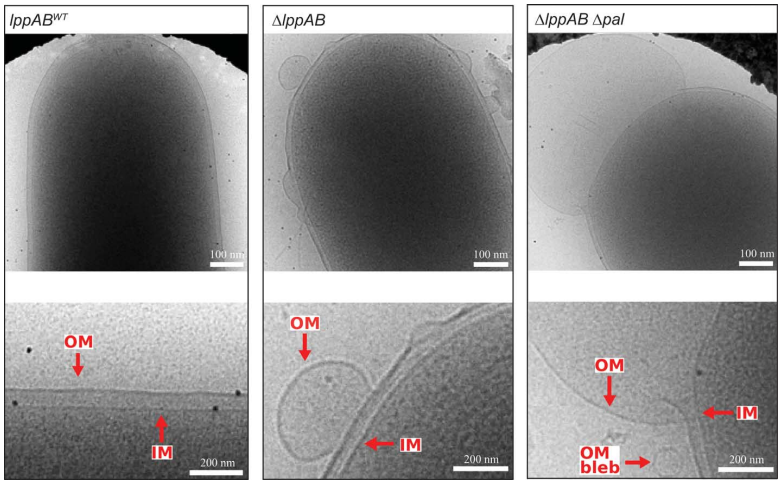

Fig. 4. LppA functions as an outer-membrane tether. Deletion of *lppAB* (strain TH22543) resulted in the formation of taut outer-membrane blebs that pulled away from the cell body. The severity of blebbing was increased in the Δ*lppAB* Δ*pal* double mutant (strain TH22569).

upon deletion of *lppA*. Western blot analysis and fluorescence microscopy confirmed that extracellular flagellin secretion and assembly in *flgG** mutants increased in the absence of LppA (fig. S4). Additionally, *flgG** mutants still produced abnormally long rods regardless of whether LppA was present or not (fig. S5). These data suggested that the outer membrane acts as a barrier to distal rod growth and prevents continuous rod polymerization.

Unlike *E. coli*, *Salmonella* has two tandem *lpp* genes, *lppA* and *lppB* (fig. S1) (*21*, *22*). The LppA protein is the equivalent of *E. coli* Lpp, whereas *lppB* is not expressed under standard laboratory conditions (*23*). LppA-length variants were constructed to test whether LppA determined the spacing between the peptidoglycan and outer membrane and whether this spacing determined distal rod length. LppA trimer formation is driven by hydrophobic interactions between seven heptad-repeat motifs within the mature 58–amino acid LppA monomers (*20*). An initial attempt to increase Lpp length by fusing LppA and LppB resulted in cells severely defective in cell shape and division (fig. S1). The LppA structure is based on heptad repeats of interacting monomers in the trimer. In an attempt to prevent cell-shape and division defects, length variants were designed that maintained interacting heptad repeats. The LppA length variants constructed included a 21–amino acid deletion and three longer variants containing insertions of 21, 42, and 63 residues (fig. S6).

To determine whether changing LppA length resulted in a concomitant change in peptidoglycan-to–outer-membrane distance, LppA length–variant cells were embedded in resin and analyzed by electron microscopy. We observed changes in peptidoglycan-to–outer-membrane spacing that were proportional to LppA lengths (Fig. 3, A and B). Electron cryomicroscopy (cryo-EM), which preserved cells in a near-native frozen-hydrated state, corroborated these results. Imaging cells harboring $lppA^{-21}$, $lppA^{+21}$, and $lppA^{WT}$ variants by using cryo-EM demonstrated that the length of LppA was a principal determinant of the inner-membrane–to–outer-membrane distance (Fig. 3C and fig. S7).

To test whether the length of the flagellar rod was dictated by periplasmic width, we measured rods isolated from the LppA-length mutants. We observed changes in the average length of the flagellar rod as the length of LppA changed (Fig. 3, D and E, and figs. S8 and S9). Taken together, the data obtained from resin-embedded electron microscopy, cryo-EM, and rod-length measurements were consistent with a model for distal rod–length control that required contact with the outer membrane.

Electron cryo-EM was then used to address whether the osmotic pressure in the periplasm mirrors that of the cytoplasm or the external environment. Suppression of the *flgG** motility defect by loss of LppA is consistent with the osmolalities in the cytoplasm and periplasm being equal, which is in agreement with previous studies (*24*, *25*). In an attempt to further address this, we imaged one mutant having *lppAB* deleted and one with both *lppAB* and *pal* deleted. Pal is another abundant outer-membrane lipoprotein that noncovalently binds peptidoglycan (*26*, *27*) and could tether the outer membrane to the peptidoglycan. We reasoned that if LppA functions as a tether under tension, as expected if the cytoplasmic and periplasmic osmolalities were equal, the absence of LppA would allow the outer membrane to pull away from the cell body as the osmolality of the periplasm equilibrates with that of the external environment.

Imaging the Δ*lppAB* mutant revealed that the outer membrane pulled away from the cell body in taut blebs. In the Δ*lppAB* Δ*pal* double mutant, more extreme blebbing was observed (Fig. 4 and fig. S7). These results support previous reports that the osmolality of the periplasm mirrors that of the cytoplasm and that the function of LppA (and perhaps other peptidoglycan-binding lipoproteins) is to act as a tether rather than a support column under normal growth conditions.

Evolution places constraints and limitations on each component of an organism in order to maximize the fitness of the organism as a whole. In addition to housing the flagellar driveshaft, the periplasm contains a multitude of other cellular machinery. We were surprised to discover that addition of 21 residues to LppA increased the apparent swim rate of *Salmonella* to a small degree (~10%) (fig. S10). Also, altering the length of LppA caused slower growth and morphological abnormalities that became more pronounced the further the length deviated from the mature wild-type LppA length of 58 residues (fig. S10). These observations suggest that the selective forces that have influenced flagellar form and function have led to a compromise on the absolute optimization of swimming ability in favor of a motility organelle that is optimized to function in harmony with other components of the cell and under various conditions.

REFERENCES AND NOTES

1. R. M. Macnab, *Annu. Rev. Microbiol.* **57**, 77–100 (2003).
2. F. F. V. Chevance, K. T. Hughes, *Nat. Rev. Microbiol.* **6**, 455–465 (2008).
3. C. J. Jones, M. Homma, R. M. Macnab, *J. Bacteriol.* **171**, 3890–3900 (1989).
4. G. J. Schoenhals, R. M. Macnab, *J. Bacteriol.* **178**, 4200–4207 (1996).
5. H. C. Berg, R. A. Anderson, *Nature* **245**, 380–382 (1973).
6. T. Hirano, S. Yamaguchi, K. Oosawa, S. Aizawa, *J. Bacteriol.* **176**, 5439–5449 (1994).
7. M. Erhardt, H. M. Singer, D. H. Wee, J. P. Keener, K. T. Hughes, *EMBO J.* **30**, 2948–2961 (2011).
8. K. Muramoto, S. Makishima, S. I. Aizawa, R. M. Macnab, *J. Mol. Biol.* **277**, 871–882 (1998).
9. K. Uchida, S. Aizawa, *J. Bacteriol.* **196**, 1753–1758 (2014).
10. N. Takahashi *et al.*, *J. Bacteriol.* **191**, 6469–6472 (2009).
11. F. F. V. Chevance *et al.*, *Genes Dev.* **21**, 2326–2335 (2007).
12. M. Homma, K. Kutsukake, M. Hasebe, T. Iino, R. M. Macnab, *J. Mol. Biol.* **211**, 465–477 (1990).
13. Y. Saijo-Hamano, N. Uchida, K. Namba, K. Oosawa, *J. Mol. Biol.* **339**, 423–435 (2004).
14. T. Fujii *et al.*, *Nat. Commun.* **8**, 14276 (2017).
15. T. Hirano, S. Mizuno, S. Aizawa, K. T. Hughes, *J. Bacteriol.* **191**, 3938–3949 (2009).
16. C. J. Jones, R. M. Macnab, H. Okino, S. Aizawa, *J. Mol. Biol.* **212**, 377–387 (1990).
17. E. J. Cohen, K. T. Hughes, *J. Bacteriol.* **196**, 2387–2395 (2014).
18. V. Braun, *Biochim. Biophys. Acta* **415**, 335–377 (1975).
19. A. Kovacs-Simon, R. W. Titball, S. L. Michell, *Infect. Immun.* **79**, 548–561 (2011).
20. W. Shu, J. Liu, H. Ji, M. Lu, *J. Mol. Biol.* **299**, 1101–1112 (2000).
21. J. Sha *et al.*, *Infect. Immun.* **72**, 3987–4003 (2004).
22. A. A. Fadl *et al.*, *Infect. Immun.* **73**, 1081–1096 (2005).
23. C. Kröger *et al.*, *Cell Host Microbe* **14**, 683–695 (2013).
24. D. S. Cayley, H. J. Guttman, M. T. Record Jr., *Biophys. J.* **78**, 1748–1764 (2000).
25. K. A. Sochacki, I. A. Shkel, M. T. Record, J. C. Weisshaar, *Biophys. J.* **100**, 22–31 (2011).
26. E. Cascales, A. Bernadac, M. Gavioli, J.-C. Lazzaroni, R. Lloubes, *J. Bacteriol.* **184**, 754–759 (2002).
27. L. M. Parsons, F. Lin, J. Orban, *Biochemistry* **45**, 2122–2128 (2006).
28. T. Nambu, T. Minamino, R. M. Macnab, K. Kutsukake, *J. Bacteriol.* **181**, 1555–1561 (1999).

ACKNOWLEDGMENTS

We thank T. Silhavy for anti-Lpp antisera and D. Blair and N. Wingreen for helpful discussions. All strains, primers, and plasmids used in this study are available upon request. This work was funded by NIH grant GM056141 (K.T.H.), Marie Curie Career Integration Grant 630988 (M.B.) and UK Medical Research Council Ph.D. Doctoral Training Partnership award MR/K501281/1 (J.L.F.).

SUPPLEMENTARY MATERIALS

www.sciencemag.org/content/356/6334/197/suppl/DC1
Materials and Methods
Figs. S1 to S10
Tables S1 and S2
References (*29*–*35*)

22 December 2016; accepted 17 March 2017
10.1126/science.aam6512

Supplementary Materials

Materials and Methods

Bacterial Strains, Plasmids and Media

Detailed information about bacterial strains and plasmids used in this study are listed in Table 1. Cells were cultured in Lysis Broth (LB). Media was supplemented with the following antibiotics when needed: chloramphenicol (12.5 µg/mL), kanamycin (50 µg/mL), tetracycline (15 µg/mL), ampicillin (100 µg/mL). Genes expressed from the chromosomal arabinose-inducible araBAD promoter (ParaBAD) were induced by the addition of L-arabinose (final concentration: 0.2%). All transductional crosses were performed using the generalized transducing phage of Salmonella typhimurium P22 HT105/1 int-201. λ-Red recombineering (29) was performed using tetracycline for selection and anhydrotetracycline/fusaric acid media for subsequent counterselection.

Swimming and Swarming Motility Assays

Swimming motility was assayed by stabbing single colonies into swimming motility plates (0.2% agar with 10 g/L tryptone and 5 g/L NaCl added) and incubated face-up at 37° C for 8-12 hours. For swarming motility assays, 1 µL of overnight cultures were spotted on swarming motility agar (0.5% agar with 10 g/L tryptone, 5 g/L yeast extract, 10 g/L NaCl and 0.5% glucose added) followed by incubating face-up at 37° C for 16-18 hours. Swim diameters were measured using ImageJ 1.50i software (National Institutes of Health (NIH)). Graphs were made with Graphpad Prism 5 software suite (Graphpad software, Inc.)

Isolation, Transmission Electron Microscopy and Measurement of Flagellar Structures:

Hook basal body (HBB) isolation was carried out by methods described previously (30), with minor modifications. Structures were not collected by CsCl or sucrose gradient centrifugation but were pelleted at 60,000 x g for 1 h using a Beckman 50.2Ti and/or S80-AT3 rotor at 12 °C.

Purified structures were applied to glow discharged carbon-coated formvar copper grids (Cu-FCF-300H grids, Electron Microscopy Sciences) and stained with 2% aqueous phosphotungstic acid (pH ~7.0). Images were captured using a JEOL JEM-1400 electron microscope at an acceleration voltage of 120 kV coupled to a Gatan CCD camera. Rod lengths were measured using NIH ImageJ 1.50i software. Statistical analysis and graphs were made using the Graphpad Prism 5 software suite (Graphpad software, Inc., Figs. 2, 3D, 3E, S8, S9)

SDS-PAGE Sample Preparation and Immunoblotting

For detection of FliC-3xHA in culture supernatants, overnight cultures were diluted 1:100 in fresh LB and grown at 37° C with aeration to O.D.600 ~1.0. Cells were harvested by centrifugation and gently resuspended in cold 0.1 M glycine, pH 2.5 and incubated on ice for 20-30 minutes to depolymerize flagellar filaments. Following depolymerization, cells were pelleted by centrifugation and the supernatant carefully decanted. 0.5 µg lysozyme was added to the supernatant to act as a carrier for TCA precipitation. The precipitant was washed twice with cold acetone and boiled in 2x SDS Laemlli buffer. Samples were run on hand-cast, 12% tris-glycine polyacrylamide gels with 0.1% SDS added. Following SDS-PAGE, proteins were transferred to nitrocellulose

by semi-dry transfer and probed with anti-HA and anti-DnaK (a cell lysis control) antisera in TBST with 5% milk added. Following incubation with 1° antibody, membranes were incubated with IRdye fluorescently labeled 2° antibody and developed on a LI-COR Biosciences Odyssey infrared imaging system.

For purification and detection of Lpp linked to cell wall sacculi, cultures were grown overnight in 10 mL of LB at 37° C with aeration. Cells were pelleted, resuspended in 3 mL saline and dripped into 6 mL of 6% SDS heated to 85-90° C with stirring. Lysates were stirred at 85-90° C for 2-3 hours followed by centrifugation at 100,000xg for 1 hour. Pellets were washed 3x with 20 mL H2O to remove all SDS and resuspended in 1 mL PBS. Lysozyme was added to the purified sacculi (final concentration: 2 mg/mL) and incubated at 37° C overnight. Lysozyme digests were concentrated by TCA precipitation and resuspended in 100 μL 2xSDS Laemlli buffer. Typically, 5-10 μL of sample were loaded to 13% tris-tricine polyacrylamide gels. Lpp was detected using anti-Lpp antisera following the protocol described above.

EM Preparation for Resin-embedded Electron Tomography

Salmonella cultures were prepared for EM by high-pressure freezing and freeze-substitution. Cells were briefly centrifuged and the pellets resuspended in culture medium containing 10% Ficoll (70kD; Sigma), which serves as an extracellular cryoprotectant. The cells were centrifuged again and the supernated removed. Pellets of Salmonella cells were transferred to brass freezing planchettes (Ted Pella, Inc.) and rapidly frozen in a HPM-010 high-pressure freezer (Leica Microsystems, Vienna Austria), then stored under liquid nitrogen. The frozen planchettes were subsequently

placed in cryotubes (Nunc) containing 2 ml of 2% glutaraldehyde in acetone and transferred to a AFS2 freeze-substitution machine (Leica Microsystems). Samples were freeze-substituted at -90°C for 60 hours, then warmed to -20° C over 8 hours. The samples were then rinsed 3x with cold acetone and processing continued at -20°C for an additional 24 hours with 2.5% OsO4, 0.05% uranyl acetate in acetone. The samples were then warmed to room temperature, rinsed 4x with acetone and infiltrated with Epon-Araldite resin (Electron Microscopy Sciences, Port Washington PA). Pellets of cells were embedded in plastic sectioning capsules and the resin polymerized at 60°C for 48 hours. Thick (400 nm) sections were cut with a UC6 ultramicrotome (Leica Microsystems) using a diamond knife (Diatome Ltd., Switzerland). And placed on Formvar-coated copper-rhodium 1mm slot grids (Electron Microscopy Sciences). Sections were stained with 3% uranyl acetate and lead citrate and colloidal gold particles (10 nm) were placed on both surfaces of the grids to serve as fiducial markers for image alignment. Grids were stabilized with evaporated carbon prior to imaging.

Electron Tomography and Peptidoglycan to Outer Membrane Measurement

Grids were placed in a Dual-Axis Tomography holder (Model 2040, Fischione Instruments, Inc., Export, PA) and imaged with a Tecnai TF30ST-FEG microscope (FEI Company, Holland) at 300 KeV. Dual-axis tilt series (+/- 64° at 1° intervals) were acquired automatically using the SerialEM software package 21). Tomographic data were aligned, analyzed and segmented using IMOD (31-32, Fig. 3B) on MacPro computers (Apple, Inc).

For measurement of cell wall peptidoglycan (PG) to outer membrane (OM) distances, 3 tomogram sections each of >3 cells per LppA length variant were saved as

.tif files and analyzed in ImageJ (NIH). Distances between the PG and OM were measured every 5-10 nm, for a total of ~200 measurements per length variant, and plotted using Graphpad Prism software (Graphpad software, Inc., Fig. 3A)

Preparation of Electron Cryo-microscopy Samples, Data Collection and Analysis

Strains were grown aerobically in LB at 37° C until an O.D.600 of 0.6 was reached. Cells were spun for 5 minutes at 6000xg and resuspended to an O.D.600 of ~18. UltraAuFoil R2/2 grids (200 mesh) (Quantifoil Micro Tools GmbH) were glow-discharged for 60s at 10mA. Cells were mixed with a solution of 10nm colloidal gold (Sigma) immediately before freezing. A 2.5µl droplet of sample was applied to the grid and plunge frozen using a Vitrobot MkIV (FEI Company) with a wait time of 60s, a blot time of 5s, a blot force of 3 and a drain time of 1s at a constant humidity of 100%. Grids were stored under liquid nitrogen until required for data collection. Projection images were collected on a 200keV FEI Tecnai TF20 FEG transmission electron microscope (FEI Company) equipped with a Falcon II direct electron detector (FEI Company) using a Gatan 626 cryogenic-holder (Gatan). Leginon automated data-collection software (33) was used to acquire images with pixel size of 0.828nm (nominal magnification 25000x) with a defocus of -5µm.

3dmod from the IMOD package (34) and custom scripting were used to manually segment inner and outer membranes of projection images of ~25 cells per mutant, measuring the periplasmic width at 0.5nm intervals, resulting in tens of thousands of data points per mutant to produce width histograms (Fig. 3C).

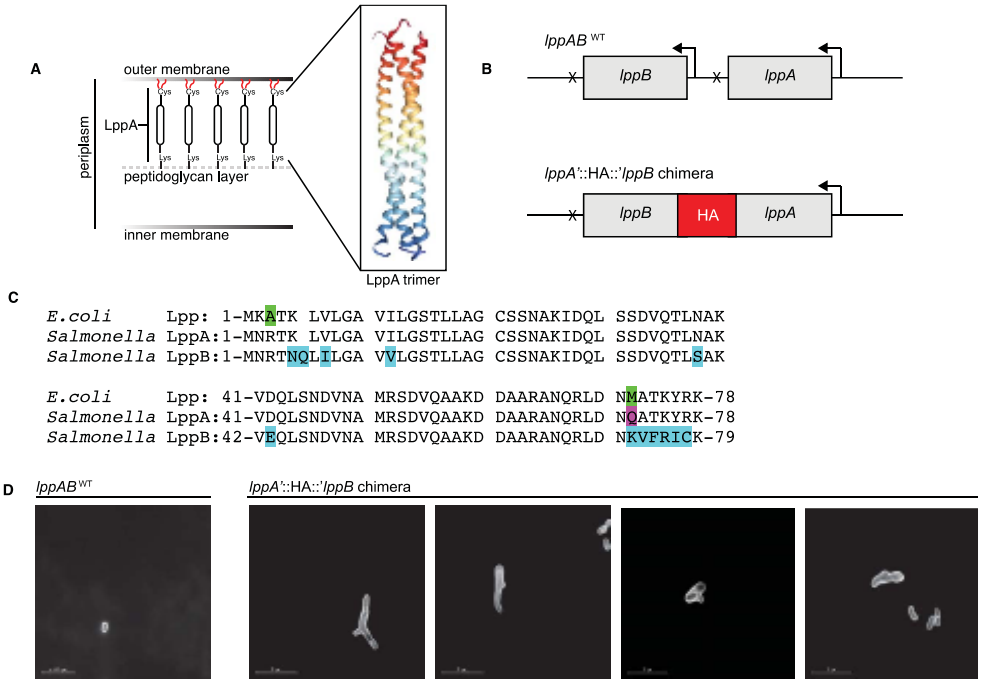

Fig. 3S.1 Mutations in LppA can cause severe morphological defects

Mature wild type LppA is a helical tether 58 amino acids in length. The attachment of a diacylglycerol moiety to the N-terminus anchors LppA in the outer membrane, while an invariant C-terminal lysine residue is covalently bound to peptidoglycan (A). The bulk of the mature LppA protein consists of seven uninterrupted heptad repeat motifs which drive trimer formation through hydrophobic interactions between LppA molecules. We attempted to create a lengthened Lpp protein by fusing LppA to LppB with a 3x hemagluttinin (HA) tag sandwiched between the two (B). Although LppA and LppB share a high degree of homology, they have diverged considerably at their N-termini, the significance of which is unknown. Cells in this background grew very slowly and exhibited gross morphological abnormalities (D). This could have been due to the heptad repeats of the chimera being out of register, the chimera being too long or the fact that the N-termini of LppA and LppB are have diverged considerably, or all three. Ribbon structure of LppA trimer sourced from RCSB Protein Data Bank (accession #1EQ7).

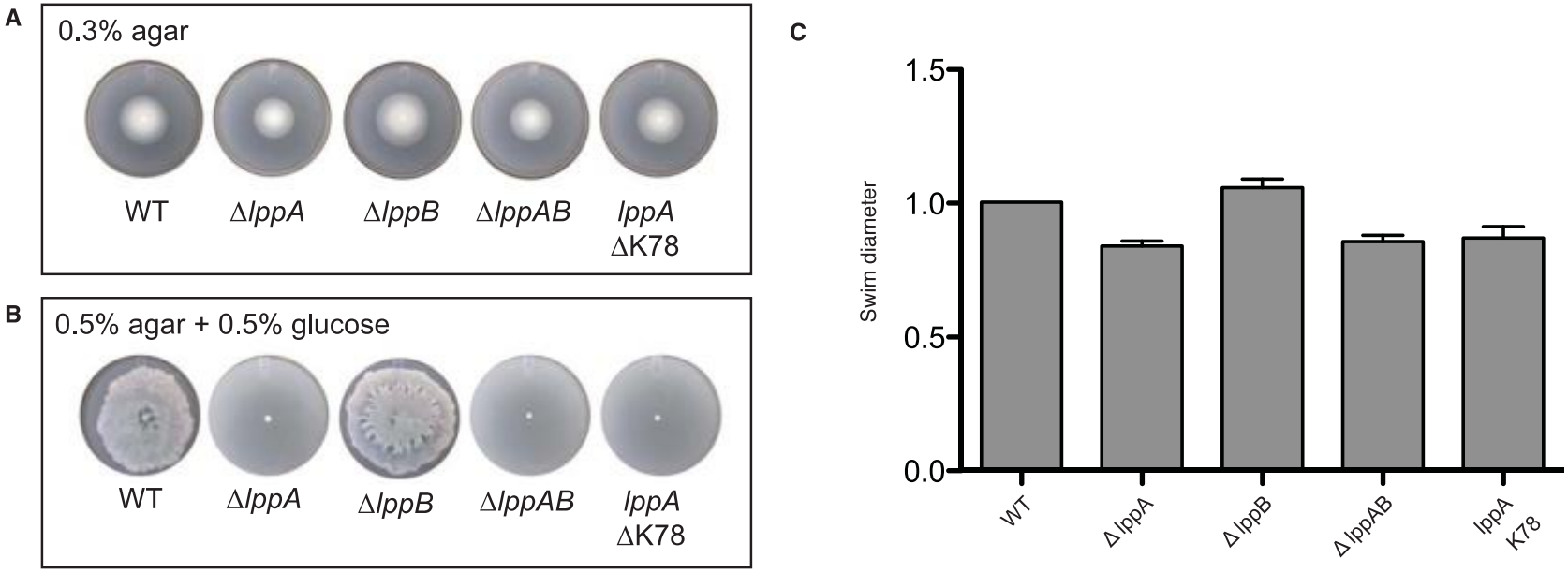

Fig. 3.S2 Deletion of *lppA* impairs swimming motility and abolishes swarming motility
Salmonella, among other species of bacteria, exhibits two distinct forms of flagella-mediated motility: swimming and swarming. Swimming motility describes the individual behaviour of a cell swimming through liquid, while swarming is a communal behavior whereby a swarm of flagellated bacteria moves across a hydrated surface (35). Swimming motility is assayed in soft agar (0.3% agar conc.), while swarming is assayed on 0.5% agar with 0.5% glucose added. Several *lpp* deletion mutations were assayed for their effects on swimming (A) and swarming (B) motility relative to WT. Motility in swim agar was reduced ~20% in the Δ*lppA*, Δ*lppAB* and $lppA^{\Delta K78}$ backgrounds (C). Motility on swarm agar was abolished in the Δ*lppA*, Δ*lppAB* and $lppA^{\Delta K78}$ backgrounds. Deletion of *lppB* had little effect on either swimming or swarming motility.

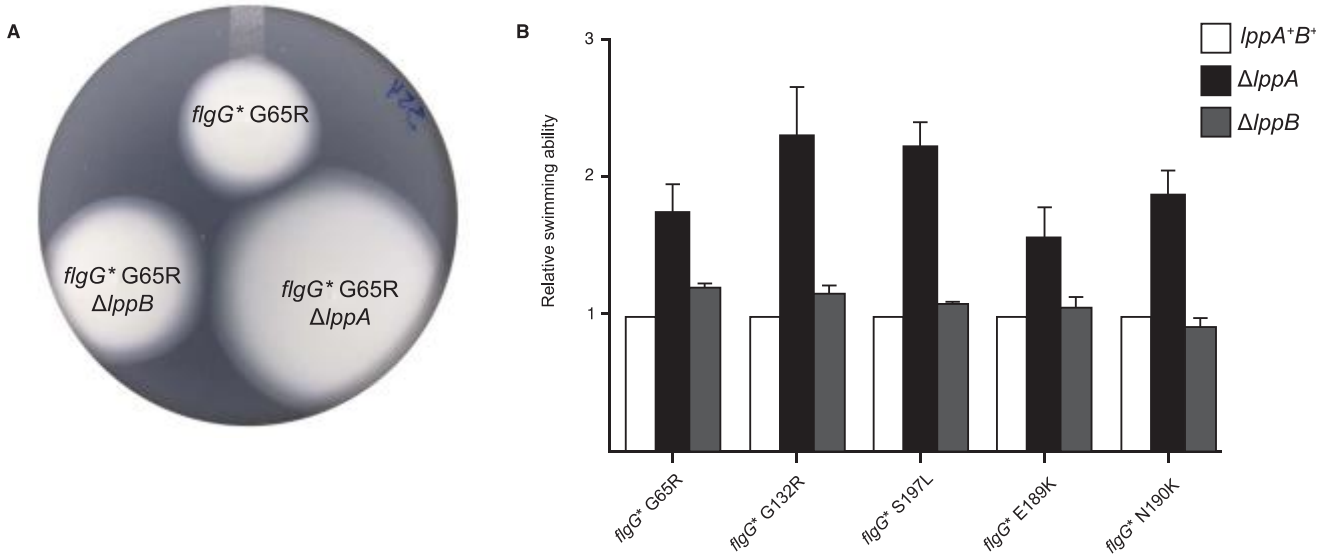

Fig. 3.S3 Deletion of *lppA* suppressed the motility defect of *flgG mutants in soft agar**
A screen for motile *flgG** revertants produced suppressor mutations that mapped to the *lpp* operon. These suppressors were all found to affect *lppA*, the equivalent of Braun's lipoprotein in *Salmonella*. To verify that suppression of the *flgG** motility defect was due to loss of *lppA*, deletions of both *lppA* and *lppB* were constructed and tested for their effect on swimming motility (A). For all five *flgG** alleles tested, deletion of *lppA* resulted in a significant increase in swim diameter, while deletion of *lppB* had little to no effect (B).

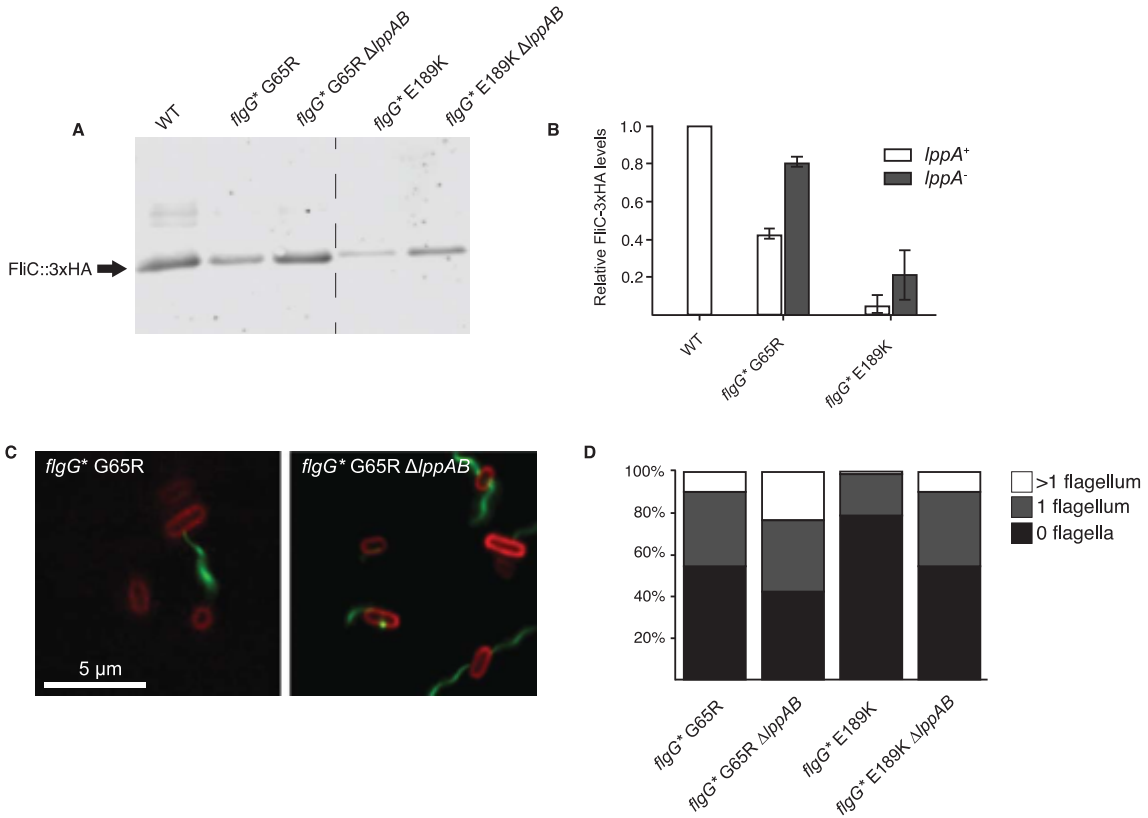

Fig. 3.S4 Deletion of LppA increases extracellular FliC secretion and filament assembly

To determine whether deletion of LppA suppressed the motility defect of filamentous distal rod mutants by increasing the likelihood of outer membrane penetration by a *flgG** hook basal body, quantitative western blots of culture supernatants probing for 3xHA-tagged flagellin (FliC::3xHA) were performed (A and B). Loss of LppA resulted in increased FliC::3xHA secretion to the culture supernatant in the *flgG** G65R and *flgG** E189K filamentous distal rod mutant backgrounds. Fluorescence microscopy was performed using these mutants in order to count the number of extracellular formed in the presence or absence of LppA (C and D). Deletion of LppA led to greater numbers of flagellated cells, and more flagella per cell, on average, in the *flgG** G65R and *flgG** E189K filamentous distal rod mutant backgrounds.

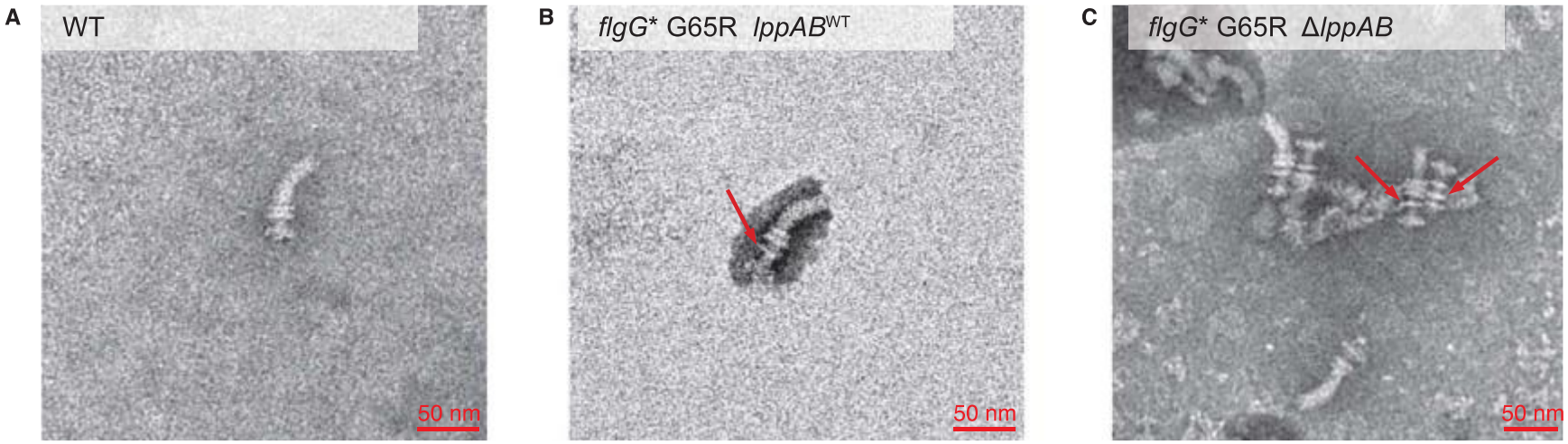

Fig. 3.S5 Deletion of *lppAB* does not prevent filamentous rod polymerization
Hook basal bodies from WT (A), *flgG** G65R *lppAB*^{WT} (B) and *flgG** G65R Δ*lppAB* (C) backgrounds were purified, negatively stained with 2% phosphotungstic acid and examined by TEM. In both *flgG** backgrounds, cells produce filamentous rods with multiple P-rings assembled along their lengh (red arrows). This demonstrated that suppression of the *flgG** motility defect upon deletion of *lppA* was not due to prevention of filamentous rod assembly.

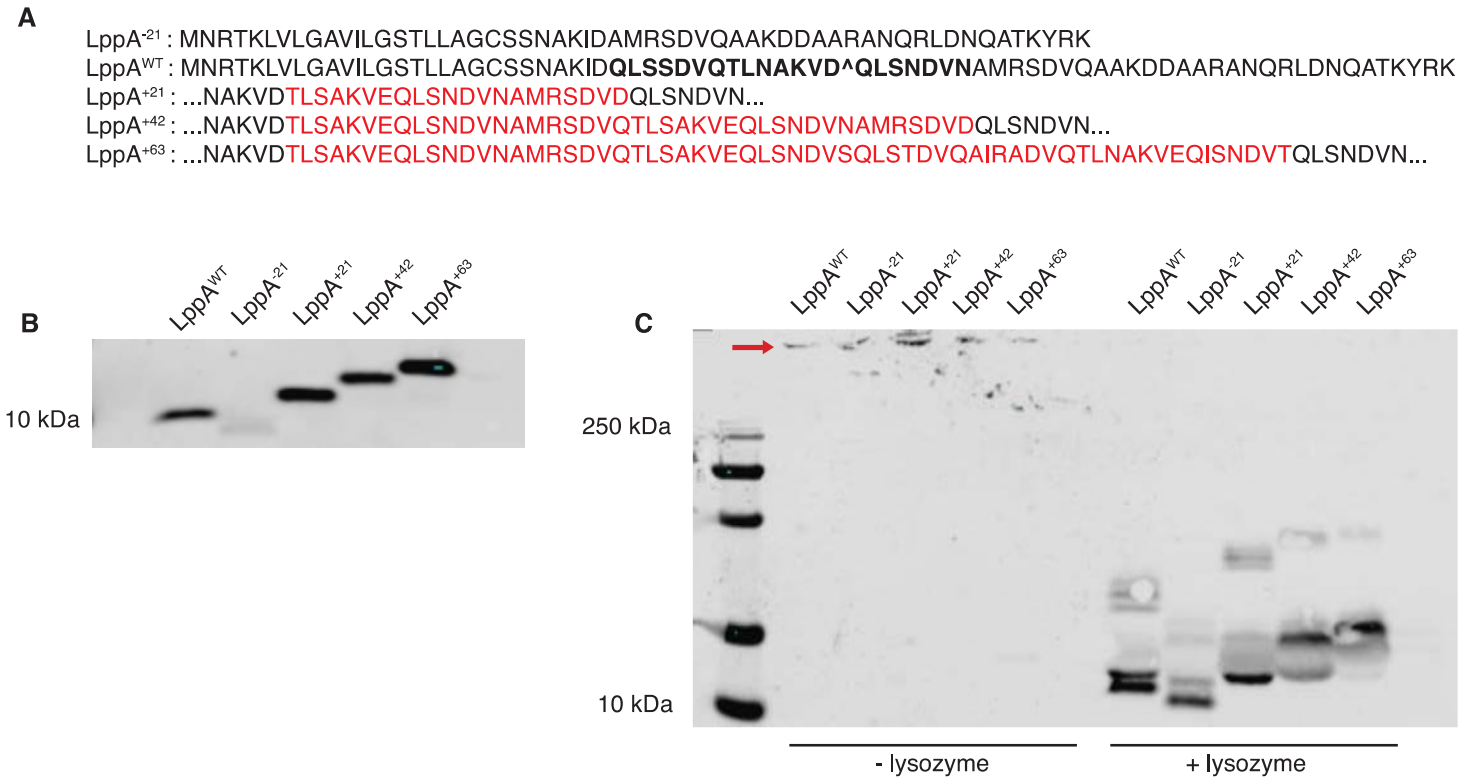

Fig. 3.S6 Longer variants of LppA were expressed and crosslinked to the cell wall
Length variants of LppA were constructed by inserting (red lettering) or deleting heptad repeats (residues deleted from $LppA^{WT}$ indicated with bold lettering) between residues D42 and Q43 (^) of wild type LppA (A). Western blots probing for LppA demonstrated that all length variants of LppA are expressed (B, cell lysate), secreted to the periplasm and crosslinked to the cell wall (C: purified cell sacculi with and without lysozyme digestion). In the absence of lysozyme treatment, the cell sacculus remains intact and prevents LppA crosslinked to peptidoglycan from migrating through an SDS-PAGE gel due to size exclusion (red arrow).

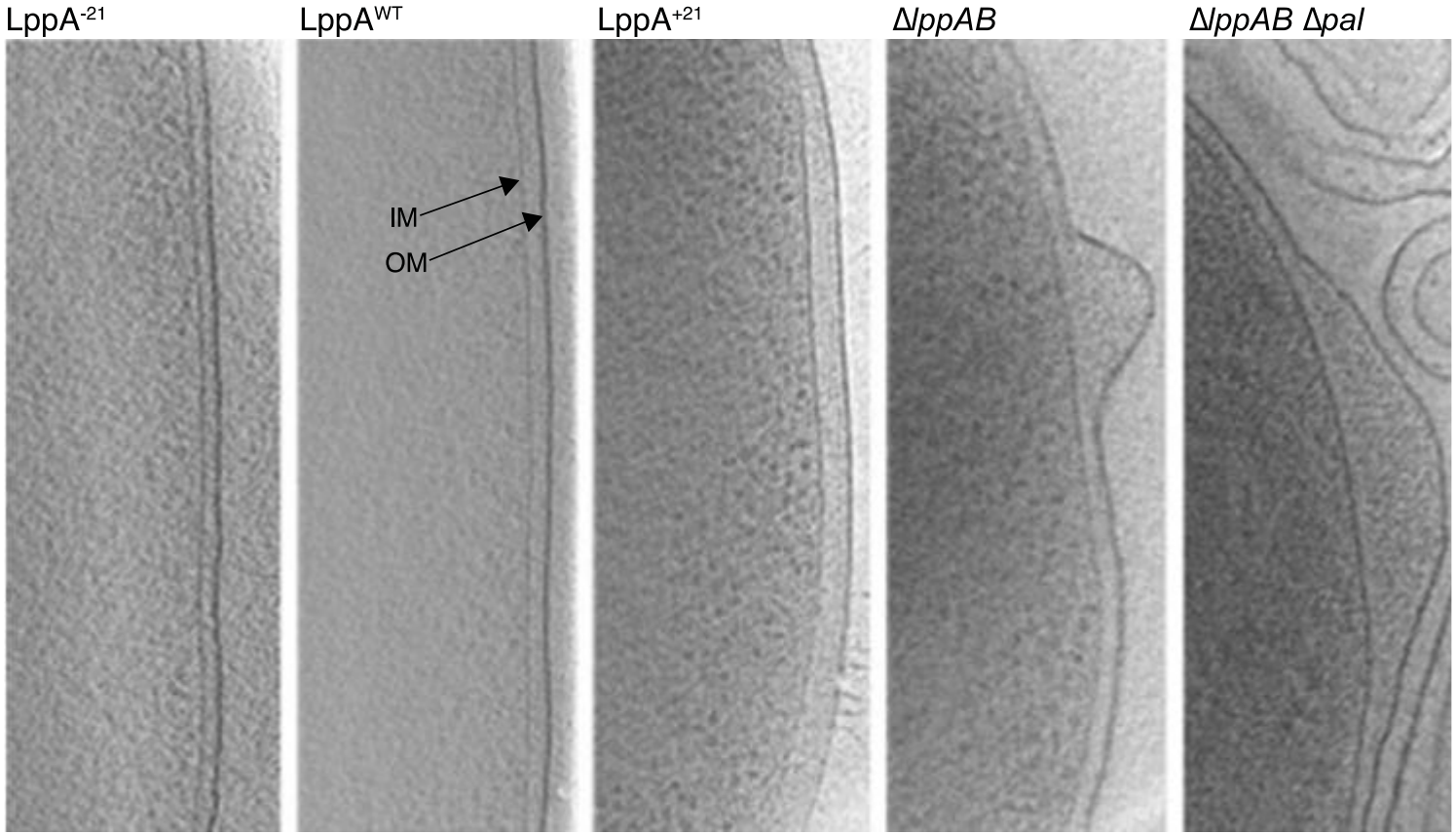

Fig. 3.S7 LppA is a major deteminant of periplasmic spacing and outer membrane stability
Electron micrographs of frozen hydrated cells demonstrated that altering the length of LppA caused a concomitant change in inner membrane (IM) to outer membrane (OM) spacing. In the absence of LppA (Δ*lppAB*), the outer membrane pulls away, or blebs, from the cell body. The blebbing phenotype was exacerbated when pal was deleted in addition to *lppAB* (Δ*lppAB* Δ*pal*).

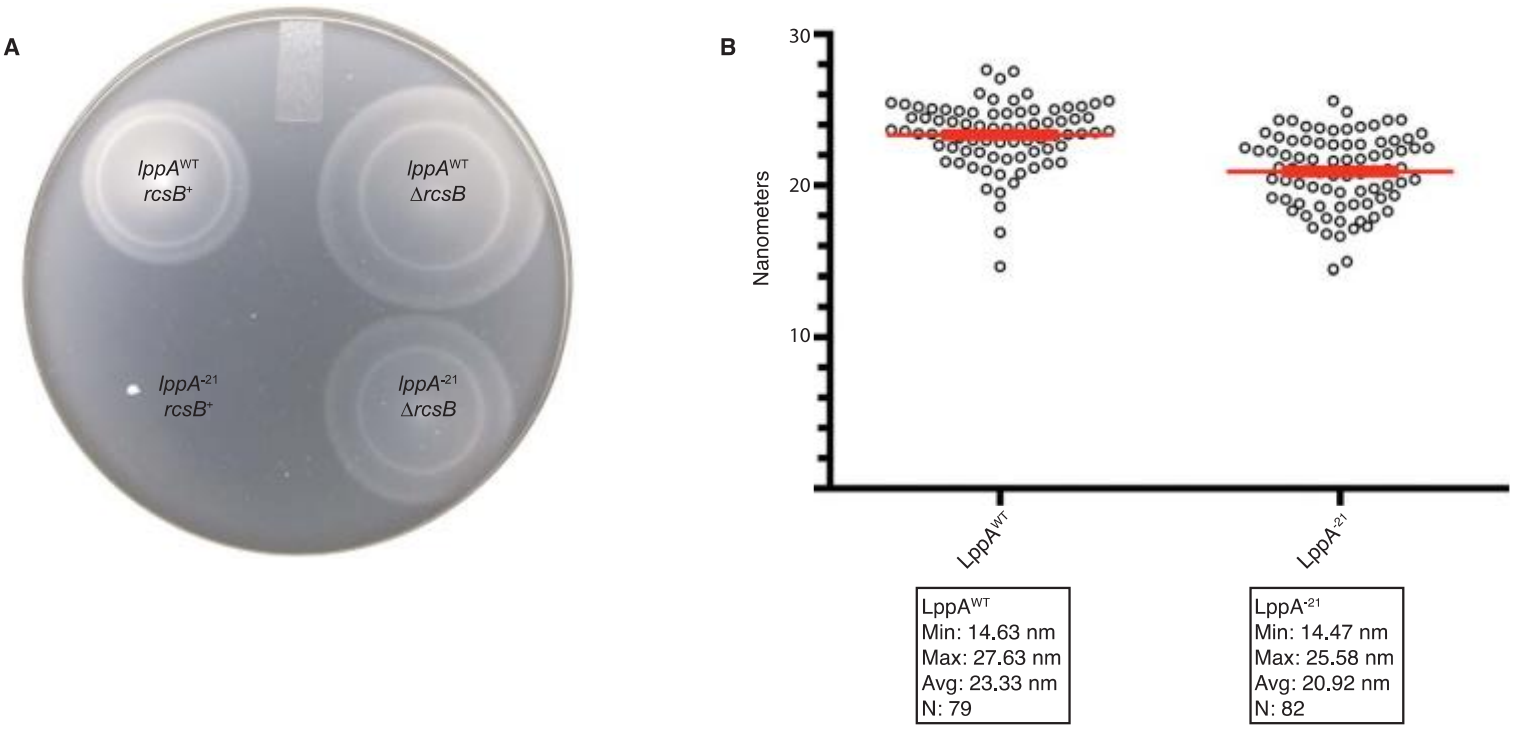

Fig. 3.S8 Shortening LppA resulted in shorter rods

Initial attempts to isolate rods from strains harboring a length variant of LppA deleted for 3 heptad repeats ($LppA^{-21}$) were unsuccessful. Using a flagellar Class I gene transcriptional reporter (*flhC5213*::Mu*dJ*), we discovered that flagellar gene expression is repressed in LppA-21 backgrounds (data not shown). We then knocked out known repressors of flagellar gene expression in the $LppA^{-21}$ background and assayed for motility in swim agar (0.3% agar conc.). Deletion of *rcsB*, a response regulator involved in responding to outer membrane stress, was found to restore motility to nearly wild-type levels in the $LppA^{-21}$ background (A). Rod structures were purified, negatively stained with 2% phosphotungstic acid and observed by TEM. Rods produced in the $LppA^{-21}$ were found to be shorter on average than those produced in the LppAWT (B, significance: $p = <0.0001$, student's two-tailed t-test, N=2, data are mean +/- SEM).

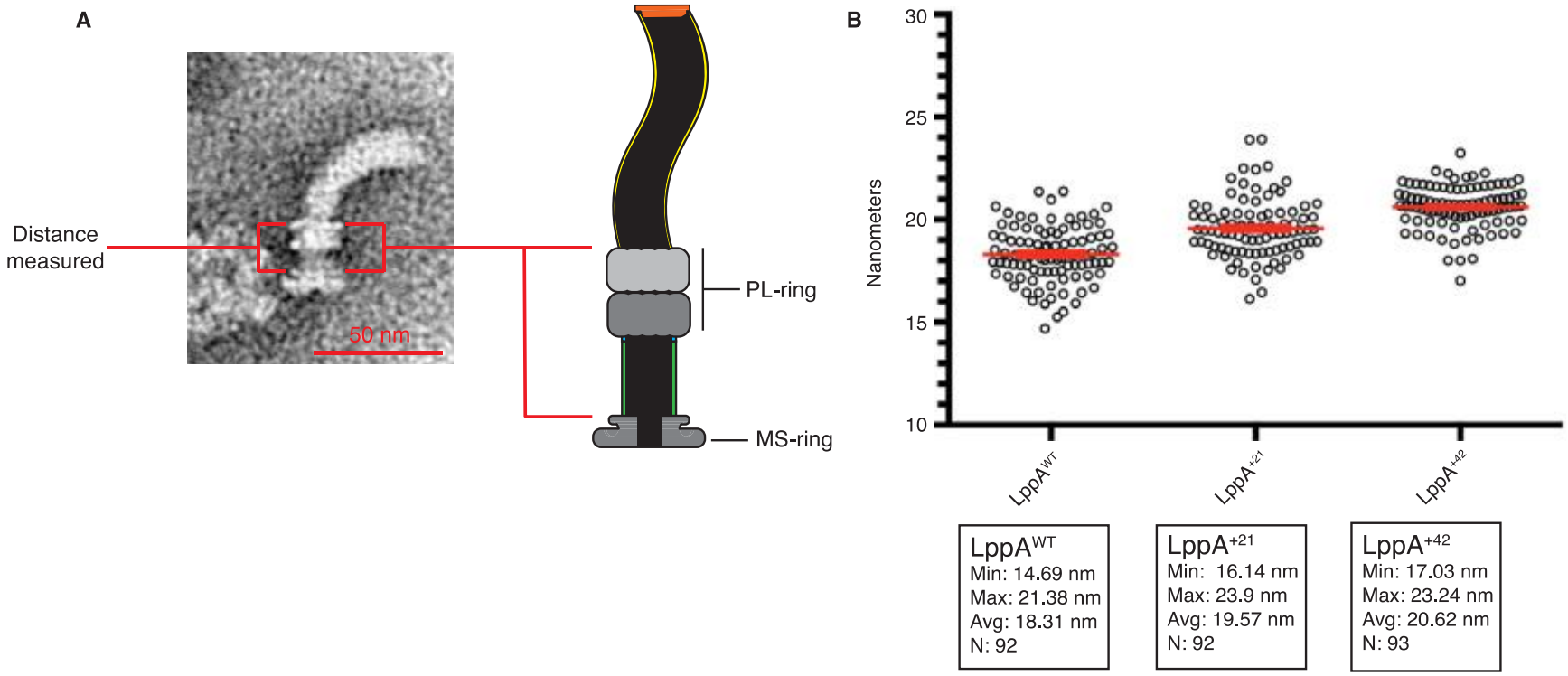

Fig. 3.S9 Lengthening LppA increased MS-ring to PL-ring distance
Hook basal bodies (HBBs) were purified from strains expressing $LppA^{WT}$, $LppA^{+21}$ and $LppA^{+42}$ (TH22638-22640), negatively stained and observed by TEM for measurement of MS-ring to PL-ring distance (A). The distances between the top of the MS-ring to the top of the PL-ring complex (red brackets) were measured in ImageJ (NIH) and plotted using Graphpad Prism (B). The MS-ring-to-PL-ring was found to increase as the length of LppA increased (significance: p = <0.0001, one-way ANOVA, N=2, data are mean +/- SEM).

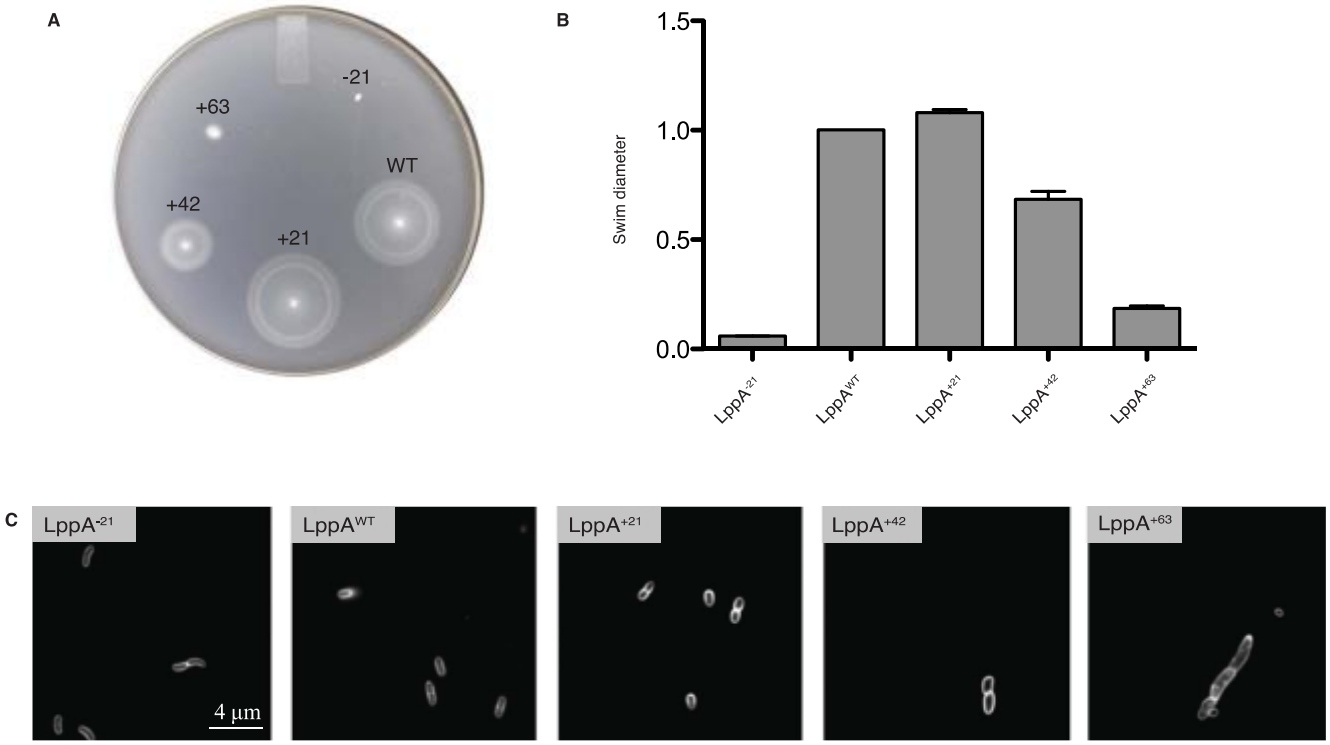

Fig. 3.S10 Altering the length of LppA affected the swimming ability and morphology of *Salmonella*
The swimming ability of mutants harboring LppA length variants was assayed using soft agar swim plates (A and B). Deletion of 21 residues abolished swimming motility, while addition of 42 or 63 residues reduced the apparent swim rate relative to WT. Addition of 21 residues to LppA increased the apparent swim rate to a small degree. All length variants were unable to swarm on 0.5% swarm agar plates (not shown). Cells from each LppA length mutant were stained with FM-43 membrane dye and observed by fluorescence microscopy (C). Cell morphology became increasingly abnormal and the growth rate in liquid LB media slowed (not shown) as the length of LppA grew longer.

Table 3.S1: List of strains used in this study

Strain	Genotype
TH437	Wild Type (LT2) strain of *Salmonella typhimurium*
TH21911	Δ*lppAB1*::*tetRA*[a]
TH21912	Δ*lppA2*::FKF[b]
TH21913	Δ*lppB3*::FCF[c]
TH22524	Δ*flgDE7756* Δ*flgH7662* pTrc99AFF4
TH22525	Δ*flgDE7756* Δ*flgH7662* pTrc99AFF4-*flgG+*
TH22526	ΔlppAB1::tetRA *flgG6705* (G65R)
TH22527	ΔlppAB1::tetRA *flgG6706* (G132R)
TH22528	Δl*ppAB1*::*tetRA flgG6707* (S197L)
TH22529	Δ*lppAB1*::tetRA *flgG6764* (E189K)
TH22530	Δ*lppAB1*::tetRA *flgG6750* (N190K)
TH22531	Δ*lppA2*::FKF *flgG6705*
TH22532	Δ*lppA2*::FKF *flgG6706*
TH22533	Δ*lppA2*::FKF *flgG6707*
TH22534	Δ*lppA2*::FKF *flgG6764*
TH22535	Δ*lppA2*::FKF *flgG6750*
TH22536	Δ*lppB3*::FCF *flgG6705*
TH22537	Δ*lppB3*::FCF *flgG6706*
TH22538	Δ*lppB3*::FCF *flgG6707*
TH22539	Δ*lppB3*::FCF *flgG6764*

Table 3.S1 continued

TH22540	Δ*lppB3*::FCF *flgG6750*
TH22543	Δ*lppAB7*[d]
TH22549	Δ*lppB3*::FCF *lppA11*[e] (lppA^{+21})
TH22550	Δ*lppB3*::FCF *lppA12*[f] (lppA^{+42})
TH22551	Δ*lppB3*::FCF *lppA13*[g] (lppA^{+63})
TH22552	Δ*lppB3*::FCF Δ*lppA14*[h] (lppA^{-21})
TH22553	*fliC7746*::3xHA Δ*hin5717*::FRT *flgG6705*
TH22554	*fliC7746*::3xHA Δ*hin5717*::FRT *flgG6706*
TH21732	*fliC7746*::3xHA Δ*hin5717*::FRT *flgG6707*
TH21733	*fliC7746*::3xHA Δ*hin5717*::FRT *flgG6764*
TH21734	*fliC7746*::3xHA Δ*hin5717*::FRT *flgG6750*
TH22555	*fliC7746*::3xHA Δ*hin5717*::FRT *flgG6705* Δ*lppAB1*::*tetRA*
TH22556	*fliC7746*::3xHA Δ*hin5717*::FRT *flgG6706* Δ*lppAB1*::*tetRA*
TH22557	*fliC7746*::3xHA Δ*hin5717*::FRT *flgG6707* Δ*lppAB1*::*tetRA*
TH22558	*fliC7746*::3xHA Δ*hin5717*::FRT *flgG6764* Δ*lppAB1*::*tetRA*
TH22559	*fliC7746*::3xHA Δ*hin5717*::FRT *flgG6750* Δ*lppAB1*::*tetRA*
TH22562	Δ*lppA16* (DK78)[i]
TH22563	Δ*lppA16 flgG6705*
TH22564	Δ*lppA16 flgG6706*

Table 3.S1 continued

TH22565	Δ*lppA16 flgG6707*
TH22566	Δ*lppA16 flgG6764*
TH22567	Δ*lppA16 flgG6750*
TH22568	Δ*pal*::FKF
TH22569	Δ*pal*::FKF Δ*lppAB7*
TH22574	Δ*flgDE7756* Δ*flgH7662* Δ*lppB3*::FCF Δ*prgH73*::*tetRA*
TH22575	Δ*flgDE7756* Δ*flgH7662* Δ*lppB3*::FCF Δ*prgH73*::*tetRA lppA11*
TH22576	Δ*flgDE7756* Δ*flgH7662* Δ*lppB3*::FCF Δ*prgH73*::*tetRA lppA12*
TH22577	Δ*flgDE7756* Δ*flgH7662* Δ*lppB3*::FCF Δ*prgH73*::*tetRA lppA13*
TH22578	Δ*lppAB17*::FKF[j]
TH22579	Δ*flgDE7756* Δ*flgH7662* Δ*lppB3*::FCF Δ*lppA14*
TH22580	Δ*flgDE7756* Δ*flgH7662* Δ*lppB3*::FCF Δ*rcsB139*::*tetRA*
TH22581	Δ*flgDE7756* Δ*flgH7662* Δ*lppB3*::FCF Δ*rcsB139*::*tetRA* Δ*lppA14*
TH22586	*fliC6500* (T237C) *flgG6705 motA5461*::Mu*dJ*
TH22587	*fliC6500* (T237C) *flgG6764 motA5461*::Mu*dJ*
TH22588	*fliC6500* (T237C) *flgG6705 motA5461*::Mu*dJ* Δ*lppAB1*::*tetRA*
TH22589	*fliC6500* (T237C) *flgG6764 motA5461*::Mu*dJ* Δ*lppAB1*::*tetRA*
TH22618	Δ*lppB3*::FCF Δ*rcsB139*::*tetRA*
TH22619	Δ*lppB3*::FCF Δ*rcsB139*::*tetRA* Δ*lppA14* (LppA^{-21})

Table 3.S1 continued

TH22634	Δ*flgDE7756* Δ*flgH7662* Δ*lppB3*::FCF Δ*sseA-ssaU*::FKF Δ*prgH73*::*tetRA*
TH22635	Δ*flgDE7756* Δ*flgH7662* Δ*lppB3*::FCF Δ*sseA-ssaU*::FKF Δ*prgH73*::*tetRA lppA11*
TH22636	Δ*flgDE7756* Δ*flgH7662* Δ*lppB3*::FCF Δ*sseA-ssaU*::FKF Δ*prgH73*::*tetRA lppA12*
TH22637	Δ*flgDE7756* Δ*flgH7662* Δ*lppB3*::FCF Δ*sseA-ssaU*::FKF Δ*prgH73*::*tetRA lppA13*
TH22638	Δ*lppB3*::FCF Δ*pal*::FKF
TH22639	Δ*lppB3*::FCF Δ*pal*::FKF *lppA11*
TH22640	ΔlppB3::FCF Δ*pal*::FKF *lppA12*

[a.] *tetRA* cassette replaces *lppA* and *lppB*, leaves first 5 residues of *lppA* and last five residues of *lppB*.

[b.] FRT-*neo*-FRT (FKF (KmR)) deletes all of *lppA* except for the first and last five residues.

[c.] FRT-*cat*-FRT (FCF (CmR)) deletes all of *lppB* except for the first and last five residues.

[d.] Clean deletion of *lppAB*, leaves first five residues of lppA and last five residues of *lppB*.

[e.] *lppA* length variant with 21 residues (3 heptad repeats) added between residues 42 and 43 of WT *lppA*.

[f.] *lppA* length variant with 42 residues (6 heptad repeats) added.

[g.] *lppA* length variant with 63 residues (9 heptad repeats) added.

[h.] *lppA* length variant with 21 residues (3 heptad repeats) deleted.

[i.] *lppA* mutant lacking the C-terminal lysine residue required for crosslinking to the cell wall peptidoglycan.

[j.] FKF replaces *lppA* and *lppB*, leaves first five residues of *lppA* and last five of *lppB*.

Table 3.S2 List of primers used in this study

#	Sequence
6572	pal::FXFa Fw 5’-attgattactaaaggaattaaagaaatgcaactgaacaaagtgtaggctggagctgcttc-3’
6573	pal::FXF Rv 5’-tctgaagttactgctcatgcaattctcttagtaaaccagtcatatgaatatcctccttag-3’
6574	lppA/B::FXF Fw 5’-taactcaatctagagggtattaataatgaatcgtactaaagtgtaggctggagct gcttc-3’
6575	lppA/B::FXF Rv 5’-cgccattttatattgtgcgtcaaattatttacagatgcggcatatgaatatcctccttag-3’
6576	lpp-tetR 5’-gttccgacgttcaggctgctaaagacgacgcagctcgcgctttaagacccactttcacat-3’
6577	lpp-tetA 5’-gctcagcgtctgtacatcggaagacaactgatcgattttagcctaagcacttgtctcctg-3’
6622	DlppAB::tetR 5’-ttaactcaatctagagggtattaataatgaatcgtactaaattaagacccactttcacat-3’
6623	DlppAB::tetA 5’-atgtgcgccattttatattgtgcgtcaaattatttacagatgctaagcacttgtctcctg-3’
6626	lppB Rv 5’-attgtgcgtcaaattatttacagat-3’
6627	lppA Fw 2 5’-cgctacatggagattaactcaat-3’
6645	lppB::FXF Fw 5’-ataaccacacaaagtataatgttattgttatgaaccgtacgtgtaggctggagctgcttc-3’
6646	lppA::FXF Rv 5’-cgccatttttattacgcaggtactattacttacggtatttcatatgaatatcctccttag-3’
6681	lppA aa42/43::tetR 5’-gctgtcttctgacgttcagactctgaacgctaaagttgacttaagacccacttt cacat-3’
6682	lppA aa42/43::tetA 5’-gaacgtcggaacgcattgcgttcacgtcgttgctcagctgctaagcacttgtc tcctg-3’
6683	lppA::lppB Fw 5’-ctgtcttctgacgttcagactctgaacgctaaagttgacacgctgagcgctaaagttgag-3’
6686	lppA::21aa-lppB Rv 5’-gaacgtcggaacgcattgcgttcacgtcgttgctcagctgatcaacgtc ggaacgcattg-3’
6732	pal Fw 5’-ttccggcaactgatggtcag-3’

Table 3.S2 continued

6733 pal Rv 5'-cgctatgccaaccagtaacga-3'

6743 lpp1b C-term tetR 5'-cacgatgtgcgccatttttattacgcaggtactattacttttaagacccactttcacatt-3'

6744 lpp1 C-term tetA 5'-cgctaaccagcgtctggacaaccaggctactaaataccgtctaagcacttgtctcctg-3'

6788 lpp1 -21 residues 5'-ctgcgtcgtctttagcagcctgaacgtcggaacgcattgcatcgattttag cgttgctggagcaaccagccagcagagta-3'

7115 lppA Del. K78 5'-aatggcgcacgatgtgcgccatttttattacgcaggtactattaacggtatttagtagcctgg ttgtccagacgctggttagcgcgagct-3'

7188 Lpp+63 mid section 5'-ctgagcgctaaagttgagcagttgtctaacgacgttaatgcgatgcgttctgacgtcc aaacattgtcagcgaaggtcgaacaattatccaac-3'

7189 Lpp+63 end section 5'-gttcaactttcgcattcagggtctgcacgtcggcacggatcgcctggacg tcggtagacagctgagagacatcgttggataattgttcgac-3'

7190 Lpp +42 mid section 5'-acgctgagcgctaaagttgagcagttgtctaacgacgttaatgcgatgcgt tctgacgtccaaacattgtcagcgaaggtcgaacaattatcgaat-3'

7191 Lpp+ 63 fill 5'-gaacgtcggaacgcattgcgttcacgtcgttgctcagctgggtcacatcgtt gctgatctgttcaactttcgcattc-3'

7192 Lpp+42 fill 5'-gaacgtcggaacgcattgcgttcacgtcgttgctcagctggtccacgtc cgatcgcatggcatttacatcattcgataattgttcgac-3'

[a]: FXF is used here as an abbreviation for the FRT-CmR-FRT and/or FRT-KmR-FRT antibiotic resistance cassettes
[b]: lpp1 refers to *lppA*

CHAPTER 4

THE FlgG L-STRETCH: DISTAL ROD RIGIDITY AND ITS CONTRIBUTION TO DISTAL ROD LENGTH CONTROL

In progress

Introduction

The work presented in this dissertation has demonstrated that distal rod length is determined by the distance between the peptidoglycan and the outer membrane (1). However, the molecular underpinnings of distal rod length control remained a mystery. In other words, the discovery that the outer membrane limits distal rod growth revealed nothing about the specific conformational changes or intermolecular interactions in the distal rod that prevent addition of additional FlgG subunits upon reaching the outer membrane.

As discussed in Chapters 2 and 3, missense and small deletion mutations that clustered in two regions (N-terminal and C-terminal) of *flgG* gave rise to the filamentous distal rod phenotype. While the C-terminal *flgG** mutations are dispersed along ~100

codons of *flgG*, the ~15 *flgG** mutations at the N-terminal end cluster tightly within codons 52-70 of *flgG* (2-3). This suggested that residues ~50-70 of FlgG play a key role in terminating distal rod growth.

The structure of the *Salmonella* HBB has recently been solved by cryo-EM (4). However, the conformation of the region (residues 40-75) of FlgG-encompassing residues 50-70 could not be determined. This suggested that this FlgG domain may be flexible and/or unstructured in the distal rod. The structure of the *C. jejuni* hook has recently been solved, including the region of *C. jejuni* FlgE ($FlgE_{Cj}$) that is homologous to residues 40-75 of *Salmonella* FlgG (Fadel Samatey, unpublished data). This stretch of amino acids was termed the "L-stretch," as it juts out from the $FlgE_{Cj}$ monomer at a roughly 90° angle, giving this domain the shape of the letter L.

In the *C. jejuni* hook, the L-stretch of one $FlgE_{Cj}$ subunit makes contact with six other $FlgE_{Cj}$ subunits across three hook protofilaments. The $FlgE_{Cj}$ L-stretch makes more intersubunit contacts than any other domain of the $FlgE_{Cj}$ hook. With each $FlgE_{Cj}$ molecule possessing an L-stretch that engages in numerous intersubunit interactions, the *C. jejuni* hook exhibits a highly interwoven character not found in the *Salmonella* hook. It is thought that the interdigitation of $FlgE_{Cj}$ subunits provided by the L-stretch enhances the strength and rigidity of the *C. jejuni* hook. A more robust HBB relative to *Salmonella* is thought to be important for *C. jejuni*'s lifestyle, allowing it to swim through the highly viscous mucous of its hosts' gastrointestinal tracts that render *Salmonella* immotile. Deletion of the *C. jejuni* L-stretch resulted in a fragile flagellum that would break at the distal rod/hook interface. This result suggests that the L-stretch provides axial flagellar structures with stability and torsional strength (5-6 and Morgan Beeby's preliminary

data).

Rigidity is another divergent characteristic between the *C. jejuni* and *Salmonella* hook. The *Salmonella* hook grows to a final length of 55 nm +/- 6 nm and is highly flexible. The *C. jejuni* hook, in contrast, polymerizes to a mature length of ~105 nm and is less flexible than that of *Salmonella* (5-8). The increased rigidity of the *C. jejuni* hook is thought to have necessitated the evolution of a longer hook. A stiffer but longer hook would allow for full articulation of the filament relative to the cell body while also being significantly stronger than the *Salmonella* hook. Further work with both *C. jejuni* and *Salmonella* will be required to determine whether this is in fact the case.

Additionally, recent work has demonstrated that increasing the length of the *Salmonella* FlgE (FlgE$_{Se}$) L-stretch to more closely resemble the FlgE$_{Cj}$ L-stretch decreases the flexibility of the hook. In *Salmonella* and *E. coli*, the L-stretch in FlgE has been truncated from the ~50 residues found in FlgG to ~30 residues. By engineering a FlgE$_{Se}$ chimera containing a portion of the FlgG L-stretch, Fujii *et al*. demonstrated that increasing the length of the FlgE$_{Se}$ L-stretch caused the hook to become rigid (4). This result is in agreement with similar TEM studies performed in our lab with FlgE$_{Se}$ chimera containing portions of the FlgG L-stretch. When we isolated HBB's from strains harboring FlgE-FlgG chimera, hooks in these backgrounds appeared to be more rigid (our unpublished data).

To further investigate the role of the L-stretch in promoting rigidity in flagellar axial structures, and the contribution of the L-stretch to distal rod length control, we constructed a *flgG* mutant deleted for a large portion of the L-stretch (residues 51-66 of FlgG (FlgG$^{\Delta 51\text{-}66}$)). We were specifically interested in determining i) whether the L-

stretch was required for assembly of the distal rod, ii) whether the L-stretch was required for P-ring assembly and iii) the effect of L-stretch truncation on distal rod rigidity.

Materials and Methods

Strain Construction

All strains constructed in this work were made in *Salmonella enterica* spp. Typhimurium LT2 background (Tables 4.1 and 4.2). For construction of *flgG* L-stretch deletions, the λRed recombinase system was employed as previously described (11). Briefly, a tetracycline resistance cassette (*tetRA*) was introduced into TH4702 that deleted codons 51-66 of the WT *flgG* gene. Transformants were selected on LB agar containing tetracycline (12.5 μg/mL). Replacement of the *tetRA* cassette, leaving clean *flgG* L-stretch deletions, was accomplished by electroporating dsDNA fragments possessing ~40 bp of homology to the *flgG* gene directly flanking the 5' and 3' ends of the *tetRA* cassette. Tetracycline sensitive (Tc^S) transformants were selected on agar media containing fusaric acid (2.4 μg/mL) and anhydrotetracycline (0.2 μg/mL). All transductional crosses to introduce *flgG* L-stretch deletions into various genetic backgrounds were carried out with using phage P22 *HT105/int*.

Electron Microscopy

To visualize flagellar structures from *flgG* L-stretch strains, structures were isolated according to the Aizawa method with minor modifications (12). Briefly, cells were incubated in 500 mL LB at 37° C with aeration until the cultures had reached $O.D._{600}$ 0.8-1.0, at which point they were placed on ice. Chilled cultures were pelleted

and resuspended in ice-cold sucrose buffer, to which was added lysozyme (2 mg/mL) and EDTA. Cell suspensions were incubated with stirring, on ice, for ~1 hour at which point they were shifted to 37° C, with stirring, for ~30 additional minutes.

Following lysozyme/EDTA digestion, 10% Triton X-100 (final concentration: 0.1%) was slowly dripped into the suspensions and allowed to incubate with stirring for ~5 minutes, at which point $MgCl_2$ was added dropwise to a final concentration of 0.1 M, followed by an additional ~5 minutes of incubation at RT. Cell lysates were centrifuged at ~4000 x g for 10 minutes to remove unlysed cells. Lysates were then adjusted to pH 11 by addition of 5N NaOH. Lysates were then centrifuged at high speed (60,000 x g for 1 hr at 10° C) to pellet flagellar structures. Structures were resuspended in pH 11 buffer and centrifuged at high speed. A second resuspension/centrifugation step using TET buffer was performed. Finally, structures were resuspended in 200 μL of TET buffer.

To visualize purified flagellar structures, ~3 μL of sample was applied to glow-discharged, formvar-coated copper TEM grids. Negative staining was performed using 2% aqueous phosphotungstic acid (pH ~7). Micrographs were captured using a JEOL JEM-1400 TEM coupled to a Gatan CCD camera. Contrast adjustment and image cropping were performed using NIH ImageJ software (version 1.50i).

Results

The flgG$^{\Delta 51\text{-}66}$ Mutant Phenocopies the flgG Mutants*

Based on the *flgG** alleles we had previously isolated and a predicted structure of FlgG that included the L-stretch (provided by Dr. Fadel Samatey), we constructed three L-stretch deletion mutants, FlgG$^{\Delta 51\text{-}66}$, FlgG$^{\Delta 46\text{-}66}$ and FlgG$^{\Delta 43\text{-}73::Gly\text{-}Gly}$, and tested their

effects on swimming motility and flagellar morphology.

The *flgG*$^{\Delta 51\text{-}66}$ deletion mutant was engineered in an otherwise wild type strain of *Salmonella* (i.e. motile). Removal of residues 51-66 resulted in small colonies relative to the parent strain. Growth of the *flgG*$^{\Delta 51\text{-}66}$ mutant was further retarded on media containing bile salts and the strain was essentially non-motile in swim agar. This suggested that deletion of residues 51-66 from FlgG led to filament polymerization in the periplasm as several of the original, spontaneous *flgG** mutations also exhibited the same phenotype. All subsequent *flgG* L-stretch deletion mutants were constructed in either a Δ*flhD*::FKF Δ*araBAD*::*flhD*$^{+}$*C*$^{+}$ or Δ*fliK* Δ*araBAD*::*fliK*$^{+}$ background. This allowed us to prevent the cytotoxic effects associated with periplasmic filament polymerization by withholding arabinose (and thereby preventing *flhDC* expression) from the culture medium.

When the *flgG*$^{\Delta 51\text{-}66}$ Δ*flhD*::FKF Δ*araBAD*::*flhD*$^{+}$*C*$^{+}$ Δ*flgDEH* strain was grown in liquid culture without arabinose added, the cell morphology was indistinguishable from WT by light microscopy. However, following arabinose induction at O.D.$_{600}$ ~0.4, the cells became abnormal in appearance over time, starting at ~30 minutes post-induction. The cell shape became elongated and contorted, suggesting that filaments were assembling in the periplasm.

All of the *flgG** mutants we had previously isolated were poorly motile in motility agar following overnight incubation. However, when incubated in motility agar for an extended period of time, motile revertants arise that swim out from the original colony, creating a motile "flare." This increased motility is the result of suppressing mutations that alleviate the swimming defect caused by the original *flgG** mutation. As

discussed in Chapter 3, one class of suppressors resulted from a deletion in the gene encoding Braun's lipoprotein, *lppA*. Suppressing mutations were also isolated in the P-ring structural gene (*flgI*), the rod-cap gene (*flgJ*) and second site suppressors in *flgG*.

We wanted to determine if suppressors of the *flgG*$^{\Delta 51\text{-}66}$ allele could be isolated and how they would compare to the *flgG** suppressing alleles that had already been obtained. Fifty independent colonies were inoculated in swim agar and incubated for 24-36 hours at which point a number of motile *flgG*$^{\Delta 51\text{-}66}$ motile revertants had arisen. Ten independent motile revertants (flares) were isolated, single colony purified and tested by P22-mediated linkage for suppressors specific to the *flg* region. Nine out of the ten revertants were linked to the *flg* operon. Additionally, introduction of an *lppAB* deletion allele suppressed the motility defect of the *flgG*$^{\Delta 51\text{-}66}$ mutant to a small degree.

Taken together, the morphological observations and results from motility experiments suggested that the *flgG*$^{\Delta 51\text{-}66}$ allele can be regarded as a synthetic *flgG** mutation.

The FlgG$^{\Delta 51\text{-}66}$ Distal Rod is Flexible

Previous work has shown that *flgG** mutations allow the distal rod to continue polymerizing past the WT length of ~18 nm to ~70 nm in Δ*flgHI fliK*$^{+}$ genetic backgrounds (2-3). Once the rod has grown to ~70 nm, the FliK-dependent secretion specificity switch occurs and periplasmic filament assembly initiates on the tip of the FlgG* distal rod. Although the preceding lines of evidence indicated that this was also the case with the *flgG*$^{\Delta 51\text{-}66}$ allele, we sought to confirm this by TEM analysis. Also, distal rods previously isolated from *flgG** backgrounds appear to retain their rigidity (i.e. they

are straight) (2-3, 9). Given that the L-stretch is truncated in $FlgE_{Se}$, we wanted to determine whether the large *flgG* L-stretch deletion (*flgG*$^{\Delta 51\text{-}66}$) affected the rigidity of the rod.

Flagellar structures from the *flgG*$^{\Delta 51\text{-}66}$ Δ*flhD*::FKF Δ*araBAD*::*flhD*$^{+}$*C*$^{+}$ Δ*flgDEH* background were isolated and observed by TEM. The majority of structures isolated and observed by TEM from this background appeared to be rigid (i.e. straight). However, a number of the structures possessed distal rods that were bent at angles ≥90° with filaments and MS-rings attached, indicating that the FlgG$^{\Delta 51\text{-}66}$ rod possessed some degree of flexibility (Fig. 4.1). This suggests that, *in vivo*, the distal rods of all *flgG*$^{\Delta 51\text{-}66}$ Δ*flgDEH* structures possessing filaments must bend as the filaments are entirely periplasmic and therefore must deflect off the outer membrane in order to accommodate the rigid flagellar filament. Since most FlgG$^{\Delta 51\text{-}66}$ rods were straight, residues or domains other than the L-stretch of FlgG are presumed to contribute to rod rigidity and hook flexibility. When removed from a cellular context and applied to an EM sample grid, these interactions could cause the distal rod to straighten *ex vivo*. In an attempt to examine the effect of a larger deletion of the FlgG L-stretch on rod rigidity, we constructed *flgG*$^{\Delta 46\text{-}66}$ and *flgG*$^{\Delta 43\text{-}76::Gly\text{-}Gly}$ mutants . However, cells in these backgrounds did not display the morphological abnormalities found in the *flgG*$^{\Delta 51\text{-}66}$ background, and we were not able to isolate flagellar structures from either the *flgG*$^{\Delta 46\text{-}66}$ or *flgG*$^{\Delta 43\text{-}76::Gly\text{-}Gly}$ backgrounds. This suggests that at least some portion of the L-stretch is required for rod polymerization.

Rod structures isolated from the *flgG**$^{\Delta 54\text{-}57}$ allele have been isolated and visualized by TEM. Distal rods from this background formed filamentous rods lacking P-

rings, suggesting that this portion of the L-stretch may be involved in P-ring assembly. However, when structures from the *flgG*$^{\Delta 51\text{-}66}$ Δ*fliK* Δ*araBAD*::*fliK*$^{+}$ Δ*flgDEH* genetic background were examined by TEM, we observed basal bodies possessing multiple P-rings along the length of the FlgG$^{\Delta 51\text{-}66}$ distal rod (Fig. 4.2), suggesting that residues 51-66 were not important for recognition of the distal rod by FlgI subunits. The observation that the *flgG**$^{\Delta 54\text{-}57}$ allele prevents P-ring assembly, but that deletion of residues 51-66 from FlgG does not affect P-ring assembly, is enigmatic and will require further investigation.

Discussion and Future Directions

The distal rod (FlgG) and the hook (FlgE) share common ancestry and architecture (4). However, the hook is remarkably flexible, an important feature given that its function is to act as a universal joint. In contrast, isolated rod structures are rigid. The difference in behavior between the two HBB substructures is thought to arise from two differences between the FlgG and FlgE proteins. Compared to FlgE, the L-stretch in FlgG is longer, and presumably engages in more intersubunit contacts, than the truncated FlgE L-stretch. The second major difference is the presence of a large, solvent-exposed globular domain in FlgE not present in FlgG (10).

The large globular domain (D3) of FlgE may promote bending in the hook through intersubunit D3-D3 domain repulsion and/or steric exclusion between neighboring D3 domains when two FlgE subunits are stacked upon one another in the hook. Alternatively, it may promote stabilizing interactions during hook rotation. Since the majority of isolated distal rods built from FlgG subunits (which lack a D3 domain)

with large L-stretch (i.e. *flgG*$^{\Delta 51\text{-}66}$) deletions are predominantly straight, the FlgE D3 domain may contribute to bending. One could potentially address this by insertion of the D3 domain from FlgE into FlgG$^{\Delta 51\text{-}66}$ followed by isolation of rod structures and visualization by TEM to determine if the distal rod becomes as flexible as the hook.

There is no evidence that a molecular ruler is utilized for distal rod length control. We have demonstrated that the outer membrane plays a role in distal rod length control by acting as a physical barrier, preventing continued distal rod polymerization beyond ~18 nm (1). However, the molecular mechanism by which the distal rod "senses" the outer membrane remains unknown. Sensing the outer membrane may involve specific conformational changes in either FlgG or in the FlgJ rod scaffold upon contact with the periplasmic face of the outer membrane. Alternatively, the available free energy (ΔG) associated with a FlgG subunit folding into its native conformation at the tip of the rod may not be large enough to overcome the energy barrier required to distort the outer membrane, which would be required to accommodate a rod longer than ~25 nm.

In either case, our experimental observations suggest that, in addition to stabilizing the flagellar driveshaft, the rigidity of the rod plays an important role in distal rod length control. By preventing the distal rod from deflecting off the inner leaflet of the outer membrane, the L-stretch ensures that termination of FlgG polymerization at the outer membrane occurs. Additionally, distal rod rigidity maintains the rod's perpendicular orientation relative to the outer membrane, which is important for L-ring polymerization and growth of the extracellular hook from the cell surface.

If it is true that *flgG** mutations increase the flexibility of the distal rods, and that this increase in flexibility is responsible for filament polymerization in the periplasm,

then reinforcing FlgG* inter-subunit interactions may restore motility in these backgrounds. To test this, we will use cysteine crosslinking to covalently bind the L-stretch of one FlgG subunit to its neighbor, resulting in a covalently networked distal rod where each subunit in the structure is bound to two of its neighbors. We predict that *flgG** alleles able to crosslink via addition of appropriately localized cysteine residues (*flgG**$^{Cys\text{-}Cys}$) will exhibit greater motility in swim agar. Furthermore, we expect that distal rods isolated from *flgG**$^{Cys\text{-}Cys}$ backgrounds will grow to WT lengths in the absence of the disulfide bond-reducing agent dithiothreitol (DTT), and filamentous in its presence. Based on the predicted structure of the distal rod, we are currently constructing Cys-Cys pairs that reside in close enough proximity in the mature structure to form disulfide bridges between neighboring FlgG molecules in the distal rod.

References

1. Cohen EJ, Ferreira JL, Ladinsky MS, Beeby M, Hughes KT, Nanoscale-length control of the flagellar driveshaft requires hitting the tethered outer membrane. *Science* 356:197-200 (2017).

2. Chevance FF *et al.*, The mechanism of outer membrane penetration by the eubacterial flagellum and implications for spirochete evolution. *Genes Dev.* 21:2326–2335 (2007).

3. Hirano T, Mizuno S, Aizawa SI, Hughes KT, Mutations in Flk, FlgG, FlhA, and FlhE that affect the flagellar Type III Secretion specificity switch in Salmonella enterica. *J. Bacteriol.* 191:3938-3949. (2009).

4. Fujii T *et al.*, Identical folds used for distinct mechanical functions of the bacterial flagellar rod and hook. *Nat. Commun.* 8:14276 (2017).

5. Beeby M *et al.*, Diverse high-torque bacterial flagellar motors assemble wider stator rings using a conserved protein scaffold. *PNAS* 113:1917-1926 (2016).

6. Muller A *et al.*, Ultrastructure and complex polar architecture of the human pathogen campylobacter jejuni. *MicrobiologyOpen* 3:702-710 (2014).

7. Minamino T, Moriya N, Hirano T, Hughes KT, Namba K, Interaction of FliK with the bacterial flagellar hook is required for efficient export specificity switching. *Mol. Microbiol.* 74:239–251 (2009).

8. Erhardt M, Singer HM, Wee DH, Keener JP, Hughes KT, An infrequent molecular ruler controls flagellar hook length in Salmonella enterica. *EMBO J.* 30:2948–2961 (2011).

9. Cohen EJ, Hughes KT, Rod-to-hook transition for extracellular flagellum assembly is catalyzed by the L-ring-dependent rod scaffold removal. *J. Bacteriol.* 196:2387-2395 (2014).

10. Samatey FA *et al.*, Structure of the bacterial flagellar hook and implication for the molecular universal joint mechanism. *Nature* 431:1062-1068 (2004).

11. Datsenko KA, Wanner BL, One-step inactivation of chromosomal genes in Escherichia coli K-12 using PCR products. *PNAS* 97:6640-6645 (2000).

12. Aizawa SI, Dean GE, Jones CJ, Macnab RM, Yamaguchi S, Purification and characterization of the flagellar hook-basal body complex of Salmonella typhimurium. *J. Bacteriol.* 161:836-849 (1985).

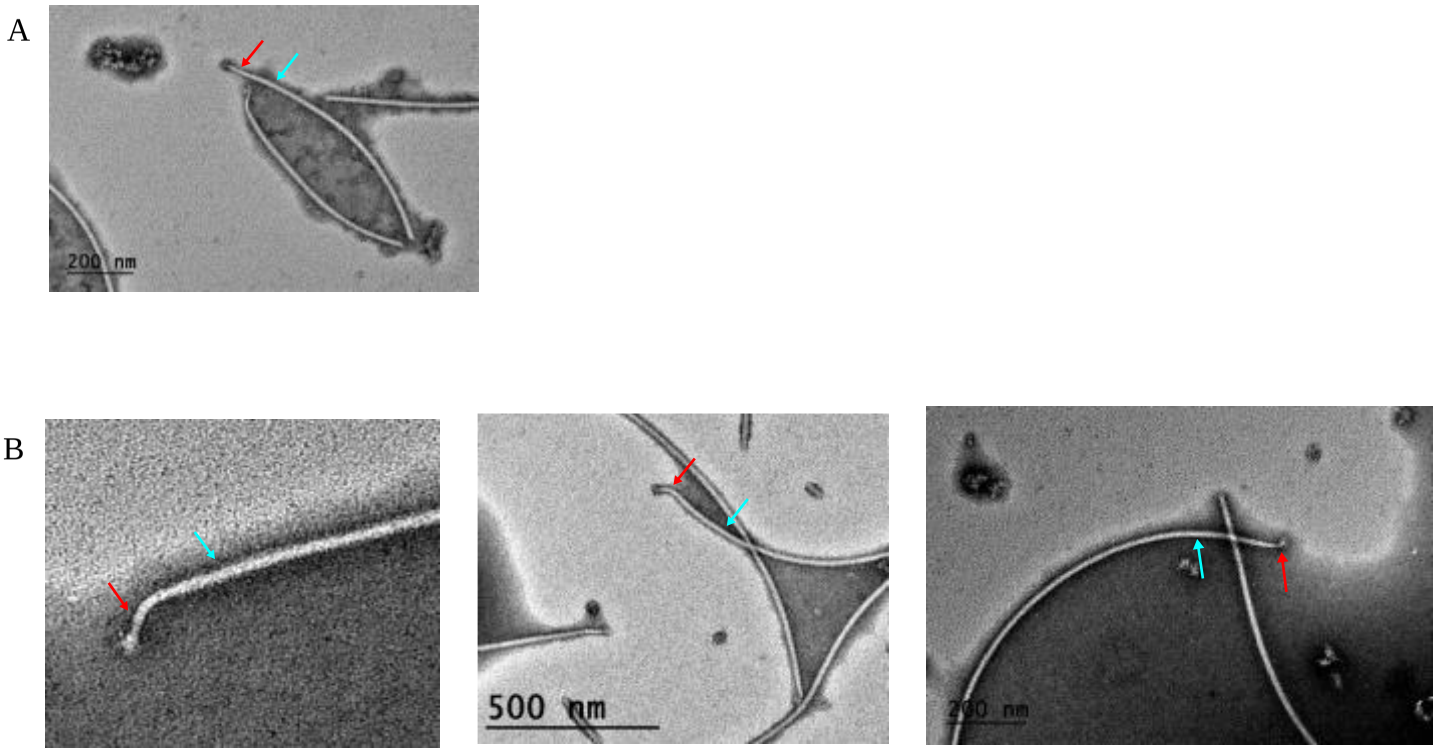

Fig. 4.1: Deletion of residues 51-66 from FlgG causes the distal rod to bend.
To determine whether the L-stretch conferred rigidity to the distal rod, and whether the distal rod could be engineered to be as flexible as the hook, codons 51-66 were deleted from *flgG*^{WT}. (A) The majority of flagella isolated from *flgG*$^{\Delta 51\text{-}66}$ backgrounds and visualized by TEM were found to possess straight distal rods (red arrows) with filaments attached directly to the distal rod (blue arrows). (B) However, some distal rods from *flgG*$^{\Delta 51\text{-}66}$ backgrounds were found to have distal rods that were bent. This result suggested that residues 51-66 of the FlgG L-stretch confer rigidity upon the rod, but are not solely responsible for promoting distal rod rigidity.

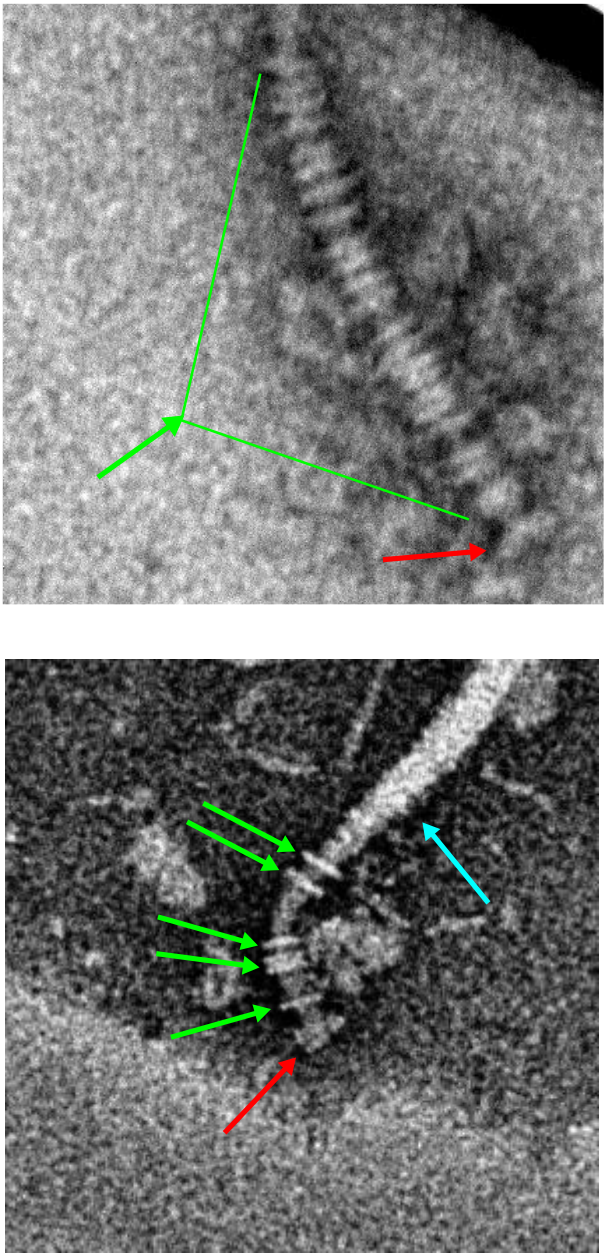

Fig. 4.2: The *flgG*$^{\Delta 51\text{-}66}$ distal rods possess P-rings
When flagella from the *flgG*$^{\Delta 51\text{-}66}$ Δ*flgDEH flgI*$^{+}$ Δ*fliK* Δ*araBAD*::*fliK*$^{+}$ background were isolated and visualized by TEM, the distal rods were found to have multiple P-rings (green arrows) with both filaments (blue arrow) and MS-rings (red arrows) attached. This result was unexpected, as the *flgG** $^{\Delta 54\text{-}57}$ mutant assembles filamentous distal rods lacking P-rings.

Table 4.1 List of *flgG* L-stretch primers

7091-flgGdel51-66-tetR	5’-GCGCGCGGTATTTGAAGATCTGTTGTATCAGACC ATCCGCTTAAGACCCACTTTCACATT-3’
7092-flgGdel51-66-tetA	5’-CAGACGCTCCGTGGCGACCGGACGCACGCCGGTACC GATTTGCTAAGCACTTGTCTCCTG-3’
7093- flgG 51-66 clean del.	5’-TCAGCGCGCGGTATTTGAAGATCTGTTGTATCAGACCA TCCGCCAAATCGGTACCGGCGTGCGTCCGGTCGCCAC GGAGC-3’
7094-flgG 51-66 clean del. fill in	5’-GCAGACGCTCCGTGGCGACCGGAC-3’
7106-DflhD::FXF FW	5’-ACAAAAATAAAGTTGGTTATTCTGGATGGGAACA ATGCATGTGTAGGCTGGAGCTGCTTC-3’
7107-DflhD::FXF RV	5’-TGAACAATGCTTTTTTCACTCATTATCATGCCC TTTTCTTCATATGAATATCCTCCTTAG-3’
7183-flgG Del. 41-73::Gly-Gly Fw	5’-ATAACCTGGCAAACGTCAGCACCAATGGTTTT AAGCGTCAGCGCGCGGTATTTGGTGGC-3’
7184-flgG Del. 41-73::Gly-Gly Rv	5’-ACAGGTTCCCCTGACTGTGCAGACGCTCCG TGGCGACCGGGCCACCAAATACCGCGCGC-3’
7198-flgG D46-66	5’-TCAGCACCAATGGTTTTAAGCGTCAGCGC GCGGTATTTGAAGATCTGTTG-3’
7199-flgG D46-66 fill in	5’-AGACGCTCCGTGGCGACCGGACGCACGCCGGT ACCGATTTGCAACAGATCTTCAAATAC-3’

Table 4.2 List of *flgG* L-stretch strains

Strain	Genotype
TH22866	*flgG*$^{\Delta 51\text{-}66}$
TH22867	*flgG*$^{\Delta 51\text{-}66}$ Δ*flgDEH* Δ*flhD*::FKF Δ*araBAD*::*flhD*$^{+}$*C*$^{+}$
TH22868	*flgG*$^{\Delta 51\text{-}66}$ Δ*flgDEHI* Δ*flhD*::FKF Δ*araBAD*::*flhD*$^{+}$*C*$^{+}$
TH22869	*flgG*$^{\Delta 46\text{-}66}$
TH22870	*flgG*$^{41\text{-}73::\text{Gly-Gly}}$

CHAPTER 5

SUMMARY

In Chapter 2, we investigated the biomechanical regulatory mechanism that synchronizes the termination of rod assembly in the periplasm with outer membrane penetration and initiation of hook assembly. It had been known that FlgH, which forms the L-ring component of the PL-ring, forms a hole in the outer membrane through which the growing flagellum exits the cell (1-2). However, it was unclear how pore formation in the outer membrane was i) coupled to the termination of rod polymerization and ii) initiation of hook polymerization.

The distal rod, hook and filament all require the presence of a scaffold, or cap, at their tip to promote incorporation of FlgG, FlgE and FliC/FljB subunits, respectively. Transition from rod to hook, or hook to filament, requires that the scaffold for the preceding structure be removed to make room at the tip of the growing structure to allow for replacement by the next scaffold, allowing assembly of the next axial structure to proceed. In the case of the hook cap, FlgD, either FlgK or FlgL likely dislodges FlgD as they assemble at the tip of the completed hook. Once the FlgKL junction has formed, the FliD filament cap can form on top of FlgL and direct assembly of the filament (3). As the filament is the last axial component of the flagellum to assemble, there is no need to

remove FliD once filament construction is complete.

In contrast to the hook-to-filament switch, which represents a switch from class II to class III substrate secretion and polymerization (4), the rod-to-hook switch is a switch in construction from one class II structure (the rod) to another class II structure (the hook). Consequently, the FlgJ rod cap must remain firmly associated with the tip of the rod to prevent co-secreted FlgD subunits from taking its place prematurely and directing hook assembly in the periplasm. It had previously been shown that FlgJ accumulates in the periplasm and was not detectable by western blot in the culture supernatant of motile cells (5). This implied that FlgJ dissociated from the tip of the distal rod before outer membrane penetration had occurred. This was perplexing, as we were unsure how periplasmic hook polymerization was prevented in the absence of the FlgJ rod cap to inhibit FlgD cap formation on the rod tip.

We presumed that if the FlgJ cap was in fact dislodged from the rod tip and secreted to the supernatant, the extracellular concentration of FlgJ was likely to be very low relative to FliC or FlgE. This presumption was informed by research demonstrating that the filament cap was formed from only five FliD subunits. As *Salmonella* constructs ~4-6 flagella/cell, one would therefore expect the average cell to release 30-40 FlgJ subunits from the rod tip into the supernatant if in fact the rod scaffold was dislodged from the rod tip into the extracellular milieu.

To address this, we constructed a version of FlgJ that contained a hemagluttinin (HA) tag in the unstructured region of FlgJ between the scaffolding domain and the PGase domain. Placement of the 3xHA tag in this position did not affect flagellum

assembly or the cell's motility phenotype and provided a sensitive method for detection of FlgJ in the culture supernatant.

Using the 3xHA-tagged variant of FlgJ, we demonstrated that FlgJ is secreted to the supernatant and that this depended on formation of the L-ring by FlgH subunits. In addition, we showed that the L-ring dislodges the FlgJ scaffold from the tip of the rod by isolating basal bodies with and without the *flgH* expressed and probing for the presence of FlgJ-3xHA associated with basal bodies. This demonstrated that the FlgJ-3xHA we detected in the supernatant represented structural FlgJ rod (i.e. the rod cap), as opposed to monomeric FlgJ that had been translocated from the cytoplasm and discarded into the culture supernatant during hook polymerization.

Using *flgG** mutants, we also demonstrated that L-ring assembly to complete the PL-ring complex prevents further distal rod assembly. Although *flgG** rods will accumulate multiple P-rings along their length, the acquisition of a single L-ring to form the PL-ring complex invariably terminated distal rod assembly. Although this observation was not pursued further, this suggested that the presence of the L-ring on the tip of the distal rod dislodges the FlgJ rod scaffold and prevents further distal rod polymerization. Whether the inability of the distal rod to polymerize past the L-ring is due to steric hindrance, specific interactions between FlgH and FlgJ or conformational changes in FlgG such that it is no longer recognized by FlgJ remains unknown (2).

In Chapter 3, we turned our attention to the distal rod. Specifically, we were interested in elucidating the mechanism by which the distal rod, constructed from ~50 copies of FlgG, controlled its own length. The axial structures of the *Salmonella* flagellum are composed of 11 protofilaments (6). Thus, with ~50 subunits required to

build the distal rod, FlgG must assemble into 4-5 stacks in order to reach the outer membrane, where polymerization of the L-ring from outer membrane-anchored FlgH subunits can occur. If FlgG is capable of stacking upon itself into multiple layers, what is to stop FlgG subunits from forming 6, or 60, layers instead of the 4-5 found in the wild type distal rod?

Based on previous estimates that the number of FlgG subunits in the distal rod was ~26 (7), a model was proposed for distal rod length control that relied solely on FlgG-FlgG interactions. This model was termed the FlgG-intrinsic model for distal rod length control. According to this model, once two stacks of FlgG had assembled, inter-FlgG interactions would prevent further distal rod polymerization. If this were the case, then overexpression of *flgG* would not have any effect on distal rod length. However, we found that the lengths of the distal rods isolated from a *flgG* overexpressing background were considerably longer than those isolated from a control background expressing *flgG* at wild type levels. This argued against the FlgG-intrinsic model for distal rod length control.

It is known that the γ-proteobacteria, the genera to which *E. coli* and *Salmonella* belong, possess a highly abundant outer membrane lipoprotein, Lpp (a.k.a. Braun's lipoprotein, LppA in *Salmonella* spp.) that is responsible for linking the outer membrane to the peptidoglycan layer. At ~10^6 copies/cell, LppA is the most abundant protein in many gram-negative species of bacteria including *Salmonella* spp. The LppA lipoprotein promotes outer membrane stability, and determines peptidoglycan-to-outer membrane spacing by tethering the outer membrane to the peptidoglycan layer. This is accomplished by anchoring LppA in the outer membrane via lipoylation of an invariant N-terminal

cysteine and covalently linking the invariant C-terminal lysine to the peptidoglycan layer. Upon searching through our strain collection, we discovered that null mutants of *lppA* had been isolated as suppressors of the motility defect in several *flgG** backgrounds. The observation that *lppA* null *flgG** mutants were able to swim better than *lppA*^{WT} *flgG** mutants suggested to us that the outer membrane might act as a barrier to extended distal rod polymerization.

To test this model, longer and shorter variants of the LppA lipoprotein were constructed to determine if varying the length of the major outer membrane lipoprotein would result in a concomitant change in rod length. Indeed, rods isolated from strains harboring longer versions of LppA were longer than those isolated from the LppA^{WT} background. The same was true for rods isolated from a strain possessing a shorter version of LppA. We also found that, as expected, varying the length of LppA changed the peptidoglycan-to-outer membrane distance.

Additionally, we were interested in addressing a longstanding question in gram negative bacterial physiology: whether the osmolality difference between the cell and the external environment existed across the cytoplasmic membrane, or the outer membrane. In other words, we wanted to determine whether the osmolality of the periplasm equaled that of the external environment, or that of the cytoplasm. As part of the distal rod length control project, we had constructed a Δ*lppAB* clean deletion mutant as well as an Δ*lppAB* Δ*pal* double mutant. Like LppA, Pal (**p**eptidoglycan **a**ssociated **l**ipoprotein) is another abundant outer membrane lipoprotein (~5x10^4 copies/cell) that is a component of the Tol-Pal trans-envelope complex responsible for the import of substances across the bacterial envelope. Pal is anchored in the outer membrane by its N-terminus and non-covalently

binds peptidoglycan.

We reasoned that if the osmolality of the periplasm was equal to the cytoplasm, deleting the proteins that tether the outer membrane to the cell body would cause the outer membrane to pull away from the cell body as water from the external environment flooded the periplasm. Conversely, if the osmolality of the periplasm equaled that of the external environment, deleting *lppA* and/or *pal* should either cause the outer membrane to collapse in on the cell, or remain morphologically unchanged. Upon deletion of *lppAB*, we observed the outer membrane blebbing away from the cell body, which was exacerbated upon deletion of *pal* in addition to *lppAB*. This result is consistent with the osmolality of the periplasm equaling that of the cytoplasm (8).

Chapter 4 presented ongoing work aimed at elucidating the molecular mechanism(s) responsible for terminating distal rod assembly upon contact with the outer membrane. Despite having demonstrated that i) termination of distal rod polymerization and PL-ring assembly are coupled events that represent an important checkpoint during flagellar assembly (Chapter 2), and ii) that termination of rod growth at ~18 nm depends on the outer membrane acting as a physical barrier to continued rod polymerization (Chapter 3), we are still unsure how termination of distal rod assembly actually occurs.

Most of the *flgG** alleles cluster in a region of the FlgG protein known as the L-stretch, which allows one FlgG subunit in the distal rod to make extensive contacts with neighboring FlgG subunits. L-stretch-dependent FlgG-FlgG interactions are thought to enhance the stability and rigidity of the rod. Furthermore, the flexible hook is composed of ~130 copies of a single protein, FlgE, that is highly homologous to FlgG, but possesses a truncated version of the L-stretch. This suggested to us that *flgG** L-stretch mutations

disrupt L-stretch-mediated FlgG-FlgG contacts and lead to filamentous distal rod growth by permitting the destabilized *flgG** distal rod to bend once it reaches the outer membrane. Bending and deflecting off the outer membrane would allow the distal rod to polymerize parallel to the outer membrane until it reaches ~70 nm, at which point filament assembly would commence in the periplasm.

Thus far, we have tested this model by looking at the effects of a single engineered mutation, *flgG*$^{\Delta 51\text{-}66}$, on motility, cell and flagellar morphology in *Salmonella*. Codons 51-66 were chosen to be deleted as these codons encompass all of the *flgG** L-stretch mutations isolated to date. We found that the *flgG*$^{\Delta 51\text{-}66}$ allele caused the same general defects as the other *flgG** L-stretch mutations. Specifically, cells in the *flgG*$^{\Delta 51\text{-}66}$ background exhibit growth and morphology defects that result from filament growth in the periplasm. Furthermore, we found that deletion of residues 51-66 did not preclude P-ring assembly along the length of the *flgG*$^{\Delta 51\text{-}66}$ filamentous rod. This was unexpected, as the cells from another *flgG** L-stretch mutant(*flgG**$^{\Delta 54\text{-}57}$) construct filamentous rods with no P-rings.

Remaining Questions

A number of questions regarding the biomechanics of rod-to-hook switching remain unanswered. As discussed in Chapter 2, rod-to-hook switching requires the FlgH lipoprotein to polymerize around the tip of the distal rod into the L-ring. L-ring formation simultaneously dislodges the FlgJ rod cap and forms a pore in the outer membrane, thereby synchronizing outer membrane penetration with the initiation of hook assembly (2).

Experimental evidence suggests that FlgH subunits recognize the P-ring, made up of FlgI subunits. This is informed by the observation that, in *flgI* null backgrounds, L-rings are never found on the rod. However, it is possible that, in addition to recognizing the P-ring, FlgH also recognizes the distal rod (FlgG) and/or the distal rod scaffold (FlgJ). It also remains a formal possibility that FlgH subunits do not recognize the P-ring *per se*. Instead, formation of the P-ring may cause conformational changes in the FlgG/FlgJ subunits directly adjacent to the P-ring, thereby exposing a FlgH-recognition motif in the distal rod required for L-ring assembly.

In any event, further work should focus on what specific features of the candlestick structure (basal bodies with P-rings) FlgH subunits use as the L-ring nucleation signal. For that matter, in much the same way that the L-ring nucleation signal(s) recognized by FlgH are unknown, the motif(s) or residues of the distal rod recognized by FlgI subunits during formation of the P-ring are also unknown at this time.

Once incorporated into the PL-ring complex, FlgH traverses the outer membrane, providing a hydrophilic barrel that the flagellar structure passes through. An open question is whether the FlgH monomer, in the absence of the basal body, traverses the outer membrane, or whether L-ring formation around the rod involves large conformational changes in FlgH that drive it through the outer membrane.

In Chapter 3, we discussed the isolation of null mutations in *lppA* that suppressed the motility defect of a number of *flgG** mutants. What was not discussed in Chapter 3 was the fact that *flgG** suppressors were also isolated in both *flgI* and *flgJ*. Similar to the *lppA* nulls, *flgI* and *flgJ* alleles increase the apparent swim rate of *flgG** mutants, although not nearly to wild type levels. The *flgI* and *flgJ* suppressors include multiple

missense mutations, but we have been most interested in two suppressor alleles, *flgI*$^{\Delta 308\text{-}320}$ and *flgJ*$^{\Delta 94\text{-}117}$, that somehow restore motility to specific *flgG** mutants. Preliminary work has demonstrated that the *flgJ*$^{\Delta 94\text{-}117}$ suppresses the *flgG**^{G65R} motility defect by retarding the polymerization of FlgG*^{G65R} subunits. Slower polymerization of the FlgG*^{G65R} rod is presumed to provide FlgH subunits more time to form the L-ring around the rod as it reaches the outer membrane. In contrast, the deletion of *lppA* does not impact the polymerization rate of the distal rod, but is thought to allow the outer membrane to flex, thereby allowing the tip of the filamentous rod to stay in contact with the outer membrane long enough to allow L-ring polymerization. Ongoing work is aimed at determining whether the *flgI*$^{\Delta 308\text{-}320}$ also retards distal rod growth, or whether it suppresses the *flgG**^{G132R} motility defect in a manner distinct from either *lppA* nulls or the *flgJ*$^{\Delta 94\text{-}117}$ suppressor.

Salmonellaceae are unique among the γ-proteobacteria in that they contain two *lpp* genes, *lppA* and *lppB*, separated by 82 base pairs (9). Thus far we have not discussed *lppB*, the gene immediately downstream of *lppA* that likely arose from a duplication of the ancestral *lpp* gene in *Salmonella* spp. The *lppB* gene is nearly identical to *lppA*, with the exception of the seven amino acid residues at their C-termini, which have diverged almost completely. With the exception of the invariant C-terminal lysine residue that is crosslinked to the peptidoglycan layer, *lppA* and *lppB* exhibit no sequence homology at their C-termini.

As previously discussed, the original selection for rescue of the *flgG** motility defect resulted in the isolation of *lppA* suppressing alleles (8). However, the original *lppA* suppressor was not simply an inactivating mutation in *lppA*, but was instead an in-frame

deletion that fused the N-terminus of *lppA* to the C-terminus of *lppB*. The *lppA-lppB* fusion codes for a chimeric Lpp molecule of wild type length, but that possesses the divergent LppB C-terminal seven residues (KVFRICK) as opposed to the LppA C-terminal amino acid sequence (QATKYRK). Although the rest of the Lpp chimera is nearly identical to LppA, the chimera is nevertheless phenotypically identical to a clean deletion of *lppA* with regard to motility and colony morphology.

The presence of a second copy of *lpp* in the *Salmonella* chromosome, and the observation that the LppA-B chimera acts as an *lppA* null, indicates that *lppB* evolved to fulfill a niche function distinct from *lppA*. Furthermore, *lppB* does not appear to be expressed under standard laboratory conditions (10). A transcriptomic approach, testing ~40 different growth conditions, indicated that *lppB* expression is induced only under anaerobic conditions. It will be interesting to determine the specific signals or environmental conditions to which *Salmonella* responds by upregulating *lppB* expression. Current work aimed at identifying the regulator(s) and signals responsible for *lppB* expression is underway.

Conclusion

The work presented in this dissertation sheds light on the biomechanical processes that regulate hook basal body assembly in *Salmonella*. The flagellar Type III Secretion System secretes substrates at a rate of thousands of amino acid residues per second. All of the distinct protein subunit types required to construct the axial structures of the HBB are secreted through the fT3SS at the same time. Consequently, the rapidly polymerizing flagellar structure requires built-in mechanisms that allow it to determine when each

substructure of the HBB has been completed and to subsequently transition to the next component. Failure to coordinate assembly or regulate the dimensions of HBB substructures has negative consequences for cell motility and morphology. Focusing on the transition from termination of intracellular HBB construction to the initiation of extracellular HBB assembly, we have shown that i) PL-ring assembly synchronizes rod-to-hook transitioning with outer membrane penetration, ii) distal rod length is determined by the distance between the peptidoglycan layer and the outer membrane, and iii) distal rod rigidity likely plays a role in preventing extended rod growth in the periplasm.

References

1. Jones CJ, Homma M, Macnab RM, L-, P-, and M-ring proteins of the flagellar basal body of Salmonella typhimurium: Gene sequences and deduced protein sequences. *J. Bacteriol.* 171:3890–3900 (1989).

2. Cohen EJ, Hughes KT, Rod-to-hook transition for extracellular flagellum assembly is catalyzed by the l-ring-dependent rod scaffold removal. *J. Bacteriol.* 196:2387-2395 (2014).

3. Yonekura K *et al.*, The bacterial flagellar cap as the rotary promoter of flagellin self assembly. *Science* 290:2148-2152 (2000).

4. Chilcott GS, Hughes KT, Coupling of flagellar gene expression to flagellar assembly in Salmonella enterica serovar Typhimurium and Escherichia coli. *Microbiol. Mol. Biol. Rev.* 64:694–708 (2000).

5. Hirano T, Minamino T, Macnab RM, The role in flagellar rod assembly of the N-terminal domain of Salmonella FlgJ, a flagellum-specific muramidase. *JMB* 312:359-369 (2001).

6. Samatey FA *et al.*, Structure of the bacterial flagellar hook and implication for the molecular universal joint mechanism. *Nature* 431:1062-1068 (2004).

7. Jones CJ, Macnab RM, Okino H, Aizawa S, Stoichiometric analysis of the flagellar hook-(basal-body) complex of Salmonella typhimurium. *J. Mol. Biol.* 212:377–387 (1990).

8. Cohen EJ, Ferreira JL, Ladinsky MS, Beeby M, Hughes KT, Nanoscale-length control of the flagellar driveshaft requires hitting the tethered outer membrane. *Science* 356:197-200 (2017).

9. Sha J, Fadl AA, Klimpel GR, Niesel DW, Popov VL, Chopra AK, The two murein lipoproteins of Salmonella enterica serovar Typhimurium contribute to the virulence of the organism. *Infection and Immunity* 72:3987-4003 (2017).

10. Kroger C *et al.,* An infection-relevant transcriptomic compendium for Salmonella enterica serovar syphimurium. *Cell Host and Microbe* 14:683-695 (2004).